REVIEWS OF GEOPHYSICS, VOL. 26, NO. 3, PAGES 407–444, AUGUST 1988

Chemistry of the Rock-Forming Silicates: Multiple-Chain, Sheet, and Framework Structures

J. J. PAPIKE

Institute for the Study of Mineral Deposits, South Dakota School of Mines and Technology, Rapid City

The crystal chemistry of 16 groups of multiple-chain, sheet, and framework silicates is reviewed. Crystal structure drawings are presented to illustrate crystal chemical features necessary to interpret chemical data for each mineral group. The 16 silicate groups considered in this review are the amphibole; nonclassical, ordered pyriboles; mica; pyrophyllite-talc; chlorite; greenalite; minnesotaite; stilpnomelane; prehnite; silica polymorphs; feldspar; nepheline-kalsilite; leucite-analcite; sodalite group; cancrinite group; and scapolite. Electron microprobe analyses should be augmented by independent determinations of Fe^{2+}/Fe^{3+} and H_2O for many of the silicate groups discussed and by determinations of CO_3^{2-}, SO_4^{2-}, S^{2-}, and Li in some of the others. However, microprobe data augmented as suggested will still be ambiguous for some of the silicate groups considered here because the structures are not completely determined or are variable, with disparate domains and/or structural modulations, e.g., pyriboles, greenalite, minnesotaite, and stilpnomelane. Nevertheless, the most rigorous way to interpret silicate mineral chemical data is based on the crystal structures involved.

CONTENTS

INTRODUCTION

The basic premise of this review of multiple-chain, sheet, and framework silicate structures is the same as that for part 1 of this synthesis [*Papike*, 1987]: that true understanding of the chemistry of minerals can be achieved only by reference to the crystal structures involved. To help investigators in the interpretation of silicate chemical data for those minerals considered in this review, I have assembled structure drawings for 16 groups of multiple-chain, sheet, and framework structures. Some of the drawings are new, and some have been adapted from previously published drawings. However, as in part 1 of this synthesis, all diagrams presented here have been selected to accurately portray sufficient detail to the noncrystallographer so that the mineral chemistry can be interpreted as rigorously as possible.

Because of length limitations, referencing has been streamlined. References necessary to convey the essentials of the structural chemistry of each mineral group are emphasized. Readers who require more detailed information are referred to *Deer et al.* [1963*a*, 1962, 1963*b*] for mutiple-chain, sheet, and framework silicates, respectively. The *Reviews in Mineralogy* series gives additional valuable information [*Ribbe*, 1983; *Veblen*, 1981; *Veblen and Ribbe*, 1982; *Bailey*, 1984]. Other amphibole reviews are by *Cameron and Papike* [1979] and *Hawthorne* [1983]. A general review of silicate crystal chemistry for 12 silicate groups is provided by *Papike and Cameron* [1976].

The elements considered for each mineral group are tabulated in Table 1. Table 2 lists recommended normalization schemes for microprobe data and criteria for good analyses. The following text documents the rationale for these recommendations.

It is my hope, as with part 1 of this synthesis, that this review will help in the rigorous interpretation of chemical analyses of silicate minerals.

Paper number 8R0240.
8755-1209/88/008R-0240$05.00

AMPHIBOLE

The amphibole group has the general formula $A_{0-1}B_2C_5T_8O_{22}(OH, F, Cl, O)_2$, where A contains Na, K at the A site, B contains Na, Li, Ca, Mn^{2+}, Fe^{2+}, Mg at the M4 site, C contains Mn^{2+}, Fe^{2+}, Mg, Fe^{3+}, Cr^{3+}, Al, Ti^{4+} at the octahedrally coordinated M1, M2, and M3 sites, and T contains Si, Al at the tetrahedral sites. The published work on this important group of rock-forming silicates is voluminous, and only a relatively brief review is presented here. For more extensive coverage the reader is referred to *Deer et al.* [1963*a*], *Papike and Cameron* [1976], *Cameron and Papike* [1979], *Veblen* [1981], *Veblen and Ribbe* [1982], and *Hawthorne* [1983].

Important aspects of the *C2/m* structure are illustrated in Figure 1*a*. The M1, M2, and M3 octahedra, which accommodate the C cations, share edges to form octahedral bands parallel to *c*. M1 and M3 are usually coordinated by four oxygens and two (OH, F) groups, whereas M2 is coordinated by six oxygens. When present, Al and Fe^{3+} usually prefer the M2 site, especially when Na occupies the adjacent M4 site. The M4 site, which accommodates the B cations, can be considered six-coordinated (a distorted octahedron) when occupied by Mn^{2+}, Fe^{2+}, and Mg and eight-coordinated when occupied by Na or Ca. The double tetrahedral chains cross-

TABLE 1. Inventory of Important Elements to Determine for Each Mineral

	Si^{4+}	Al^{3+}	Fe^{3+}	Ti^{4+}	Mg^{2+}	Fe^{2+}	Mn^{2+}	Ca^{2+}	Ba^{2+}	Li^{+}	Na^{+}	K^{+}	Rb^{+}	Cs^{+}	H_2O	F^{-}	Cl^{-}	CO_3^{2-}	SO_4^{2-}	S^{2-}
Amphibole group	X	X	X*	X	X	X	X	X		X*	X	X			X*	X	X			
Pyriboles	X	X			X	X	X	X			X				X*					
Mica	X	X	X*	X	X	X	X	X		X*	X	X	X	X	X*	X				
Pyrophyllite-talc	X	X	X	X	X	X	X	X			X	X			X*					
Chlorite	X	X	X*	X	X	X	X								X*					
Greenalite	X	X			X	X	X								X*					
Minnesotaite	X	X	X*		X	X	X	X			X	X			X*					
Stilpnomelane	X	X	X*		X	X	X	X			X	X			X*					
Prehnite	X	X	X*	X	X	X	X	X			X				X*					
Silica polymorphs	X	X	X	X	X	X	X	X			X	X								
Feldspar	X	X	X*	X	X	X	X	X	X		X	X								
Nepheline-kalsilite	X	X	X	X	X			X			X	X								
Leucite-analcite	X	X	X	X	X	X		X			X	X			X*					
Sodalite group	X	X	X					X			X	X					X		X*	X
Cancrinite group	X	X			X			X			X	X			X*		X	X*	X*	
Scapolite	X	X						X			X	X					X	X*	X*	X

*Determinations recommended to supplement microprobe data.

TABLE 2. Recommended Normalization Schemes for Microprobe Data and Criteria for Good Analyses

	Normalization		Criteria for Good Analyses			
	Fixed Number of Oxygens	Fixed Number of Cations	100% Anhydrous Sum	Total Silicons	Selected Cation Sum	Compare With Table Analyses
Amphibole	23		no		$\sum$ Si, ^{IV}Al = 8 $\sum$ Mn, Fe, Mg, Ti, Cr, Al $\geq$ 5 octahedral cations in excess of 5 (exoct) should sum to $\leq$2 $\sum$ exoct, Ca $\leq$ 2 $\sum$ exoct, Ca, Na, Li = 2 A site occupancy (Na, K) $\leq$ 1	
Pyriboles						
Clinojimthompsonite	34		no	12	$\sum$ Al, Mg, Fe^{2+}, Mn, Ca = 10	
Jimthompsonite	34		no	12	$\sum$ Al, Mg, Fe^{2+}, Mn, Ca = 10	
Chesterite	57		no	20	$\sum$ Al, Mg, Fe^{2+}, Mn, Ca = 17	
Mica	11		no		$\sum$ Si, Al $\geq$ 4 Si $\leq$ 4 octahedral cations $\leq$ 3 X cations $\leq$ 1	
Pyrophyllite	11		no	4	^{VI}Al = 2	
Talc	11		no	4	$\sum$ Mg, Fe, Al = 3	
Chlorite	14		no		Octahedral cations = 5.5–6.0 Si = 2.34–3.45	
Greenalite	7		no		Octahedral cations = 2.73–2.85 Si = 2.06–2.13	
Minnesotaite	11		no			X
Stilpnomelane		$\sum$ Si, Al, Fe^{3+}, Mg, Fe^{2+}, Mn = 15				X
Prehnite	11		no		Ca + Na = 2 $\sum$ Si, Al, Fe^{3+}, Ti, Mg, Fe^{2+}, Mn = 5	
Quartz	2		yes	1		
Tridymite	2		yes		^{IV}Al + $^{IV}Fe^{3+}$ = 2(Mg, Fe^{2+}, Mn^{2+}, Ca) + Na + K	
Feldspar	8		yes		$\sum$ Na, K, Ca, Ba, Fe^{2+}, Mg = 1 $\sum$ Al, Si, Fe^{3+}, Ti = 4	
Nepheline-kalsilite	16		yes		$\sum$ Si, Al, Fe^{3+} = 8	
Leucite	6		yes		$\sum$ K, Na, Ca = 1 $\sum$ Si, Al, Fe^{3+}, Ti = 3	
Analcite	6		no		$\sum$ Na, K, Ca = 1 $\sum$ Al, Si = 3	
Sodalite group		$\sum$ Si, Al, Fe^{3+} = 12	no			X
Cancrinite group		$\sum$ Si, Al = 12	no			X
Scapolite		$\sum$ Si, Al = 12	no			X

It is assumed that Fe^{2+}/Fe^{3+} is determined independently, and therefore cations are not adjusted to estimate Fe^{2+}/Fe^{3+}.

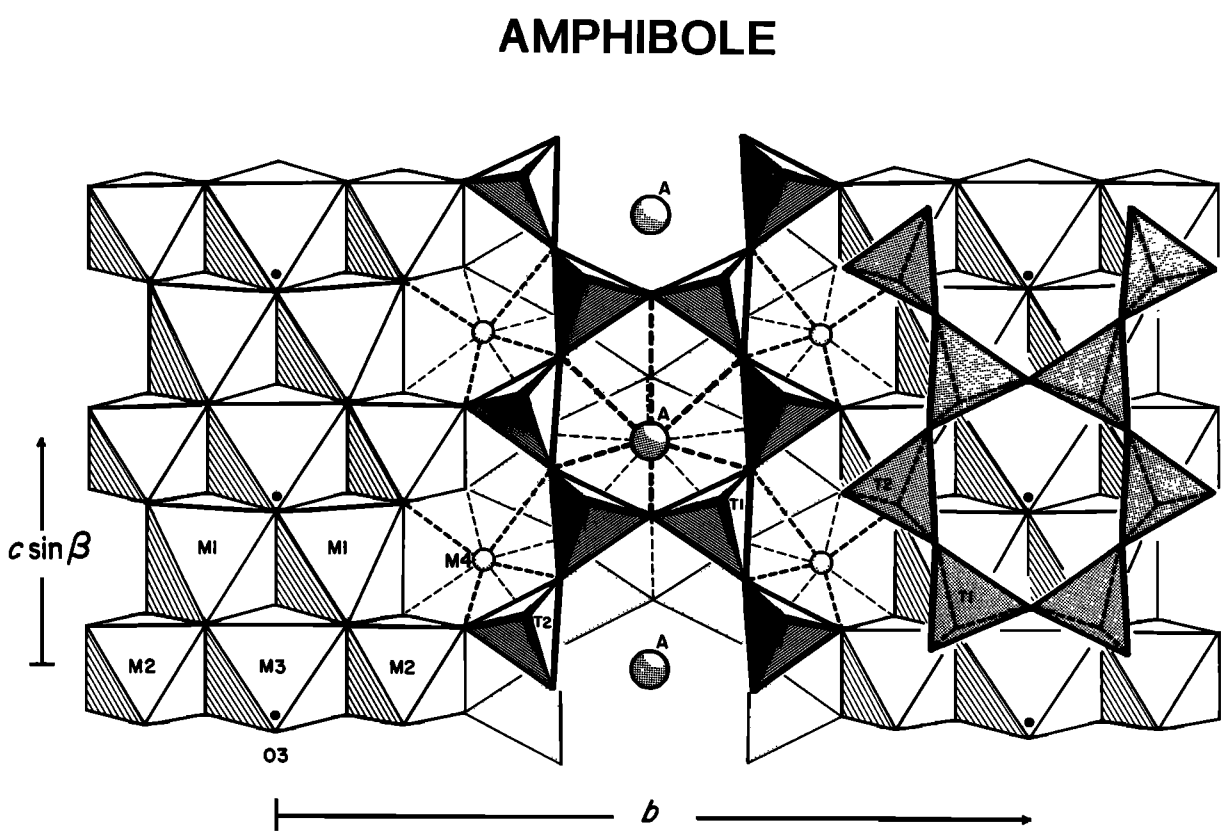

Fig. 1*a*. The crystal structure of a *C*2/*m* amphibole projected down *a* [from *Papike and Cameron*, 1976].

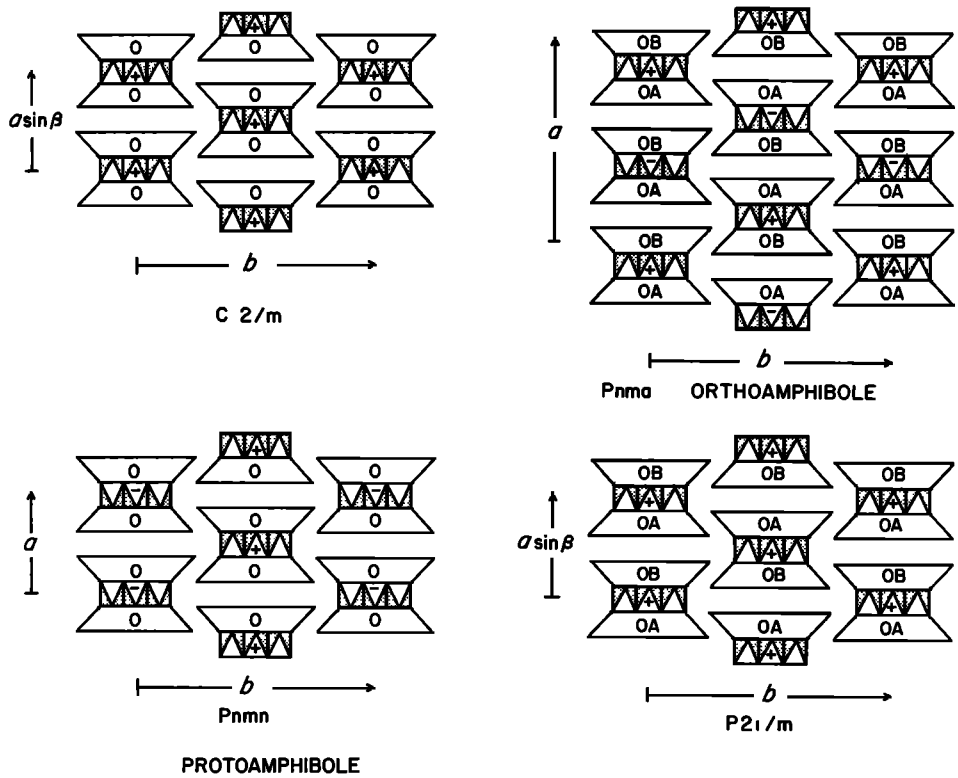

Fig. 1*b*. Amphibole structural topology [from *Papike and Cameron*, 1976].

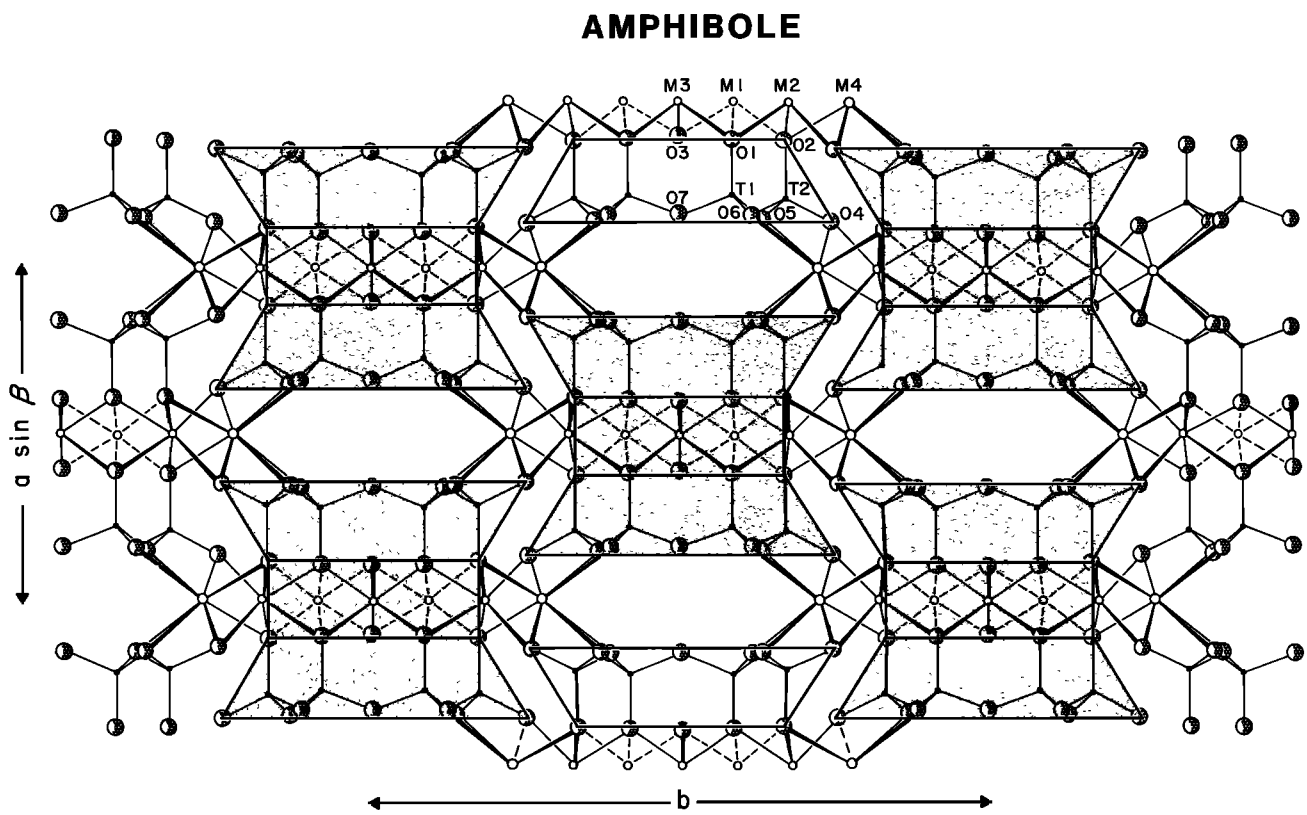

Fig. 1*c*. The crystal structure of *C2/m* amphibole projected down [001]. Stippled areas outlined I beams depicted in Figure 1*b* [from *Cameron and Papike*, 1979].

link the octahedral strips and are composed of two independent tetrahedral sites, T1 and T2. The T1 site, which shares three oxygens with other tetrahedra, is more regular and smaller than T2. The T2 site shares two oxygens with adjacent tetrahedra. The large and highly distorted A polyhedron occurs between the tetrahedral chains. This site can be vacant, partially filled, or fully occupied by Na and/or K in the *C2/m* structures. The O3 site is usually occupied by an $(OH)^-$ group or, less commonly, by F^- and Cl^-. Oxyamphiboles predominantly have O^{2-} at the O3 position.

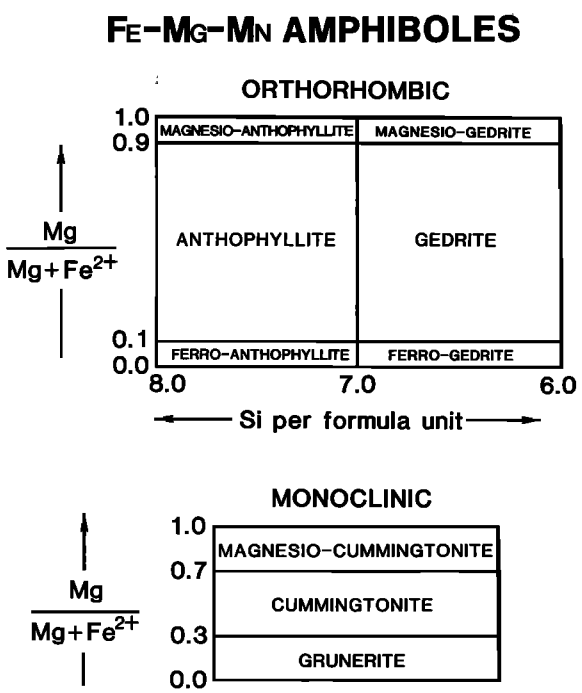

Fig. 1*d*. Classification of Fe-Mg-Mn amphiboles [after *Leake*, 1978].

The major topologic aspects of the structures are summarized in Figure 1*b*. Each "I beam" represents a tetrahedral-octahedral-tetrahedral (T-O-T) unit. The rotational aspect of the tetrahedral chain relative to the octahedral strip is *S* if the tetrahedra and octahedra have the same orientation and is *O* if the tetrahedra and octahedra have opposite orientations [*Thompson*, 1970; *Papike and Ross*, 1970]. A stacking sequence of the octahedral layers is defined as positive or negative depending on whether the apex of an octahedron points to $+a$ or $-a$ when viewed in the $+c$ direction, as in Figure 1*b*. The designations A and B refer to two tetrahedral sheets in a T-O-T unit that are symmetrically distinct. The absence of these designations indicates that the tetrahedral sheets in a T-O-T unit are symmetrically equivalent and are related by a twofold axis parallel to *b*.

The *C2/m* amphiboles have the octahedral stacking sequence $+, +, +, \cdots$ and only *O* rotations of the tetrahedral layers. The tetrahedral layers are related by a twofold axis parallel to *b*. The $P2_1/m$ structure has the same $+, +, +, \cdots$ stacking sequence as the *C2/m* structure, but it has lost the twofold axis parallel to *b*. Thus it has symmetrically distinct A and B tetrahedral chains. The orthorhombic (*Pnmn*) protoamphibole structure has the stacking sequence $+, -, +, -, \cdots$ and *O* rotations of tetrahedra. Orthorhombic *Pnma* structures have octahedral stacking sequences $+, +,$

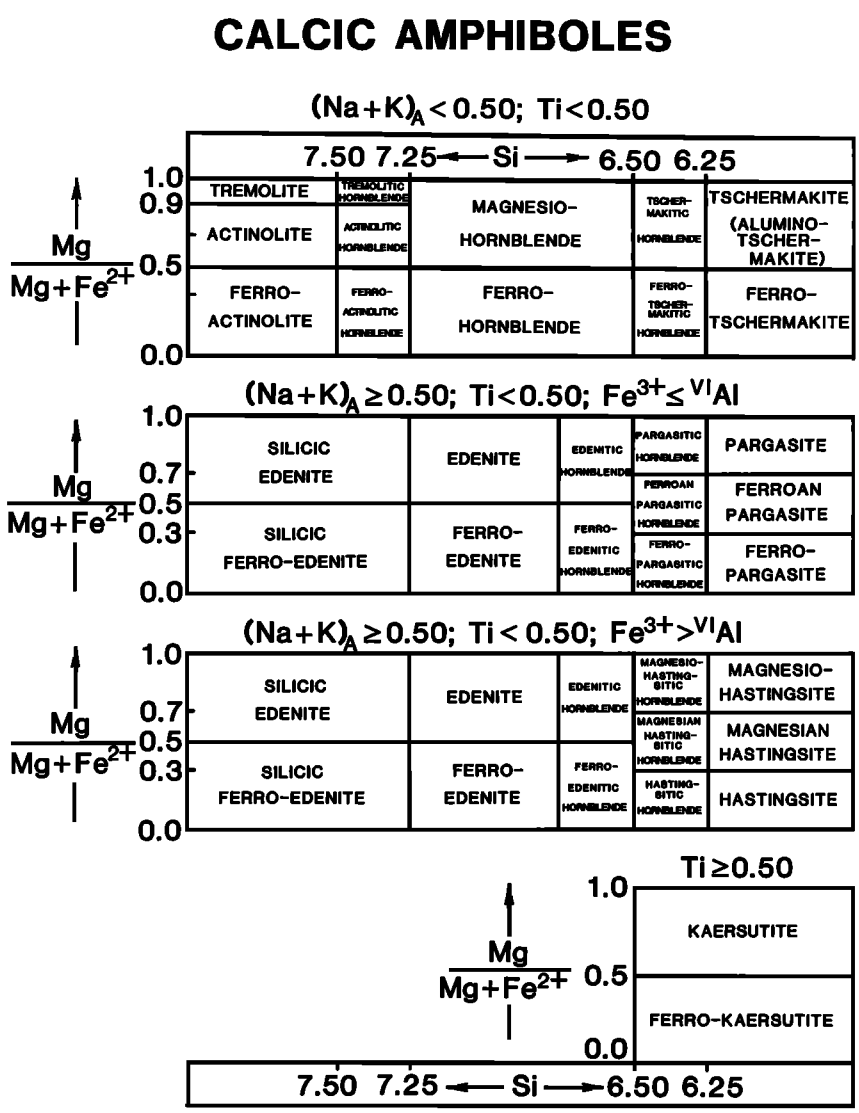

Fig. 1*e*. Classification of calcic amphiboles [after *Leake*, 1978].

−, −, +, +, ⋯; A and B tetrahedral chains, and *O* rotations of tetrahedra.

The *a* axes are similar in length for the *C*2/*m*, $P2_1/m$, and *Pnmn* amphiboles; however, for the *Pnma* orthoamphiboles the distance along *a* that must be traversed before arriving at a symmetrically identical point is twice as long because of the different octahedral stacking sequence. The T-O-T I beams are only schematic, and the relationship between the I beams and the polyhedral representation is shown in Figure 1*c*.

The range of substitutions and therefore the number of possible end-members are very large in the amphibole group. Fortunately, the International Mineralogical Association (IMA) subcommittee on amphibole nomenclature addressed this problem and arrived at a recommended classification [*Leake*, 1978]. This system divides the amphiboles into four chemical groups in terms of atoms per formula unit (apfu) as follows: (1) iron-magnesium-manganese group, where $^{B}(Ca + Na) < 1.34$, (2) calcic group, where $^{B}(Ca + Na) \geq 1.34$ and $^{B}Na < 0.67$, (3) sodic-calcic group, where $^{B}(Ca + Na) \geq 1.34$ and $0.67 < {}^{B}Na < 1.34$, and (4) alkali group, where $^{B}Na \geq 1.34$.

Tables 3*a*–3*d* list the 58 recommended end-member names and formulae for rock-forming amphiboles. The IMA system requires that the amphibole first be identified with one of the four groups on the basis of the critical ratios given above. In the next step we use one of our sets of *x*-*y* plots (Figures 1*d*–1*g*) to arrive at the most appropriate name for the amphibole. See *Leake* [1978] for details. Last, provision is made to denote by prefixes the presence of substantial substitutions that are not essential constituents of the end-members (Table 3*e*).

Table 3*f* presents several sets of unit cell data for a variety of amphibole structure types. Figure 1*h* shows the amphibole quadrilateral and illustrates the approximate compositional control for the *C*2/*m*, $P2_1/m$, and *Pnma* amphiboles in the Ca-Fe^{2+}-Mg system.

Table 3*g* presents some representative amphibole analyses from *Deer et al.* [1963*a*]. For a detailed recent review of the chemistry of amphiboles the reader is referred to *Veblen and Ribbe* [1982]. Readers who need a refresher on mineral formula calculations are referred to *Deer et al.* [1966, Appendix I]. Table 3*g* presents amphibole formulae based on a normal-

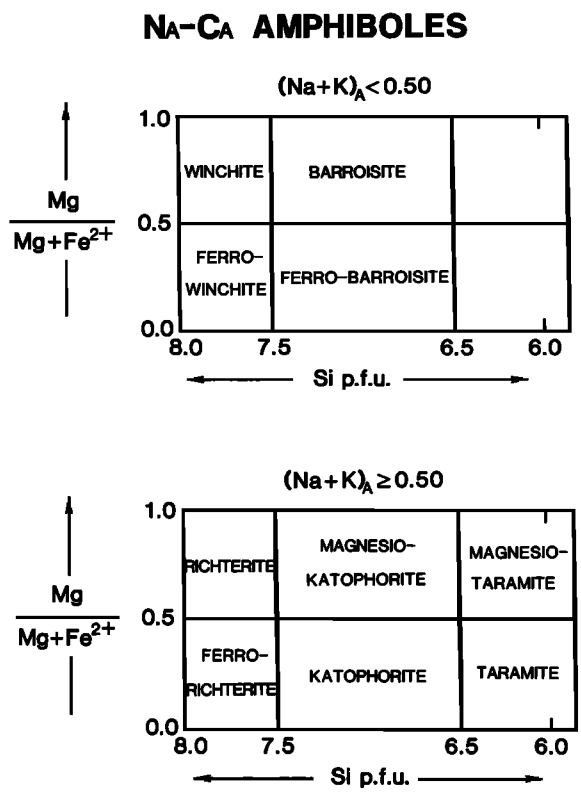

Fig. 1*f*. Classification of Na-Ca amphiboles [after *Leake*, 1978].

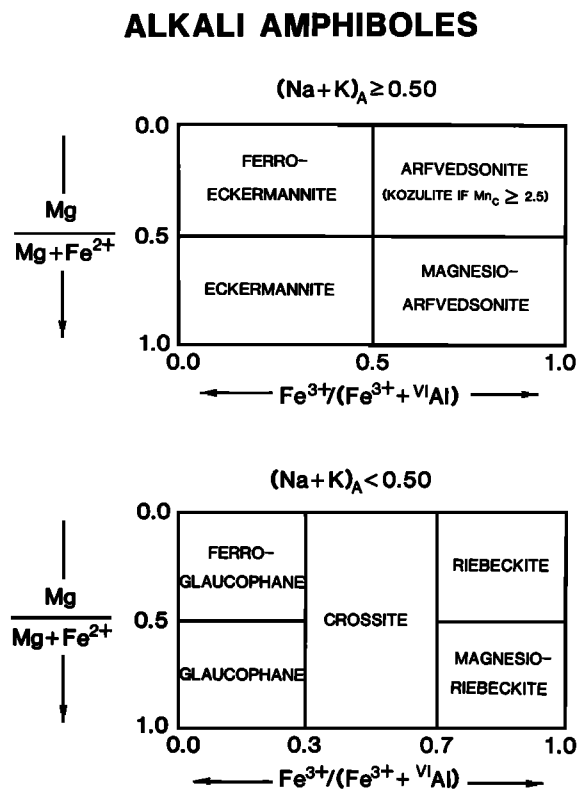

Fig. 1*g*. Classification of alkali amphiboles [after *Leake*, 1978].

ization to 24 (O, OH, F), and this is the recommended way to normalize amphibole analyses if reliable H_2O and F analyses are available. If H_2O and F are not analyzed, then the recommended normalization is to 23 oxygens or 46 negative charges. This is also the recommended way to normalize microprobe analyses. Of course, this assumes no oxyamphibole component, which can be a dangerous assumption in certain cases. Criteria for good analyses include: (1) Si + ^{IV}Al should total to approximately eight; (2) the octahedral cations (Mn, Fe, Mg, Ti, Cr, Al) should sum to greater than or equal to five; (3) the octahedral cations in excess of the five needed to fill the M1, M2, and M3 sites ("exoct") should be less than or equal to two; (4) exoct plus Ca should be less than or equal to two; (5) the M4 site occupancy (exoct, Ca, Na, Li) should sum to approximately two; and (6) the A site (Na, K) should sum to less than or equal to one. See *Cameron and Papike* [1979, p. 32] for additional charge balance criteria.

Note that there are various ways of estimating Fe^{3+} from microprobe data (see *Hawthorne* [1983] for a review); however, none are accurate, and none are recommended. I strongly recommend a direct determination of Fe^{2+}/Fe^{3+} [e.g., *Goldich*, 1984].

PYRIBOLES (NONCLASSICAL, ORDERED)

Much of this discussion concerning pyriboles and biopyriboles is extracted from a review by *Veblen* [1981]. The term biopyribole was introduced by *Johannsen* [1911] to collectively consider the micas (biotites), pyroxenes, and amphiboles. Johannsen also used the term pyribole to refer to the biopyriboles excluding the micas. *Thompson* [1970, 1978] used this terminology and extended it to include other minerals (hypothetical at that time) that could be thought of as assembled from slabs of pyroxene and mica. Here we consider only the nonclassical (excluding pyroxenes and amphiboles), ordered (ordered sequences of mixed double and triple chains along *b*) pyriboles.

The first silicates to be recognized with wider than a double chain were synthetic barium silicates [*Katscher and Liebau*, 1965; *Liebau*, 1980]. However, the tetrahedral chains in these structures are topologically distinct from those in pyroxenes and amphiboles. The first report of a structurally ordered, nonclassical biopyribole that can be constructed from mica and pyroxene units was of a synthetic reported by *Drits et al.* [1974]. This silicate contained Na and Mg at crystallographic sites analogous to the amphibole M4 site and the M1, M2, and M3 octahedral sites, respectively.

Veblen and Burnham [1975] discovered four new minerals in this series; these were intergrown with anthophyllite and cummingtonite in an alteration zone of a metamorphosed ultramafic body near Chester, Vermont. Structurally, the new minerals are similar to pyroxenes and amphiboles but contain either triple chains or both triple and double chains. Figure 2*a* provides a comparison of idealized pyroxene, amphibole, and the new triple chains. There is a remarkable analogy of these four new minerals to the pyroxene and amphibole groups. Figure 2*b* presents I beam diagrams comparing pyroxene, amphibole, jimthompsonite (triple chains only), and chesterite (triple and double chains that alternate along *b*). Table 4*a* tabulates unit cell parameters, space groups, and the number of formula units per unit cell (*Z*) for jimthompsonite and chesterite.

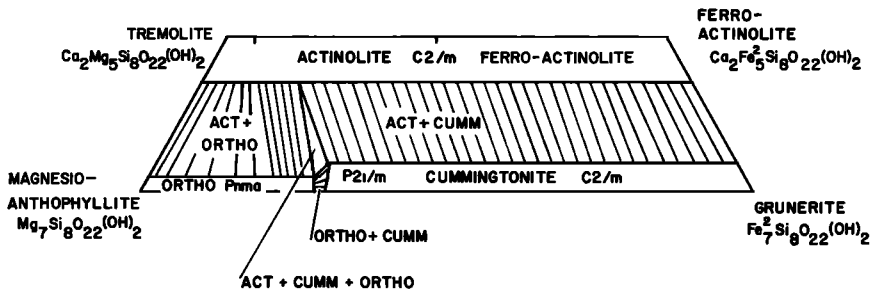

Fig. 1*h*. The amphibole quadrilateral [from *Papike and Cameron*, 1976].

Structural details for clinojimthompsonite, jimthompsonite, and chesterite are illustrated in Figures 2*c* 2*d*, and 2*e*, respectively. For a detailed discussion of these structures, refer to *Veblen and Burnham* [1978*b*].

Clinojimthompsonite is composed of triple silicate chains; in one tetrahedral layer parallel to (100) the tetrahedra point alternately in the $+a$ and $-a$ directions (the pointing directions of apical oxygens). These $+a$ and $-a$ chains are related by a 2_1 axis parallel to *b*. The M5 site is equivalent to the M4 site in amphibole or the M2 site in pyroxene. The M1, M2, M3, and M4 octahedral sites are equivalent to the M1, M2, and M3 sites in amphibole or the M1 site in pyroxene. Because of the triple chains in clinojimthompsonite, the mirror plane which runs through the double chains in amphibole is lost and is replaced by a *c* glide plane (g_c), and the space group is *C*2/*c*, as in diopside.

Jimthompsonite (space group *Pbca*) is related to clinojimthompsonite in the same way that orthoamphibole is related to clinoamphibole, i.e., the octahedral stacking sequence is +, +, −, −. +, +, ⋯ (note Figure 2*b*).

TABLE 3*a*. Iron-Magnesium-Manganese Amphiboles

	Formula
Orthorhombic Pnma	
Anthophyllite	
Mangesioanthophyllite	$Mg_7Si_8O_{22}(OH)_2$
Ferroanthophyllite	$Fe_7^{2+}Si_8O_{22}(OH)_2$
Sodium anthophyllite	$Na(Mg, Fe^{2+})_7Si_7O_{22}(OH)_2$
Gedrite	
Magnesiogedrite	$Mg_5Al_2Si_6Al_2O_{22}(OH)_2$
Ferrogedrite	$Fe_5^{2+}Al_2Si_6Al_2O_{22}(OH)_2$
Sodium gedrite	$Na(Mg, Fe^{2+})_6AlSi_6Al_2O_{22}(OH)_2$
Holmquistite	
Magnesioholmquistite	$Li_2Mg_3Al_2Si_8O_{22}(OH)_2$
Ferroholmquistite	$Li_2Fe_3^{2+}Al_2Si_8O_{22}(OH)_2$
Monoclinic C2/m or P2₁/m	
Cummingtonite	
Magnesiocummingtonite	$Mg_7Si_8O_{22}(OH)_2$
Grunerite	$Fe_7^{2+}Si_8O_{22}(OH)_2$
Tirodite	$Mn_2^{2+}Mg_5Si_8O_{22}(OH)_2$
Dannemorite	$Mn_2^{2+}Fe_5^{2+}Si_8O_{22}(OH)_2$
Clinoholmquistite	
Magnesioclinoholmquistite	$Li_2Mg_3Al_2Si_8O_{22}(OH)_2$
Ferroclinoholmquistite	$Li_2Fe_3^{2+}Al_2Si_8O_{22}(OH)_2$

Chesterite (space group $A2_1ma$) is composed of alternating triple and double tetrahedral chains along *b*. Because of the double chains the mirror planes parallel to (010) are present as well as the glide planes (g_c) parallel to (010) and running through the triple tetrahedral chains.

Selected microprobe analyses [*Veblen and Burnham*, 1978*a*] are presented in Table 4*b* for anthophyllite, chesterite, jimthompsonite, and clinojimthompsonite. The method of normalizing the microprobe data by *Veblen and Burnham* [1978*a*] is also recommended here, i.e., 34 oxygens for clinojimthompsonite and jimthompsonite and 57 oxygens for chesterite. Checks for good clinojimthompsonite and jimthompsonite analyses include Si summing to approximately 12 and octahedral cations summing to approximately 10. Checks for good chesterite analyses include Si summing to approximately 20 and octahedral cations summing to approximately 17.

MICA

The mica group of layer silicates has the general formula $X_{0-1}Y_{2-3}(Z_4O_{10})(OH, F, Cl, O)_2$. The major X cations are Na, K, Ca, and in the ideal, undistorted mica structure they are 12-coordinated. Other X cations include Ba and NH_4. The Y cations are octahedrally coordinated and include Mg, Fe^{2+},

TABLE 3*b*. Calcic Amphiboles (Monoclinic *C*2/*m*)

	Formula
Tremolite	$Ca_2Mg_5Si_8O_{22}(OH)_2$
Ferroactinolite	$Ca_2Fe_5^{2+}Si_8O_{22}(OH)_2$
Edenite	$NaCa_2Mg_5Si_7AlO_{22}(OH)_2$
Ferroedenite	$NaCa_2Fe_5^{2+}Si_7AlO_{22}(OH)_2$
Pargasite	$NaCa_2Mg_4AlSi_6Al_2O_{22}(OH)_2$
Ferropargasite	$NaCa_2Fe_4^{2+}AlSi_6Al_2O_{22}(OH)_2$
Hastingsite	$NaCa_2Fe_4^{2+}Fe^{3+}Si_6Al_2O_{22}(OH)_2$
Magnesiohastingsite	$NaCa_2Mg_4Fe^{3+}Si_6Al_2O_{22}(OH)_2$
Aluminotschermakite	$Ca_2Mg_3Al_2Si_6Al_2O_{22}(OH)_2$
Ferroaluminotschermakite	$Ca_2Fe_3^{2+}Al_2Si_6Al_2O_{22}(OH)_2$
Ferritschermakite	$Ca_2Mg_3Fe_2^{3+}Si_6Al_2O_{22}(OH)_2$
Ferriferrotschermakite	$Ca_2Fe_3^{2+}Fe_2^{3+}Si_6Al_2O_{22}(OH)_2$
Aluminomagnesiohornblende	$Ca_2Mg_4AlSi_7AlO_{22}(OH)_2$
Aluminoferrohornblende	$Ca_2Fe_4^{2+}AlSi_7AlO_{22}(OH)_2$
Kaersutite	$NaCa_2Mg_4TiSi_6Al_2O_{22}(O, OH)_2$
Ferrokaersutite	$NaCa_2Fe_4^{2+}TiSi_6Al_2O_{22}(O, OH)_2$

TABLE 3c. Sodic-Calcic Amphiboles (Monoclinic *C2/m*)

	Formula
Richterite	$NaCaNaMg_5Si_8O_{22}(OH)_2$
Ferrorichterite	$NaCaNaFe_5^{2+}Si_8O_{22}(OH)_2$
Ferriwinchite	$CaNaMg_4Fe^{3+}Si_8O_{22}(OH)_2$
Aluminowinchite	$CaNaMg_4AlSi_8O_{22}(OH)_2$
Ferroaluminowinchite	$CaNaFe_4^{2+}AlSi_8O_{22}(OH)_2$
Ferroferriwinchite	$CaNaFe_4^{2+}Fe^{3+}Si_8O_{22}(OH)_2$
Aluminobarroisite	$CaNaMg_3Al_2Si_7AlO_{22}(OH)_2$
Ferroaluminobarroisite	$CaNaFe_3^{2+}Al_2Si_7AlO_{22}(OH)_2$
Ferribarroisite	$CaNaMg_3Fe_2^{3+}Si_7AlO_{22}(OH)_2$
Ferroferribarroisite	$CaNaFe_3^{2+}Fe_2^{3+}Si_7AlO_{22}(OH)_2$
Magnesioferrikatophorite	$NaCaNaMg_4Fe^{3+}Si_7AlO_{22}(OH)_2$
Magnesioaluminokatophorite	$NaCaNaMg_4AlSi_7AlO_{22}(OH)_2$
Ferrikatophorite	$NaCaNaFe_4^{2+}Fe^{3+}Si_7AlO_{22}(OH)_2$
Aluminokatophorite	$NaCaNaFe_4^{2+}AlSi_7AlO_{22}(OH)_2$
Ferritaramite	$NaCaNaFe_3^{2+}Fe_2^{3+}Si_6Al_2O_{22}(OH)_2$
Magnesioferritaramite	$NaCaNaMg_3Fe_2^{3+}Si_6Al_2O_{22}(OH)_2$
Aluminotaramite	$NaCaNaFe_3^{2+}Al_2Si_6Al_2O_{22}(OH)_2$
Magnesioaluminotaramite	$NaCaNaMg_3Al_2Si_6Al_2O_{22}(OH)_2$

TABLE 3d. Alkali Amphiboles (Monoclinic *C2/m*)

	Formula
Glaucophane	$Na_2Mg_3Al_2Si_8O_{22}(OH)_2$
Ferroglaucophane	$Na_2Fe_3^{2+}Al_2Si_8O_{22}(OH)_2$
Magnesioriebeckite	$Na_2Mg_3Fe_2^{3+}Si_8O_{22}(OH)_2$
Riebeckite	$Na_2Fe_3^{2+}Fe_2^{3+}Si_8O_{22}(OH)_2$
Eckermannite	$NaNa_2Mg_4AlSi_8O_{22}(OH)_2$
Ferroeckermannite	$NaNa_2Fe_4^{2+}AlSi_8O_{22}(OH)_2$
Magnesioarfvedsonite	$NaNa_2Mg_4Fe^{3+}Si_8O_{22}(OH)_2$
Arfvedsonite	$NaNa_2Fe_4^{2+}Fe^{3+}Si_8O_{22}(OH)_2$
Nyboite	$NaNa_2Mg_3Al_2Si_7AlO_{22}(OH)_2$
Kozulite	$NaNa_2Mn_4(Fe^{3+}, Al)Si_8O_{22}(OH)_2$

TABLE 3e. Recommended Prefixes for Amphibole Names

	Condition
Chlor	Cl ≥ 1.00 (about 4% Cl)
Chromium	Cr ≥ 1.00 (about 9% Cr_2O_3)
Chromian	Cr = 0.25–0.99 (about 2.3–9% Cr_2O_3)
Ferri	Fe^{3+} ≥ 1.00 (about 9% Fe_2O_3) except in alkali amphiboles and hastingsite
Ferrian	Fe^{3+} = 0.75–0.99 (about 6.8–9% Fe_2O_3) except in alkali amphiboles and hastingsite
Fluor	F ≥ 1.00 (about 2% F)
Hydro	OH ≥ 3.00 (about 3% H_2O)
Lithian*	Li ≥ 0.25 (about 0.4% Li_2O) except in the alkali amphiboles, where Li ≥ 0.50
Manganese	Mn ≥ 1.00 (about 10% MnO) except in end-members containing Mn

*Not used with holmquistite and clinoholmquistite.

Fe^{3+}, Al, Li, and occasionally Ti and Cr. The tetrahedral sites (Z) are occupied principally by Si and Al. Fluorine and, less commonly, Cl, S, and O may substitute for OH^-. Ideal end-member compositions of selected micas are presented in Table 5*a* from *Bailey* [1984].

Much of the following discussion is from *Papike and Cameron* [1976]. Micas in which two thirds of the octahedral sites are filled (usually by triply charged Y cations) are termed dioctahedral, whereas those in which all octahedral sites are filled (usually by three doubly charged cations) are termed trioctahedral. If X is monovalent (usually K, Na), the mineral is a common or true mica; if X is divalent (Ca), it is a brittle mica.

A basic feature of the mica structure is sheets of hexagonal or pseudohexagonal rings of tetrahedra stacked along the *c* direction. The tetrahedra within one sheet all point in the same direction, and two tetrahedral sheets point inward and are cross-linked by octahedrally coordinated cations, e.g., aluminum in muscovite. In order to maintain octahedral coordination the upper tetrahedral sheet is staggered by $\sim a/3$ (Figure 3*a*) in either a positive or a negative direction along any of the three pseudohexagonal axes (six possible directions). Although this stagger reduces the symmetry within each T-O-T subcell to monoclinic, it does not affect the hexagonal or pseudohexagonal local symmetry of the surfaces of the subcells. The centers of the hexagonal rings of adjacent subcells superimpose directly. The X cations, which are necessary for charge balance, occur between these T-O-T units (Figures 3*a* and 3*b*). For further details of specific mica structures the reader is referred to *Bailey* [1984].

The configuration of the octahedral sheet is determined, in large part, by the distribution and valence of cations within the sheet. In dioctahedral micas the octahedrally coordinated vacancies (M1 site) are ordered, and the triply charged cations (M2 site) are arranged in hexagons around each vacant site (Figure 3*c*). Structural adjustment occurs because of cation repulsion and involves the moving apart of adjacent cations. Concomitant movement of the anions on shared edges toward one another shortens each shared edge. These structural adjustments produce (1) thinning of the octahedral sheet along the sheet normal and expansion laterally within the sheet and (2) distortion of the hexagonal pattern of the anions by alternate clockwise and counterclockwise twisting of two thirds of the octahedral edges.

In trioctahedral micas the cations are doubly charged, and thus lateral cation repulsion is less. In addition, each anion is now pulled in three directions along three shared edges. Because the direction of their movement is limited, shared edges are only slightly shorter than unshared edges, and the octahedra do not have twisted edges.

In structures where the octahedral sheet is smaller than the tetrahedral sheet, the latter is reduced in size by rotation of

TABLE 3f. Selected Amphibole Unit Cell Data

Amphibole	Space Group	*a*, Å	*b*, Å	*c*, Å	β, deg	*Z**
Tremolite [*Papike et al.*, 1969]	*C2/m*	9.82	18.05	5.28	104.6	2
Grunerite [*Finger*, 1969]	*C2/m*	9.56	18.39	5.34	101.89	2
Primitive cummingtonite [*Papike et al.*, 1969]	$P2_1/m$	9.55	18.01	5.30	102.65	2
Gedrite [*Papike and Ross*, 1970]	*Pnma*	18.53	17.74	5.25	90	4
Protoamphibole [*Gibbs*, 1969]	*Pnmn*	9.33	17.88	5.29	90	2

*Number of formula units per unit cell.

TABLE 3*g*. Amphibole Analyses

	Fe-Mg-Mn Group				Calcic Group				Sodic-Calcic Group		Alkali Group		
	Sample 1 (DHZ217-8)	Sample 2 (DHZ218-2)	Sample 3 (DHZ231-2)	Sample 4 (DHZ237-7)	Sample 5 (DHZ252-10)	Sample 6 (DHZ275-6)	Sample 7 (DHZ281-35)	Sample 8 (DHZ288-14)	Sample 9 (DHZ354-5)	Sample 10 (DHZ360-2)	Sample 11 (DHZ336-1)	Sample 12 (DHZ337-8)	Sample 13 (DHZ366-1)
						Major Oxides							
SiO_2	55.34	45.50	59.58	50.78	51.60	52.78	41.32	40.14	56.74	46.87	57.73	54.56	58.65
Al_2O_3	2.56	17.64	7.19	1.77	2.35	5.77	11.19	13.92	0.71	7.97	12.04	8.29	5.98
Fe_2O_3		2.16	9.35	1.88	2.60	2.45	9.34	6.49	4.71	5.52	1.16	7.94	2.37
TiO_2		0.23		0.40	0.50	0.43	0.02	1.98	0.28	1.03		0.23	
MgO	22.80	20.51	11.66	11.83	12.91	17.43	7.94	10.94	21.95	13.22	13.02	8.74	18.56
FeO	15.29	9.04	4.88	29.64	15.21	6.61	15.83	9.56	0.87	8.57	5.41	10.31	1.34
MnO	0.51	0.16	0.41	0.14	0.20	0.17	0.28	0.26	0.07	1.18		0.13	
CaO	0.63	0.87	0.06	1.33	10.97	11.90	10.24	11.93	6.15	7.69	1.04	0.81	1.40
Li_2O			3.54										
Na_2O	0.19	1.73	0.50	0.00	0.91	0.68	1.33	2.01	5.15	4.46	6.98	6.71	9.30
K_2O	0.12	0.00	0.27	0.00	0.53	0.07	0.29	0.79	1.80	1.75	0.68	0.14	1.10
F		0.02	0.21			0.01		0.22	1.30				
H_2O^+	2.34	2.12	2.23	2.01	2.05	2.10	1.89	1.83	0.87	1.87	2.27	2.18	2.20
Total	99.78	99.98	99.88	99.78	99.83	100.40	99.67	100.07	100.6	100.13	100.33	100.04	100.90
Minus O = F		0.07	0.10			0.01		0.09	0.54				
New total	99.78	99.91	99.78	99.78	99.83	100.39	99.67	99.98	100.06	100.13	100.33	100.04	100.90
						Number of Ions Based on 24 (O, OH, F, Cl)							
Si	7.759	6.313	7.951	7.708	7.598	7.393	6.314	5.968	7.920	6.885	7.789	7.722	7.912
Al	0.241	1.687	0.049	0.292	0.402	0.607	1.686	2.032	0.080	1.115	0.211	0.278	0.088
Σ tetrahedra	8.000	8.000	8.000	8.000	8.000	8.000	8.000	8.000	8.000	8.000	8.000	8.000	8.000
Al	0.181	1.197	1.081	0.025	0.005	0.345	0.330	0.408	0.037	0.265	1.704	1.105	0.864
Fe^{3+}		0.224	0.938	0.215	0.288	0.258	1.074	0.726	0.495	0.609	0.118	0.845	0.240
Ti		0.024		0.046	0.056	0.045	0.002	0.222	0.029	0.114		0.025	
Mg	4.765	3.555	2.319	2.676	2.833	3.639	1.808	2.424	4.439	2.894	2.618	1.844	3.732
Fe^{2+}	0.054		0.544	2.038	1.873	0.713	1.786	1.189		1.053	0.56	1.181	0.151
Mn^{2+}			0.046		0.025			0.031		0.065			
Li			0.072										
Σ M1, M2, M3 sites	5.000	5.000	5.000	5.000	5.080	5.000	5.000	5.000	5.000	5.000	5.000	5.000	4.987
Mg		0.686							0.127				
Fe^{2+}	1.739	1.049		1.726		0.061	0.237		0.102		0.051	0.039	
Mn^{2+}	0.061	0.018		0.018		0.020	0.036	0.002	0.008	0.082		0.015	
Ca	0.094	0.129	0.009	0.216	1.731	1.786	1.677	1.901	0.920	1.210	0.150	0.122	0.203
Li			1.828										
Na	0.052	0.118	0.130		0.260	0.133	0.050	0.097	0.843	0.708	1.799	1.824	1.797
Σ M4 site	1.946	2.000	1.967	1.960	1.991	2.000	2.000	2.000	2.000	2.000	2.000	2.000	2.000
Na		0.348				0.052	0.392	0.481	0.551	0.563	0.027	0.016	0.635
K	0.022	0.000	0.046		0.098	0.012	0.056	0.150	0.319	0.327	0.117	0.025	0.190
Σ A site	0.022	0.348	0.046	0.000		0.064	0.448	0.631	0.870	0.890	0.144	0.041	0.825
F		0.008	0.088			0.007		0.104	0.574				
OH	2.190	1.962	1.986	2.036	2.014	1.962	1.926	1.816	0.810	1.832	2.043	2.058	1.980
Σ O3 site	2.190	1.970	2.074	2.036	2.014	1.969	1.926	1.920	1.384	1.832	2.043	2.058	1.980

All analyses are from *Deer et al.* [1963*a*]; for example, DHZ217-8 refers to page 217, column 8 of Deer et al. Following are the names according to the IMA classification: (1) anthophyllite, (2) gedrite, (3) magnesioholmquistite, (4) cummingtonite, (5) actinolite, (6) actinolitic hornblende, (7) ferrotschermakitic hornblende, (8) magnesian hastingsite, (9) richterite, (10) magnesiokatophorite, (11) glaucophane, (12) crossite, and (13) eckermannite.

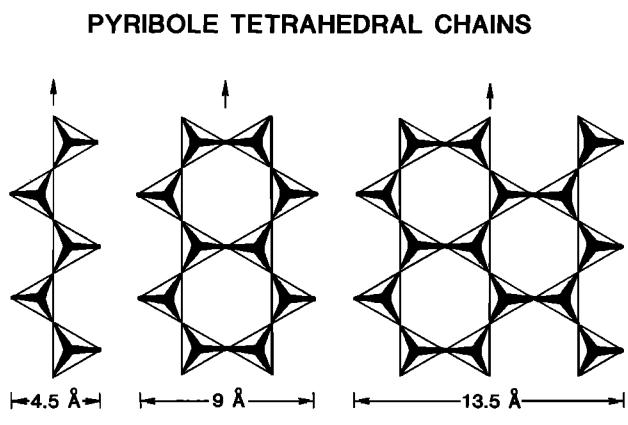

Fig. 2*a*. Pyribole tetrahedral chains [after *Veblen et al.*, 1977].

the tetrahedra about an axis normal to the sheet. Clockwise and counterclockwise rotations of alternate tetrahedra reduce the lateral dimensions of the sheet and change the shape of the six-membered tetrahedral rings from hexagonal to ditrigonal (Figure 3*c*).

Because the surface symmetry of the mica subcells is hexagonal or pseudohexagonal, it is possible to rotate each subcell by 60° increments without affecting the packing at the surfaces of the units. These six possible rotations of the $a/3$ stagger produce various layer stacking sequences, or polytypes.

The stagger within the subcell can be represented by an interlayer vector of projected magnitude $a/3$ drawn from the center of the hexagonal ring in the lower tetrahedral sheet to the center of the ring in the upper tetrahedral sheet. The angle between two interlayer vectors, as projected onto the (001) plane and measured in a counterclockwise direction, is called the interlayer stacking angle. In an experimental and theoretical study of mica polymorphs, *Smith and Yoder* [1956] determined that there are six different stacking sequences (Figure 3*d*) that can be formed if only one interlayer stacking angle is present in each crystal. Figure 3*d* also presents some of the space group and unit cell dimension data for specific polytypes. Table 5*b* [*Bailey*, 1984] documents the natural occurrence of mica polytypes.

Unfortunately, the classification and nomenclature for micas has not been developed to the extent that it has for amphiboles. Nevertheless, a good start at classifying lithium and related micas has been made. The classification, reviewed in some detail by *Černý and Burt* [1984], uses exchange operators (isomorphic substitutions) that are important in micas, e.g., KNa_{-1}, $FeMg_{-1}$, and $F(OH)_{-1}$. The condensed composition polyhedron is illustrated in Figure 3*e*. Three exchange operators are used in the classification: $LiAlFe^{2+}{}_{-2}$, $Fe^{2+}SiAl_{-2}$, and $\square\ Al_2Fe^{2+}{}_{-3}$. The end-members considered in this polyhedron are siderophyllite (Sdp), synthetic mica (Synth), ephesite (Kep), annite (Ann), protolithionite (Pro), zinnwaldite (Znw), trilithionite (Tri), muscovite (Mus), phengite (Phn), celadonite (Cld), montdorite (Mtd), taeniolite (Fet), and polylithionite (Ply). Note that end-members are represented as two of the standard formula units, e.g., muscovite is represented by $K_2{}^{VI}(Al_4)^{IV}(Si_6Al_2)O_{20}(OH, F)_4$. More detailed slices through this compositional polyhedron are illustrated in Figures 3*f*–3*i*. Figure 3*f* represents the basal plane of the polyhedron (Li-free micas). Figure 3*g* represents the large front face (reversed), which includes Fe-free micas. Figure 3*h* represents the large back face (reversed), which includes trioctahedral micas (zero octahedral vacancies). Figure 3*i* represents the right side of the polyhedron and includes the tetrasilicic micas (tetrahedral silicon is equal to four atoms per formula unit or eight atoms per two formula units).

Table 5*c* presents some representative chemical analyses of micas taken from *Deer et al.* [1962]. I recommend that the microprobe data be reduced by normalization to 11 oxygens or 22 negative charges, i.e., $O_{10}(OH, F, Cl)_2$. However, this assumes no oxycomponent. I also recommend that Fe^{2+}/Fe^{3+} be determined directly. Checks for good analyses are few because of the possibility of vacancies at all but the tetrahedral positions and because of solid solution between dioctahedral and trioctahedral micas. However, the sum of Si, Al, and Fe^{3+} should be greater than or equal to four, with Si less than or equal to four (the number of tetrahedral sites per formula unit), that of the octahedral cations should be less than or equal to three and that of the X cations should be less than or equal to one.

PYROPHYLLITE-TALC

Pyrophyllite, $Al_2Si_4O_{10}(OH)_2$, crystallizes as a one-layer triclinic polytype 1 *Tc* in space group $C\bar{1}$ ($a = 5.16$ Å, $b = 8.97$ Å, $c = 9.35$ Å, $\alpha = 91.2°$, $\beta = 100.5°$, $\gamma = 89.6°$, and $Z = 2$ [*Lee and Guggenheim*, 1981]). The crystal structure (schematic) is

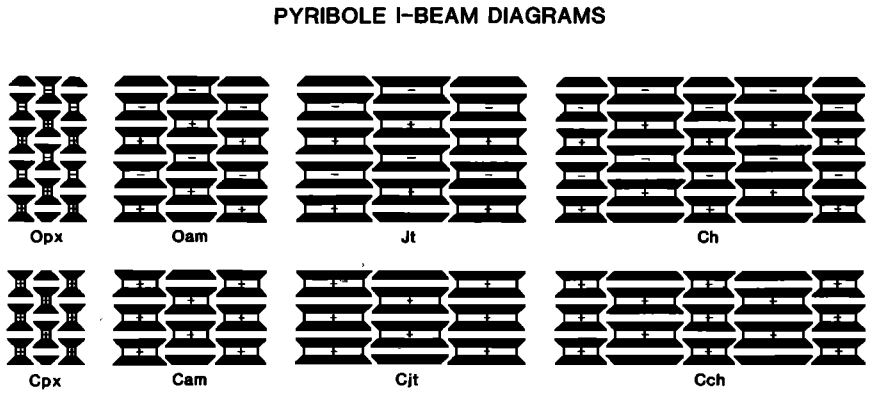

Fig. 2*b*. Pyribole I beam diagrams [after *Veblen et al.*, 1977] comparing pyroxene (Opx and Cpx), amphibole (Oam and Cam), jimthompsonite (Jt and Cjt), and chesterite (Ch and Cch).

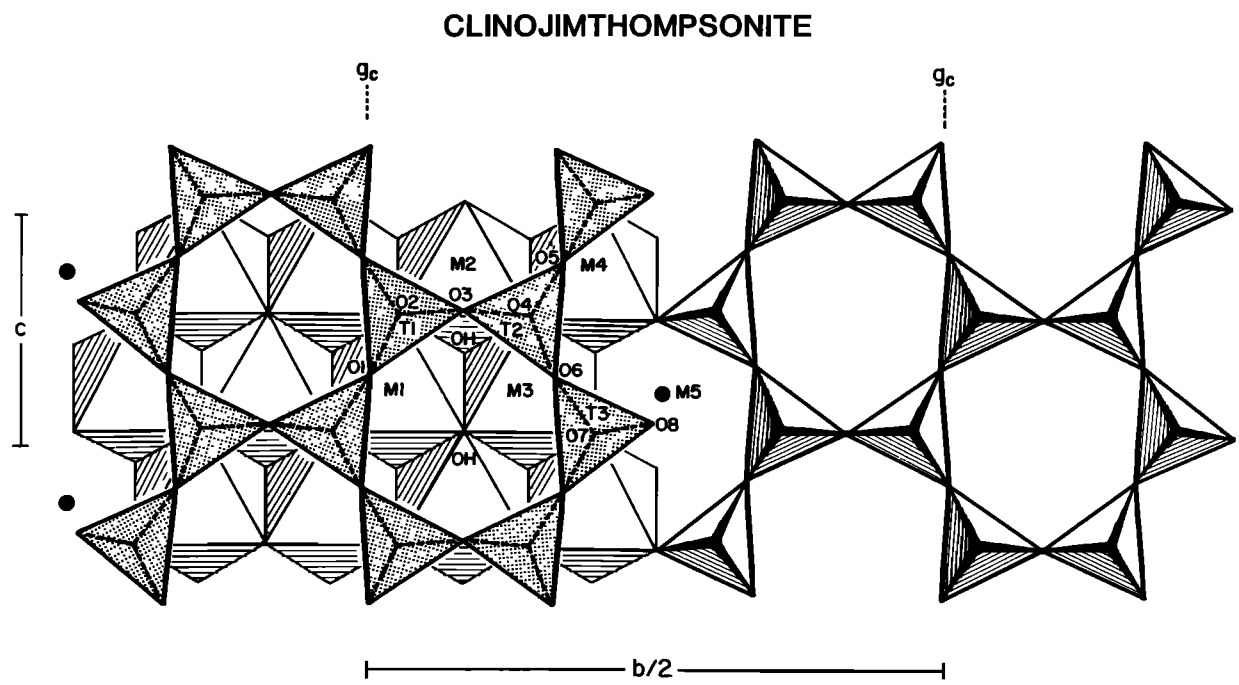

Fig. 2*c*. Crystal structure of clinojimthompsonite projected onto (100) [after *Veblen and Burnham*, 1978*b*].

illustrated in Figure 4. Pyrophyllite has a layered structure similar to that of the micas, in which an octahedral sheet is sandwiched between two tetrahedral sheets (T-O-T unit). The structure is dioctahedral with two thirds of the available octahedral sites occupied by aluminum. The positions of the (OH^-) groups are indicated by solid circles, and the oxygen ligands are indicated by open circles. In ideal end-member pyrophyllite, each T-O-T unit is electrically neutral, and therefore the bonding (Van der Waals') between the layers is weak, accounting for the highly flexible nature of the structure.

A detailed and precise refinement of a one-layer triclinic polytype (1 *Tc*) of pyrophyllite was reported by *Lee and Guggenheim* [1981]. *Rayner and Brown* [1964] studied a partially disordered pyrophyllite 2 *M* single crystal, and powder data were analyzed for 1 *Tc* pyrophyllite by *Wardle and Brindley* [1972]. However, the first study to be carried out on well-

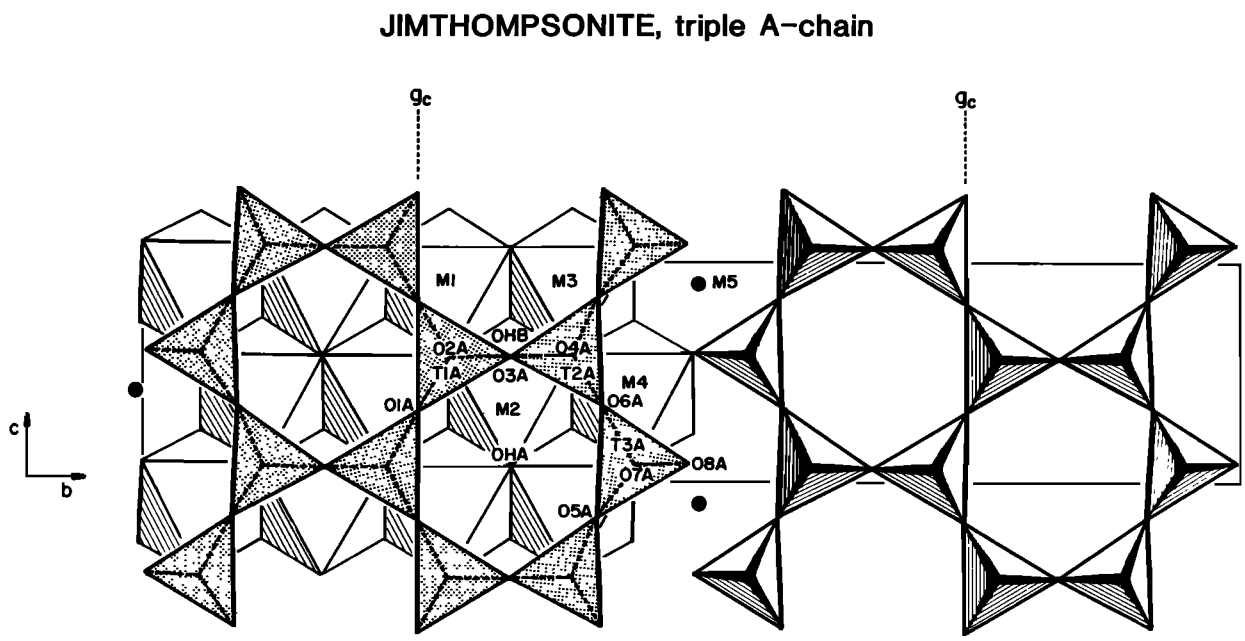

Fig. 2*d*. Crystal structure of jimthompsonite projected onto (100). The *c* glide is labeled as g_c [after *Veblen and Burnham*, 1978*b*].

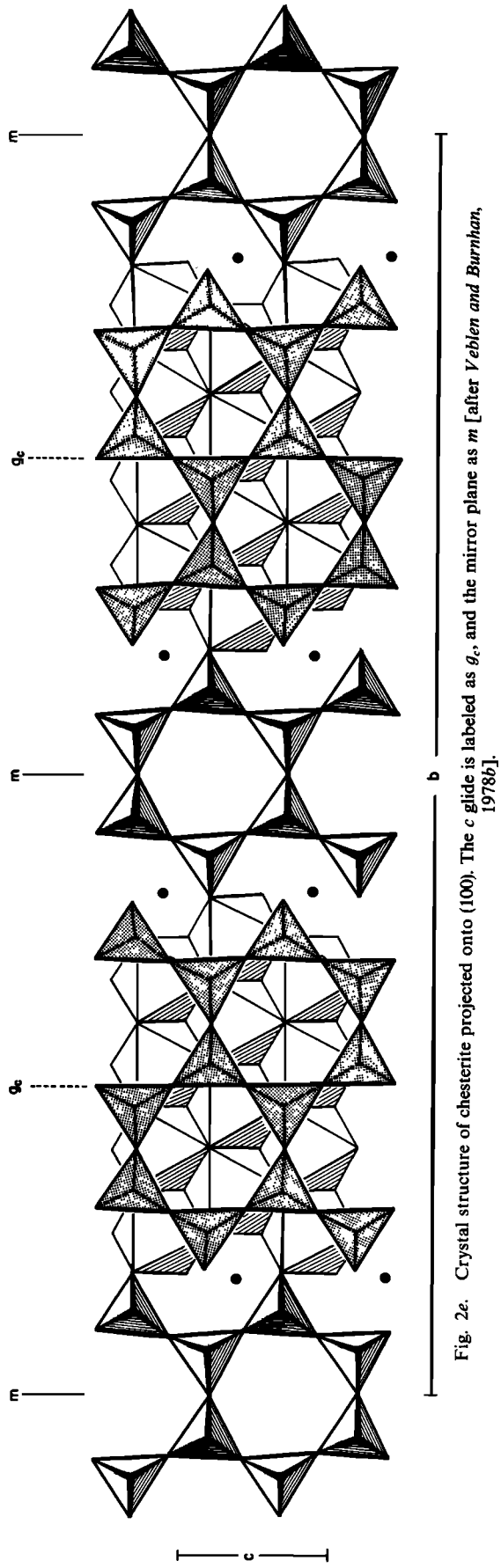

Fig. 2e. Crystal structure of chesterite projected onto (100). The c glide is labeled as g_c, and the mirror plane as m [after *Veblen and Burnham*, 1978*b*].

crystallized material was that by *Lee and Guggenheim* [1981].

Pyrophyllite shows little deviation from the ideal formula [*Deer et al.*, 1962]. Slight substitution of Al for Si at the tetrahedral sites and of Mg, Fe^{2+}, Fe^{3+}, for Al at the octahedral sites may occur. Small amounts of K, Na, and Ca also can occur at the interlayer site to compensate for small amounts of tetrahedral Al. Because adsorbed water may cause problems in the determination of H_2O, the formula for pyrophyllite is commonly calculated on the basis of 11 oxygen (22 negative charges equivalent to 10 oxygens plus two OH^- groups). Table 6 presents two pyrophyllite analyses calculated in this manner. Microprobe data should also be reduced on the basis of an 11-oxygen normalization. Good, near-end-member formulae will have Si approximately equal to four and ^{VI}Al approximately equal to two.

Talc, $Mg_3Si_4O_{10}(OH)_2$, crystallizes predominantly as a one-layer triclinic polytype 1 *Tc* in space group $C\bar{1}$, with $a = 5.29$ Å, $b = 5.30$ Å, $c = 9.47$ Å, $\alpha = 86.1°$, $\beta = 98.9°$, $\gamma = 120.0°$, and $Z = 2$ [*Rayner and Brown*, 1973]. The crystal structure of talc was first determined by *Gruner* [1934]. *Rayner and Brown* [1973] provided a detailed structure analysis of a 1 *Tc* talc, and the structures was further refined by *Perdikatsis and Burzlaff* [1981].

The structure of talc is very similar to that of pyrophyllite (Figure 4) except that it is trioctahedral with all of the octahedral sites occupied by magnesium. There is little variation in the chemical composition of talc [*Deer et al.*, 1962]. However, small amounts of Al may substitute for silicon, and small amounts of Fe^{2+}, Fe^{3+}, Mn, and Al may replace Mg in octahedral coordination. Also, small amounts of Na, K, and Ca may occur at the interlayer site to charge-compensate for tetrahedral Al. Because of problems with accurate determination of H_2O, chemical formulae should be calculated (as for pyrophyllite) on an 11-oxygen normalization basis. Table 6 gives two representative talc analyses. Near-end-member analyses should give formulae with Si approximately equal to four and Mg (plus slight Fe, etc.) approximately equal to three.

CHLORITE

Chlorite, $(\square, Mg, Fe^{2+}, Al, Fe^{3+})_6(Si, Al)_4O_{10}(OH)_8$, crystallizes in a number of space groups with numerous ordered polytypes of great complexity [e.g., *Bailey*, 1975]. However, discussion of details of structural variability and polytype systematics, though interesting, is beyond the scope of this paper. A common polytype crystallizes in monoclinic space group $C2/m$, with $a \sim 5.3$ Å, $b \sim 9.2$ Å, $c \sim 14.3$ Å, $\beta \sim 97°$, and $Z = 2$ [*Deer et al.*, 1962], and this will be the structure type used for reference here. The structure with a 14-Å repeat is composed of a T-O-T unit (talc-like layer, ideally an Mg_3, trioctahedral) alternating with an $Mg_3(OH)_6$, trioctahedral, brucite-like sheet. Figure 5 illustrates aspects of the structure and distinguishes OH (solid circles) and oxygen (open circles) ligands. The basic features of the structure were first described by Pauling [1930*b*], and since then, numerous structure determinations and refinements have been reported (see *Bailey*, [1975] for an excellent review). Many classifications have been proposed for chlorite (they are reviewed by *Bailey* [1975]); see, for example, the one presented by *Foster* [1962]. The classification reported by Foster is based on two series of ionic replacements: (1) replacement of Mg by Fe^{2+} and (2) replacement of tetrahedral and octahedral Al by Si and Mg, respec-

TABLE 4*a*. Cell Parameters and Space Groups of Low-Calcium Chain Silicates, Chester, Vermont

	Space Group	*a*, Å	*b*, Å	*c*, Å	β, deg	V, Å^3	*Z**
			Orthorhombic				
Jimthompsonite	*Pbca*	18.6263(3)	27.2303(6)	5.2970(3)		2686.6(2)	4[(Mg, Fe)$_{10}$Si$_{12}$O$_{32}$(OH)$_4$]
Chesterite	$A2_1ma$	18.6140(3)	45.306(1)	5.2966(3)		4466.8(3)	4[(Mg, Fe)$_{17}$Si$_{20}$O$_{54}$(OH)$_6$]
			Monoclinic				
Clinojimthompsonite	*C2/c*	9.874(4)	27.24(3)	5.316(3)	109.47(3)	1347(3)	2[(Mg, Fe)$_{10}$Si$_{12}$O$_{32}$(OH)$_4$]
Clinochesterite	*A2/m*, *Am*, or *A2*	9.867	45.31	5.292	109.7	2227	2[(Mg, Fe)$_{17}$Si$_{20}$O$_{54}$(OH)$_6$]

Numbers in parentheses are standard deviations.
*Number of formula units per unit cell.

tively. Divisions with respect to Fe^{2+}/R^{2+}, where R^{2+} = Mg + Fe^{2+} + Mn^{2+}, are placed at 0.25 and 0.75, thus defining three categories in terms of Mg, Fe^{2+} as magnesian, intermediate, and ferroan chlorites. These categories are further subdivided according to Si at 2.75 and 3.10 Si per formula unit. The limits of variation for silicon found since the Foster study are 2.25–3.60 Si per four tetrahedral sites. Eight chlorite analyses [*Bailey*, 1975] corresponding to this range of composition are presented in Table 7. However, the IMA commission on mineral names has now approved the simplified nomenclature of *Bayliss* [1975] for trioctahedral chlorites. The end-member compositions in this classification are clinochlore, $(Mg_5Al)(Si_3Al)O_{10}(OH)_8$; chamosite, $(Fe_5^{2+}Al)(Si_3Al)(OH)_8$; nimite, $(Ni_5Al)(Si_3Al)O_{10}(OH)_8$; and pennantite, $(Mn, Al)_6(Si, Al)_4O_{10}(OH)_8$. Trioctahedral chlorite (which is by far the most common chlorite) is composed of talc-like T-O-T layers of composition $(R^{2+}, R^{3+})_3(Si_{4-x}Al_x)O_{10}(OH)_2$ that alternate with octahedral brucite-like sheets of composition $(R^{2+}, R^{3+})_3(OH)_6$, where R^{3+} is Al, Fe^{3+}, Cr^{3+}. Chromium can be quite abundant in chlorites (e.g., Cr_2O_3 is approximately 3.5 wt % [*Bailey*, 1975]), but these chromium varieties will not be considered in this paper. The tetrahedral sheets in the T-O-T units have a negative charge because of the substitution of Al (less commonly Fe^{3+}, Cr^{3+}) for Si, whereas the brucite sheet has a positive charge because of the substitution of R^{3+} for R^{2+} cations. Ni, Mn, V, Cu, and Li can also substitute in the octahedral sheets. *Foster* [1962] showed that if the total number of the trivalent octahedral cations is equal to tetrahedral Al, the octahedral occupancy is close to six cations per formula unit. However, if the total number of trivalent octahedral cations is greater than the number of tetrahedral cations, the total octahedral occupancy is less than six by an amount equal to one half the excess of the octahedral trivalent cations over tetrahedral Al. This reflects the additional charge balance mechanism $^{VI}\square \leftrightarrows {}^{VI}2R^{3+}$, in which each substitution of R^{3+} for R^{2+} in octahedral coordination causes a charge excess of 1^+, whereas each vacancy substitution for R^{2+} causes a charge deficiency of 2^-. Mg-Fe^{2+} substitution in

TABLE 4*b*. Pyribole Analyses

	Anthophyllite	Chesterite	Jimthompsonite	Clinojimthompsonite
		Major Oxides		
SiO_2	56.55	57.95	57.78	58.55
Al_2O_3	0.24	0.25	0.29	0.37
MgO	23.44	24.24	25.14	24.93
FeO*	16.03	14.14	12.22	12.13
MnO	1.15	0.99	0.72	0.73
CaO	0.50	0.42	0.38	0.50
Na_2O	0.04	0.03	0.12	0.10
H_2O†	2.12	2.60	2.92	2.93
Total	100.07	100.62	99.57	100.24
		Number of Ions‡		
Si	7.96	19.94	11.91	11.97
Al	0.04	0.05	0.07	0.03
Σ tetrahedral sites	8.00	19.99	11.98	12.00
Al	0.00	0.00	0.00	0.05
Mg	4.92	12.43	7.73	7.59
Fe^{2+}	1.89	4.07	2.11	2.07
Mn	0.14	0.29	0.13	0.13
Ca	0.08	0.16	0.08	0.11
Σ octahedral sites	7.03	16.95	10.05	9.95
Na(A-site)	0.01	0.02	0.05	0.04

Analyses are from *Veblen and Burnham* [1978*a*].
*All iron calculated as Fe^{2+}.
†Amount of water calculated by assuming that all OH sites are filled with OH^-.
‡Number of ions based on 23 oxygens for anthophyllite, 57 for chesterite, and 34 for jimthompsonite and clinojimthompsonite.

TABLE 5a. Classification of the Micas

Subgroup, Species	Ideal Formula Units
	*True Micas**
Trioctahedral	
phlogopite	$KMg_3(Si_3Al)O_{10}(OH, F)_2$
biotite	$K(Mg_{0.6-1.8}Fe_{2.4-1.2})(Si_3Al)O_{10}(OH, F)_2$
annite	$KFe_3^{2+}(Si_3Al)O_{10}(OH, F)_2$
ferriannite	$KFe_3^{2+}(Si_3Fe^{3+})O_{10}(OH, F)_2$
polylithionite	$K(Li_2Al)Si_4O_{10}(F, OH)_2$
trilithionite	$K(Li_{1.5}Al_{1.5})(Si_3Al)O_{10}(F, OH)_2$
taeniolite	$K(Mg_2Li)Si_4O_{10}(F, OH)_2$
zinnwaldite	$K[Fe_{1.5-0.5}^{2+}Li_{0.5-1.5}(Al, Fe^{3+})](Si_{3.5-2.5}Al_{0.5-1.5})O_{10}(F, OH)_2$
masutomilite	$K(Mn_{1.0-0.5}^{2+}Li_{1.0-1.5}Al)(Si_{3.5-3.0}Al_{0.5-1.0})O_{10}(F, OH)_2$
hendricksite	$K(Zn, Mn)_3(Si_3Al)O_{10}(OH, F)_2$
sodium phlogopite	$NaMg_3(Si_3Al)O_{10}(OH)_2$
wonesite	$[(Na, K)_{0.5}\square_{0.5}][(Mg, Fe)_{2.5}Al_{0.5}](Si_3Al)O_{10}(OH, F)_2$
siderophyllite	$K(Fe_2^{2+}Al)(Si_2Al_2)O_{10}(OH, F)_2$
ephesite	$Na(LiAl_2)(Si_2Al_2)O_{10}(OH, F)_2$
preiswerkite	$Na(Mg_2Al)(Si_2Al_2)O_{10}(OH)_2$
montdorite	$K(Fe^{2+}, Mn, Mg)_{2.5}Si_4O_{10}(F, OH)_2$
Dioctahedral	
muscovite	$KAl_2(Si_3Al)O_{10}(OH, F)_2$
paragonite	$NaAl_2(Si_3Al)O_{10}(OH, F)_2$
phengite	$K[Al_{1.5}(Mg, Fe^{2+})_{0.5}](Si_{3.5}Al_{0.5})O_{10}(OH, F)_2$
illite	$\sim K_{0.75}(Al_{1.75}R_{0.25}^{2+})(Si_{3.50}Al_{0.50})O_{10}(OH, F)_2$
chernykhite	$(Ba, Na, NH_4)(V^{3+}, Al)_2(Si, Al)_4O_{10}(OH)_2$
roscoelite	$K(V^{3+}, Al, Mg)_2(Si_3Al)O_{10}(OH)_2$
celadonite	$K(Mg, Fe^{2+})(Fe^{3+}, Al)Si_4O_{10}(OH)_2$
glauconite	$\sim K(R_{1.33}^{3+}R_{0.67}^{2+})(Si_{3.67}Al_{0.33})O_{10}(OH)_2$
tobelite	$(NH_4, K)Al_2(Si_3Al)O_{10}(OH)_2$
	Brittle Micas†
Trioctahedral	
clintonite	$Ca(Mg_2Al)(SiAl_3)O_{10}(OH, F)_2$
kinoshitalite	$Ba(Mg, Mn, Al)_3(Si_2Al_2)O_{10}(OH, F)_2$
anandite	$BaFe_3^{2+}(Si_3Fe^{3+})O_{10}(OH)S$
bityite	$Ca(Al_2Li)(Si_2AlBe)O_{10}(OH, F)_2$
Dioctahedral	
margarite	$CaAl_2(Si_2Al_2)O_{10}(OH, F)_2$

*X is a monovalent cation.
†X is a divalent cation.

chlorites can be complete. Foster's study showed that whereas most chlorites have H_2O contents reflecting the ideal eight (OH) groups per formula unit, some analyses indicated less than eight suggesting an oxycomponent. Despite this observation, microprobe data will normally be reduced assuming eight (OH) groups. In addition to trioctahedral chlorites a few examples of dioctahedral chlorites [*Bailey*, 1975] have been reported. However, these will not be discussed further here.

Microprobe analyses for chlorite should be reduced on a 14-oxygen (assumes 10 oxygen plus eight (OH), or 28 negative charges) basis, realizing that this ignores a possible oxycomponent. I strongly suggest that a direct determination of Fe^{3+} [e.g., *Goldich*, 1984] be made because Fe^{3+} substitution in chlorite can be significant. There are few firm criteria for assessing the accuracy of chlorite microprobe analyses. The sums will be low (~88%) because of the lack of an H_2O determination. However, for most good (approximately trioctahedral) analyses the octahedral occupancy will vary between 5.5 and 6.0 atoms per formula unit (apfu), and silicon will fall in the range 2.25–3.60 apfu.

GREENALITE

Greenalite, $(Fe, Mg, Mn)_{2.73-2.85}Si_{2.06-2.13}O_5(OH)_4$, is a complex iron silicate with a modulated layer structure composed of tetrahedral-octahedral (T-O) units somewhat analogous to that of antigorite, $Mg_{3-x}Si_2O_5(OH)_{4-2x}$, but with some significant differences. *Gruner* [1936] suggested that greenalite was the ferroan iron analogue of serpentine (antigorite). However, *Floran and Papike* [1975] found that electron microprobe data for greenalite deviated from antigorite stoichiometry by having excess silicon (greater than 2.0) and deficient octahedral occupancy (less than 3.0) when the formula was calculated on the basis of seven oxygens (14 negative charges equivalent to $O_5(OH)_4$). Floran and Papike suggested that modulations involving tetrahedral inversions could explain the observed chemical compositions.

The most detailed structural study of greenalite [*Guggenheim et al.*, 1982] reported new information about this important silicate but did not come up with a complete structural solution. Guggenheim et al. found that greenalite is not just an analogue of serpentine but that it is composed of a mixture of both a trigonal and a monoclinic phase. This is also true for the Mn analogue of greenalite, caryopilite. Satellites present on electron diffraction photographs indicated a modulation of the structure that ranged from 23 Å in greenalite to 17 Å in

TABLE 5b. Observed Natural Mica Structures

Species	Abundance		
	High	Medium	Low
	Trioctahedral Micas		
Phlogopite	1*M*, 1*Md*	3*T*	$2M_1$
Manganoan phlogopite	1*M*	$2M_1$	
Sodium phlogopite	1*M*		
Biotite	1*M*, 1*Md*	3*T*	$2M_1$
Annite	1*M*		
Ferriannite	1*M*		
"Lepidolite"	1*M*, $2M_2$	3*T*	$2M_1$
Taeniolite	1*M*, 3*T*	$2M_1$	
Zinnwaldite	1*M*, 1*Md*	$2M_1$, 3*T*	
Masutomilite	1*M*	$2M_1$	
Hendricksite	1*M*	$2M_1$	3*T*
Wonesite	1*Md*		
Preiswerkite	$2M_1$		
Siderophyllite	1*M*		
Ephesite	$2M_1$	1*M*	
Clintonite	1*M*		3*T*, $2M_1$
Anandite	2*Or*	$2M_1$, 1*M*	
Kinoshitalite	1*M*, $2M_1$		
Bityite	$2M_1$		
	Dioctahedral Micas		
Muscovite	$2M_1$	1*M*, 1*Md*	3*T*
Paragonite	$2M_1$	3*T*	
Lithian muscovite	$2M_1$		
Manganian muscovite	$2M_1$, 3*T*	1*M*	
Chromian muscovite	$2M_1$, 1*M*		
Phengite	1*M*, 1*Md*, 3*T*	$2M_1$	$2M_2$
Roscoelite	1*M*		
Chernykhite	$2M_1$		
Tobelite	1*M*, $2M_1$		
Illite	1*M*, 1*Md*		3*T*
Glauconite	1*M*, 1*Md*		
Celadonite	1*M*, 1*Md*		
Margarite	$2M_1$		

TABLE 5c. Mica Analyses

	Muscovite		Paragonite	Phlogopite	Biotite			Lepidolite	Margarite
	Sample 1 (DHZ16-1)	Sample 2 (DHZ16-2)	Sample 3 (DHZ33-3)	Sample 4 (DHZ46-1)	Sample 5 (DHZ59-8)	Sample 6 (DHZ60-15)	Sample 7 (DHZ63-9)	Sample 8 (DHZ88-4)	(Sample 9 (DHZ97-3)
				Major Oxides					
SiO_2	45.87	45.24	44.41	42.70	37.88	37.01	35.42	48.98	30.84
Al_2O_3	38.69	36.85	40.09	12.21	12.87	15.89	19.04	22.21	50.76
Fe_2O_3		0.09	1.72	0.06	4.86		2.70	1.55	0.12
TiO_2		0.01	0.22		0.62	0.02	3.15	0.00	
MgO	0.10	0.08	0.16	28.58	8.22	0.22	9.56	0.03	0.35
FeO		0.02	0.28		21.03	30.16	16.11	1.52	0.35
MnO		0.12	0.02		0.88	1.01	0.25	0.75	0.11
CaO		0.00	0.67			0.10	0.24	0.10	10.52
Li_2O		0.49				1.01		4.99	0.23
Na_2O	0.64	0.64	5.80	0.06	1.53	0.58	0.40	0.53	1.68
K_2O	10.08	10.08	2.22	10.92	8.65	9.02	9.30	8.62	0.32
Rb_2O		0.93				0.19		3.80	
Cs_2O		0.20						1.08	
F	0.00	0.91	0.08	9.20		3.88	0.37	6.69	
H_2O^+	4.67	4.12	4.45	0.20	3.51	1.92	3.48	1.46	4.97
Total	100.05	99.78	100.12	103.93	100.05	101.01	100.02	102.31	100.25
Minus O = F	0.00	0.38	0.03	3.87		1.68	0.16	2.62	
New total	100.05	99.40	100.09	100.06	100.05	99.33	99.86	99.69	100.25
				Number of Ions Based on 12 (O, OH, F)					
Si	3.046	3.025	2.877	2.980	2.947	2.976	2.674	3.377	2.026
Al	0.954	0.975	1.123	1.005	1.053	1.024	1.326	0.623	1.974
Σ tetrahedra	4.000	4.000	4.000	3.985	4.000	4.000	4.000	4.000	4.000
Al	1.988	1.930	1.940		0.127	0.482	0.366	1.184	1.958
Fe^{3+}		0.046	0.084		0.284		0.153	0.080	0.006
Ti			0.011		0.036		0.178		
Mg	0.010	0.011	0.016	2.987	0.954	0.027	1.076	0.003	0.034
Fe^{2+}		0.001	0.015		1.369	2.028	1.016	0.088	0.020
Mn^{2+}		0.007			0.058	0.069	0.016	0.044	0.006
Li		0.132				0.327		1.385	0.061
Σ octahedra	1.998	2.127	2.066	2.987	2.828	2.933	2.805	2.784	2.085
Ca			0.046			0.009	0.020	0.008	0.740
Na	0.082	0.083	0.729	0.008	0.231	0.091	0.058	0.070	0.214
K	0.853	0.860	0.184	0.973	0.859	0.925	0.896	0.759	0.027
Rb		0.040				0.010		0.168	
Cs		0.006						0.032	
Σ X site	0.935	0.989	0.959	0.981	1.09	1.035	0.974	1.037	0.981
F		0.192	0.016	2.031		0.986	0.088	1.460	
OH	2.068	1.838	1.923	0.084	1.822	1.029	1.751	0.672	2.178
Σ F, OH	2.068	2.030	1.939	2.115	1.822	2.015	1.839	2.132	2.178

All analyses are from *Deer et al.* [1962]; for example, DHZ16-1 refers to page 16, column 1 of Deer et al. The names applied to individual analyses are also based on the work of *Deer et al.* [1962].

caryopilite. High-resolution transmission electron micrographs suggest saucer-shaped island domains. Because a trioctahedral sheet (all octahedra filled by Mg, Fe, Mn) is inherently larger than a tetrahedral sheet composed of tetrahedra occupied by silicon only, it is not surprising that the structure deviates from a simple T-O layer structure. One way to make the octahedral sheet smaller is to incorporate vacancies, and indeed, the results of Guggenheim et al. indicate that rows of octahedra around the island edges may be vacant. Figure 6 is an idealized model of the tetrahedral sheet in greenalite [*Guggenheim et al.*, 1982]. Domains of six-membered rings of tetrahedra link to octahedra filled by Fe, Mg, Mn to form T-O units in small domains. The solid tetrahedra would thus connect downward in this diagram to a domain of filled octahedra (not shown). These T-O domains are cross-linked by both three-membered (trigonal) and four-membered rings of tetrahedra which face the opposite way (up) from the solid tetrahedra (pointing down). This can be referred to as tetrahedral inversion. Such tetrahedral inversion and the presence of the three- and four-membered rings make the tetrahedral sheet larger in lateral dimensions and thus facilitate the linkage of tetrahedral and octahedral sheets in greenalite.

Obviously, because the structure is not completely solved, it is difficult to give criteria for good microprobe analyses. As a provisional measure I suggest comparing greenalite microprobe analyses and formulae (calculated on a seven-oxygen basis) to those reported in Table 8. These analyses, taken from *Guggenheim et al.* [1982], show silicon ranging from 2.06 to

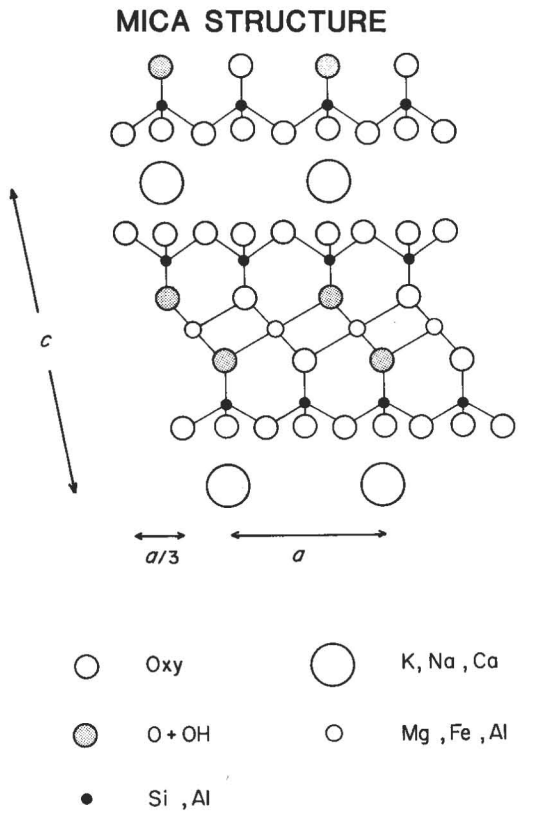

Fig. 3*a*. Projection down *b* of the muscovite structure showing a T-O-T subcell. The upper tetrahedral sheet is staggered (offset) with respect to the lower sheet by *a*/3 [from *Papike and Cameron*, 1976].

2.13 and a total octahedral occupancy ranging from 2.73 to 2.85. Na, K, and Ca, when determined, are very low.

MINNESOTAITE

Magnesian minnesotaite has a dominant primitive lattice, $P\bar{1}$ ($a = 28.0$ Å (~ 5 times a_{talc}), $b = 9.4$ Å, $c = 12.4$ Å, $\alpha = 101°$, $\beta = 127°$, $\gamma = 90°$, and $Z = 1$), with the ideal formula $(Fe, Mg)_{30}Si_{40}O_{96}(OH)_{28}$, or, to compare with talc stoichiometry, $(Fe, Mg)_3Si_4O_{9.6}(OH)_{2.8}$. Ferroan minnesotaite has a dominantly *C*-centered lattice, $C\bar{1}$ ($a = 50.6$ Å (~ 9 times a_{talc}), $b = 9.6$ Å, $c = 12.4$ Å, $\alpha = 101°$, $\beta = 127°$, $\gamma = 90°$, and $Z = 2$), with the ideal formula $(Fe, Mg)_{27}Si_{36}O_{86}(OH)_{26}$, or, to compare with talc stoichiometry, $Fe_3Si_4O_{9.55}(OH)_{2.89}$. The definitive structural study of this complex silicate series is by *Guggenheim and Eggleton* [1986], and this summary derives largely from that paper. Although *Gruner* [1944] suggested that minnesotaite is the ferrous iron analogue of talc, we now know that is not the case. The basic structural problem in this silicate series is that although the silicon tetrahedral sheet fits comfortably on the magnesian trioctahedral sheet of talc, a ferrous iron trioctahedral layer is just too large for a silicon tetrahedral sheet. Therefore there has to be structural adjustment in the tetrahedral sheet to make it larger. Figure 7*a* illustrates the tetrahedral sheet for the primitive unit (*P*) cell. The tetrahedral strip width in the *P* cell is four tetrahedra wide along *a*. These strips are held together by continuous silicate chains running parallel to *b*. The chains are located in the interlayer region, i.e., the region occupied by potassium in muscovite and biotite. The tetrahedra located in the upper four-tetrahedra-wide strip link upward to an octahedral strip (not shown in Figure 7*a*), whereas the lower tetrahedral strip links downward to another octahedral strip (not shown in Figure 7*a*). Figure 7*b* shows the minnesotaite *P* cell projected down *b*. The small amount of alkalis reported for minnesotaite (Table 9) could be located in the interlayer cavities. The *C*-centered structure is similar to the *P* structure described above, but it has three-tetrahedra-wide chains alternating with four-tetrahedra-wide chains along *a* instead of just the four-tetrahedra-wide chains that occur in the primitive structure. The different strip widths are thought to result from the different linkage requirements in Mg-minnesotaite versus Fe-minnesotaite. Ten tetrahedra (4 + 1 + 4 + 1) span nine octahedra parallel to *a* for the *P* cell which occurs in magnesian compositions. For the *C* cell with the larger, iron-containing octahedra, nine tetrahedra (4 + 1 + 3 + 1) span eight octahedra.

As with greenalite, it is difficult to give criteria for good microprobe analyses because of the structural complexity in the minnesotaite series. However, analyses reduced on the basis of 11 oxygens (22 negative charges) should be similar to those listed in Table 9.

STILPNOMELANE

Stilpnomelane has a complex modulated structure crystallizing in space group $P\bar{1}$ ($a \cong b = 21.72$ Å, $c = 17.74$ Å, $\alpha = 124°$, $\beta = 96°$, $\gamma = 120°$, and $Z = 1$). Important papers contributing to our understanding of stilpnomelane include those by *Eggleton* [1972] and *Eggleton and Chappell* [1978], and much of this discussion derives from these two publications. Stilpnomelane is remarkable in that it can accommodate a wide range of Fe^{2+}/Fe^{3+} ratios without major structural change. An ideal end-member ferrostilpnomelane can be represented by $K_5Fe_{48}{}^{2+}(Si_{63}Al_9)O_{168}(OH)_{48} \cdot 12H_2O$, and an ideal end-member ferristilpnomelane can be represented by $K_5Fe_{48}{}^{3+}(Si_{63}Al_9)O_{216} \cdot 36H_2O$. However, neither end-member composition has been reported. A convenient approximation to the structural formula using a one-eighth subcell is $K_{0.6}(Mg, Fe^{2+}, Fe^{3+})_6Si_8Al(O, OH)_{27} \cdot 2$–$4H_2O$. Ferristilpnomelane is thought to result from oxidation after primary crystallization. A convenient ternary dia-

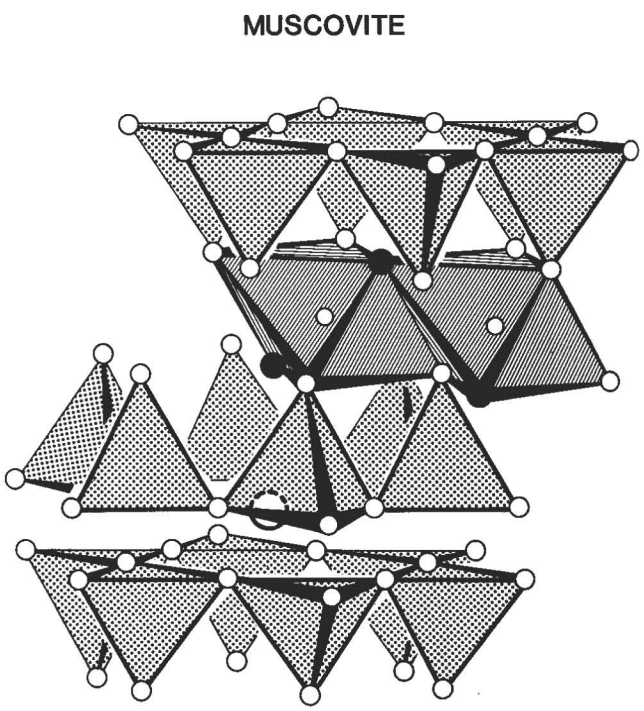

Fig. 3*b*. Crystal structure of muscovite [after *Hurlbut and Klein*, 1977]. Solid circles represent OH^- groups.

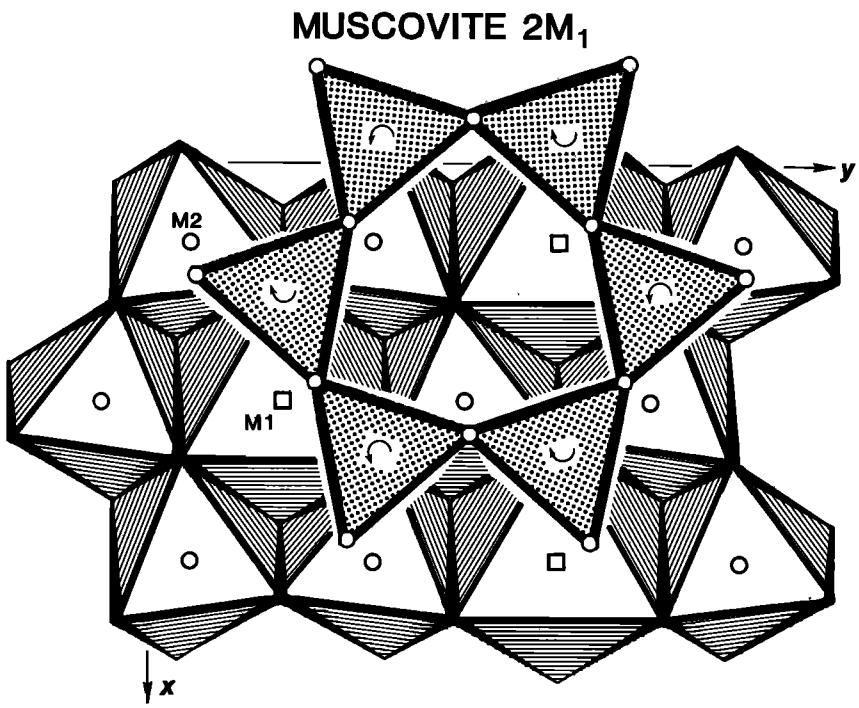

Fig. 3c. The crystal structure of muscovite showing the filled M2 sites (circles) and vacant M1 sites (squares) [after *Bailey*, 1984].

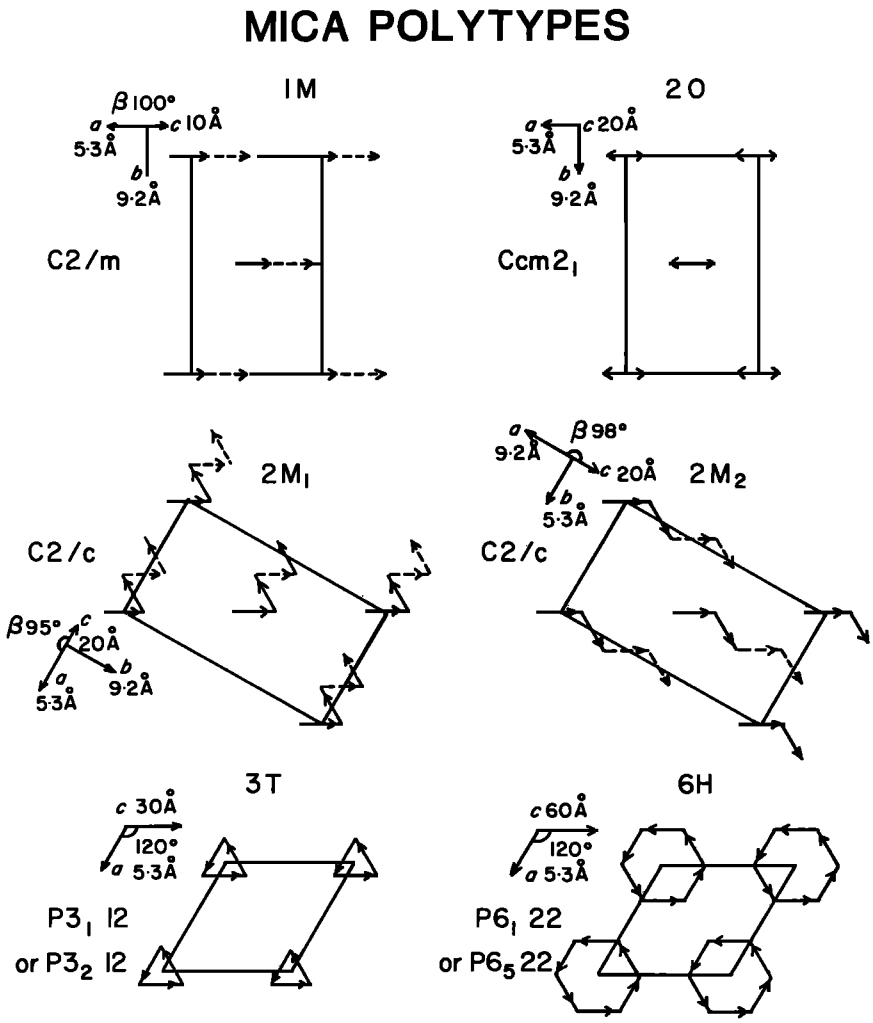

Fig. 3d. The six mica polytypes derived by assuming that only one interlayer stacking angle is present in each crystal [from *Papike and Cameron*, 1976].

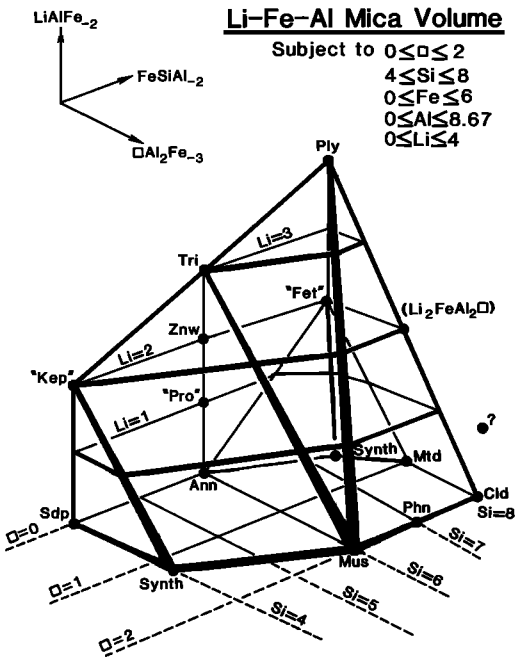

Fig. 3*e*. Mica classification [after *Cerný and Burt*, 1984]. The end-members are synthetic mica (Synth), siderophyllite (Sdp), ephesite (Kep), annite (Ann), protolithionite (Pro), zinnwaldite (Znw), trilithionite (Tri), muscovite (Mus), phengite (Phn), celadonite (Cld), montdorite (Mtd), taeniolite (Fet), and polylithionite (Ply).

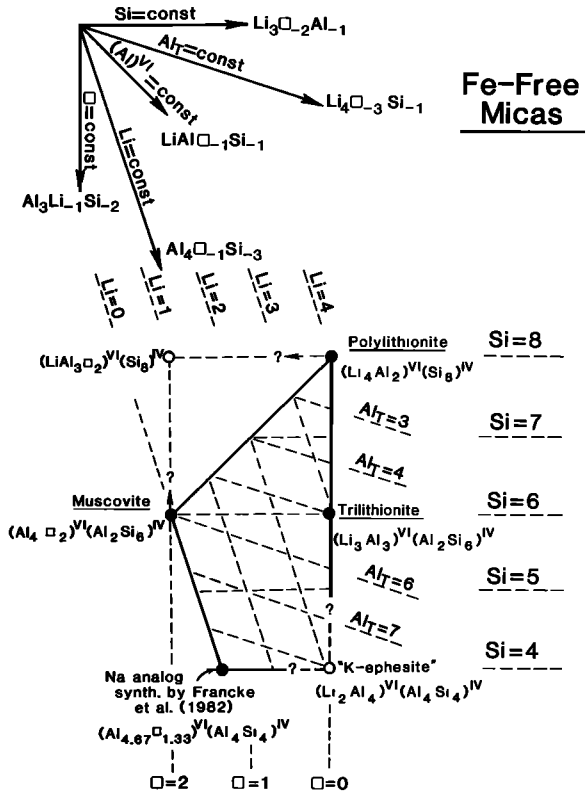

Fig. 3*g*. Mica classification [after *Cerný and Burt*, 1984].

gram that compares greenalite, minnesotaite, and stilpnomelane compositions is illustrated in Figure 8*a*.

As mentioned above, an iron-bearing octahedral sheet has lateral dimensions too large to permit linkage of a continuous hexagonal sheet of silica tetrahedra [*Eggleton*, 1972]. In stilpnomelane (Figures 8*b* and 8*c*), linkage between the octahedral and the tetrahedral sheets is maintained over a distance of seven linked tetrahedra, resulting in an island of 24 tetrahedra linked in a hexagonal array and articulating to a continuous

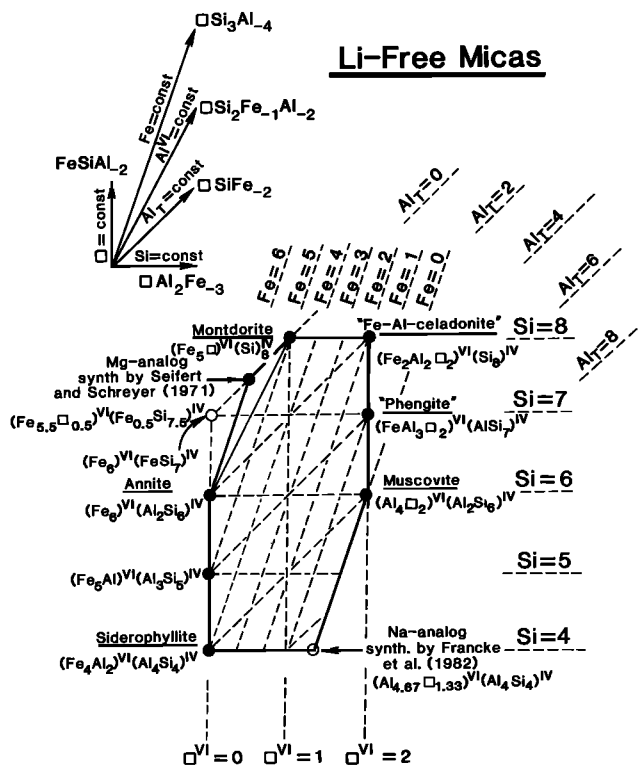

Fig. 3*f*. Mica classification [after *Cerný and Burt*, 1984].

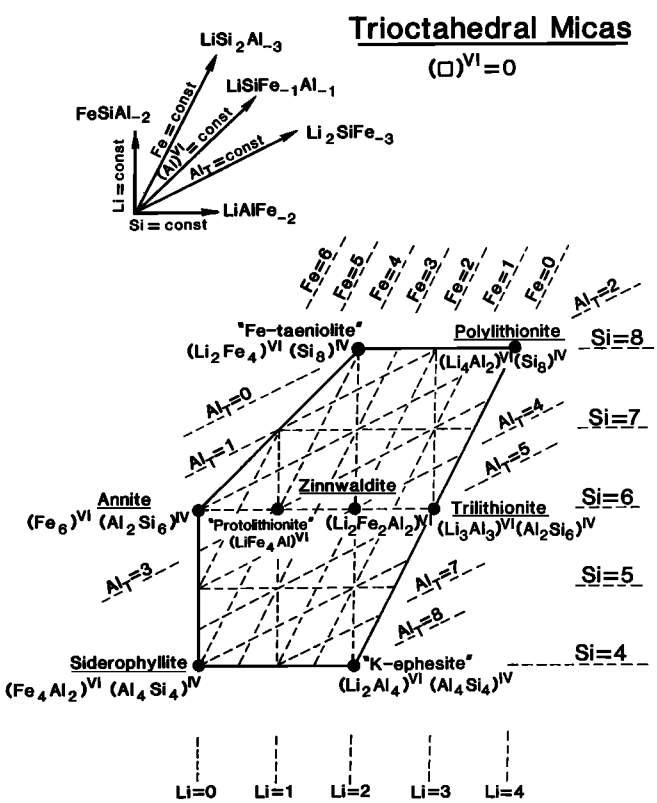

Fig. 3*h*. Mica classification [after *Cerný and Burt*, 1984].

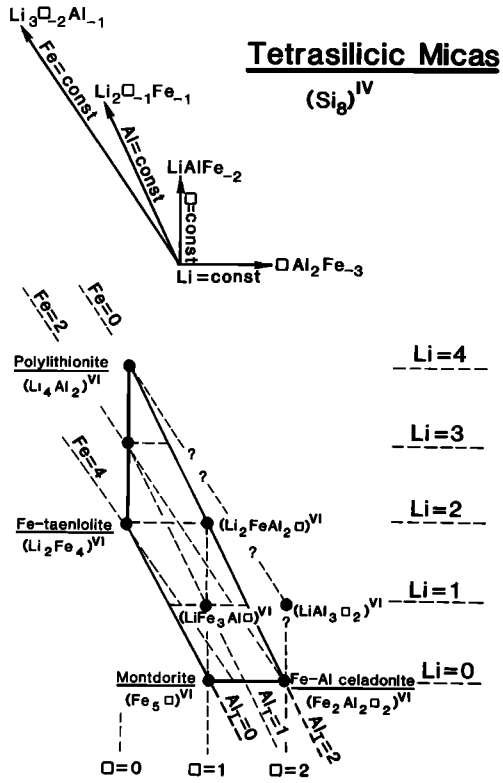

Fig. 3*i*. Mica classification [after *Černý and Burt*, 1984].

octahedral sheet. The islands are linked by six-membered (trigonal) rings of tetrahedra whose apices point in the opposite direction from those of island tetrahedra (tetrahedral inversion). The island tetrahedra and the trigonal rings form

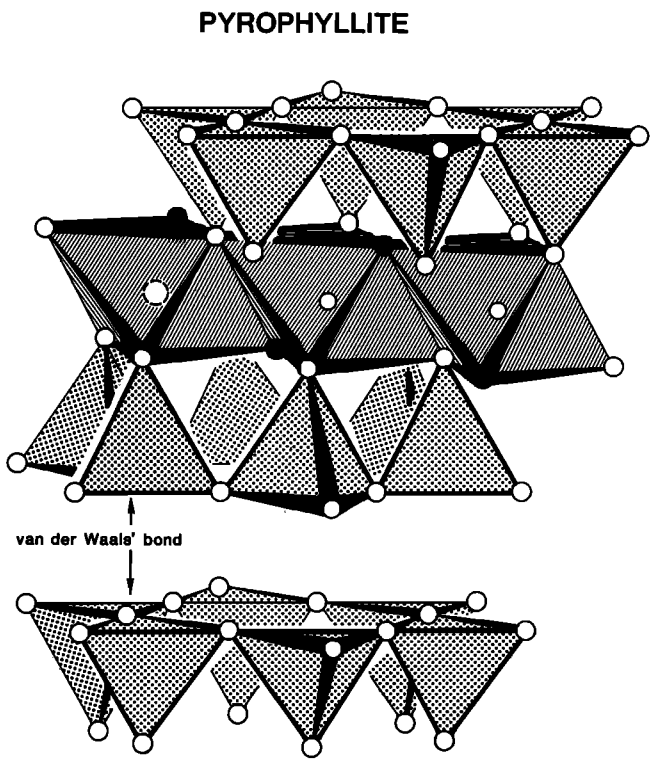

Fig. 4. Crystal structure of pyrophyllite [after *Hurlbut and Klein*, 1977]. Note that this is only a schematic diagram. Solid circles represent OH^- groups.

TABLE 6. Pyrophyllite-Talc Analyses

	Pyrophyllite		Talc	
	Sample 1*	Sample 2† (DHZ118-1)	Sample 3‡	Sample 4† (DHZ123-6)
		Major Oxides		
SiO_2	66.04	63.57	63.22	60.02
Al_2O_3	28.15	29.25		1.88
Fe_2O_3	0.64	0.10	0.33	
TiO_2		0.04		
MgO	0.04	0.37	30.45	30.39
FeO		0.12	0.89	1.51
MnO		0.00		
CaO	0.01	0.38		1.00
Na_2O	0.04	0.02	0.02	
K_2O			0.05	
H_2O^+	5.27	5.66	4.78	5.37
Total	100.19	99.51	99.74	100.17
		Number of Ions Based on 11 Oxygens		
Si	3.976	3.882	4.022	3.861
Al	0.024	0.118		0.139
Σ tetrahedra	4.000	4.000	4.022	4.000
Al	1.974	1.988		0.002
Fe^{3+}	0.029	0.004	0.016	
Ti				
Mg	0.004	0.034	2.884	2.914
Fe^{2+}		0.006	0.047	0.081
Mn^{2+}				
Σ octahedra	2.007	2.032	2.947	2.997
Ca	0.001	0.020		0.069
Na	0.005		0.002	
K			0.004	
Σ X site	0.006	0.020	0.006	0.069

*From *Lee and Guggenheim* [1981].
†From *Deer et al.* [1962]; for example, DHZ118-1 refers to page 118, column 1 of Deer et al.
‡From *Rayner and Brown* [1973].

five-membered rings at their boundaries. Figure 8*c* illustrates several possible locations for K, Na, and Ca in the interlayers. However, the exact locations of these cations has not been determined.

Once again, the complexity of the stilpnomelane structure and chemistry makes it difficult to give criteria for good microprobe analyses. Therefore it is suggested that microprobe analyses, after reduction based on 15 tetrahedral and octahedral cations (Si, Al, Fe^{3+}, Mg, Fe^{2+}, Mn), be compared to the range of analyses presented in Table 10.

PREHNITE

Prehnite, $Ca_2{}^{VI}(Al, Fe^{3+})(Si_3Al)O_{10}(OH)_2$, has a relatively complex silicate sheet structure [*Peng et al.*, 1959; *Preisinger*, 1965; *Papike and Zoltai*, 1967]. Determination of the correct space group has been challenging. *Gossner and Mussgnug* [1931] suggested that the space group is either *P2cm* or *Pncm*, and *Nuffield* [1943] reported that single-crystal X ray diffraction photographs display systematically missing diffraction spots indicative of space group *Pncm*. However, as this space group is not consistent with the pyroelectric character of prehnite, he concluded that the crystal he studied was twinned, with the untwinned material having space group *P2cm*. *Peng et al.* [1959] solved the crystal structure assuming space group

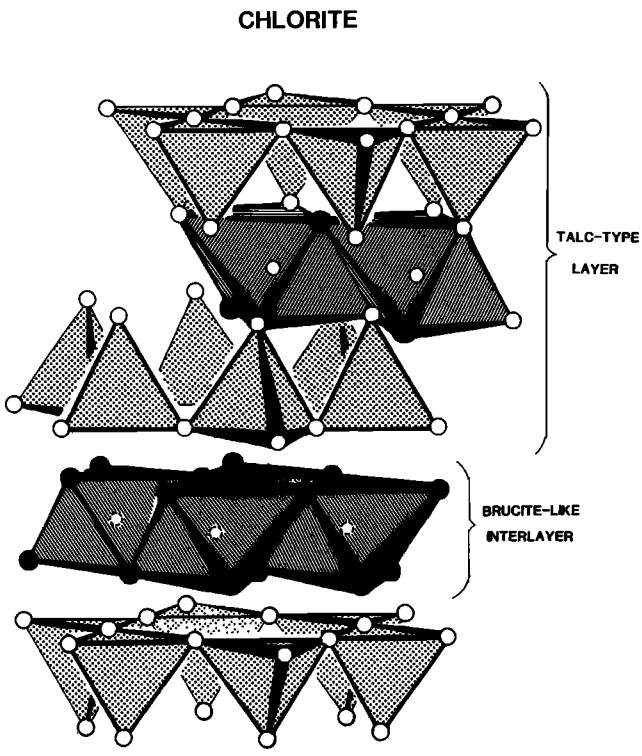

Fig. 5. Crystal structure of chlorite [after *Hurlbut and Klein*, 1977]. Solid circles represent OH^- groups.

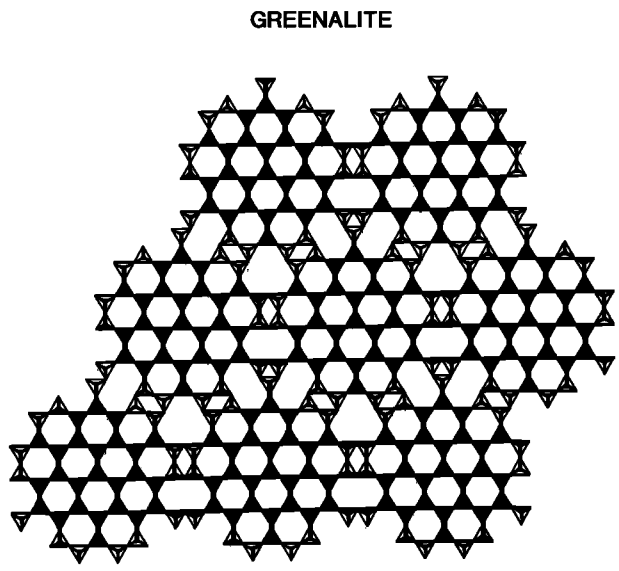

Fig. 6. The modulated tetrahedral sheet of greenalite [after *Guggenheim et al.*, 1982].

Pncm. However, *Preisinger* [1965] refined the structure of a prehnite in space group *P2cm*. *Papike and Zoltai* [1967] refined the "average structure" of prehnite in space group *Pncm*, with $a = 4.65$ Å, $b = 5.48$ Å, $c = 18.49$ Å, and $Z = 2$. However, Papike and Zoltai claim that the *Pncm* structure represents an average structure composed of *P2cm* and *P2/n* domains. Figure 9*a* is a schematic drawing of the silicate layer showing three levels of tetrahedra along the *c* axis that make up these relatively complex silicate sheets [*Quint*, 1987]. *Quint* [1987] compares the layer structure of a newly described mineral, amstallite, $CaAl(OH)_2(Al_{0.8}Si_{3.2})O_8OH_2 \cdot [(H_2O)_{0.8}Cl_{0.2}]$, with that of prehnite. *Liebau* [1985] classifies such layers as open-branched "zweier" single-layer silicates. *Moore* [1986] compares the silicate linkage as portrayed in Figure 9*b* with a portion of the crystal structure of high quartz.

The structural study of *Papike and Zoltai* [1967] shows that the T1 tetrahedra (Figure 9*b*) are occupied by silicon only, whereas the T2 are occupied by 50% Al and 50% Si. If *Pncm* were the correct space group, then each T2 tetrahedron (multiplicity 4) would be statistically occupied by 0.5 Al, 0.5 Si. However, this is not thought to be the case. *Papike and Zoltai*

TABLE 7. Chlorite Analyses

	Sample 1	Sample 2	Sample 3	Sample 4	Sample 5	Sample 6	Sample 7	Sample 8
				Major Oxides				
SiO_2	27.30	30.60	33.78	25.12	28.15	30.76	22.30	26.56
Al_2O_3	24.17	16.80	13.24	24.02	15.17	12.12	16.81	20.19
Fe_2O_3	1.87	2.18	1.50	4.86	3.85	9.12	15.13	1.27
TiO_2								0.24
MgO	29.24	32.18	34.41	12.19	14.56	12.36	1.30	2.68
FeO	5.15	5.02	3.07	23.26	25.23	22.76	32.78	36.51
MnO			0.16	0.18	0.21	1.24		2.04
H_2O^+	12.64	12.76	13.89	10.90	11.25	9.76	11.04	9.97
Total	100.37	99.54	100.05	100.53	98.42	98.12	99.36	99.46
				Number of Ions Based on 18 (O, OH)				
Si	2.59	2.94	3.23	2.59	3.02	3.27	2.58	2.93
Al	1.41	1.06	0.77	1.41	0.98	0.73	1.42	1.07
Σ tetrahedra	4.00	4.00	4.00	4.00	4.00	4.00	4.00	4.00
Al	1.30	0.85	0.71	1.50	0.94	0.78	0.88	1.56
Fe^{3+}	0.13	0.16	0.11	0.38	0.31	0.73	1.32	0.11
Ti								0.02
Mg	4.14	4.61	4.89	1.87	2.33	1.96	0.22	0.44
Fe^{2+}	0.41	0.40	0.24	2.00	2.26	2.02	3.18	3.37
Mn^{2+}			0.01	0.02	0.02	0.11		0.19
Σ octahedra	5.98	6.02	5.96	5.77	5.86	5.60	5.60	5.69

All analyses are from *Bailey* [1975].

TABLE 8. Greenalite Analyses

	Sample 1	Sample 2	Sample 3	Sample 4	Sample 5	Sample 6	Sample 7
			Major Oxides				
SiO_2	34.7	36.5	35.9	34.4	35.9	36.5	36.3
Al_2O_3	0.90	0.25	0.16	0.05	0.06	0.16	0.10
MgO	4.98	3.75	4.13	0.26	3.83	4.53	3.80
FeO*	47.3	40.2	47.8	55.5	50.0	46.7	50.4
MnO	0.15	8.71	1.78	0.18	0.06	1.50	0.06
Total	88.03	89.41	89.77	90.39	89.85	89.39	90.66
			Number of Ions Based on Seven Oxygens				
Si	2.057	2.129	2.099	2.079	2.103	2.123	2.106
Al	0.063	0.017	0.011	0.004	0.004	0.011	0.007
Mg	0.440	0.326	0.360	0.023	0.334	0.393	0.328
Fe	2.344	1.961	2.337	2.805	2.450	2.272	2.446
Mn	0.007	0.431	0.088	0.009	0.003	0.074	0.003
Σ cations other than Si	2.854	2.735	2.796	2.841	2.791	2.750	2.784

All analyses are from *Guggenheim et al.* [1982, Table 2].
*All iron calculated as FeO.

[1967] suggest that the *Pncm* structure is an average of two types of domains with *P2cm* and *P2/n* symmetry, each with a different ordering scheme, as shown in Figure 9*c*.

Prehnite does not show much compositional variability (Table 11). The only appreciable substitution is of Fe for Al in octahedral coordination. Table 11 presents prehnite analyses from *Deer et al.* [1962], and the formulae are calculated on the basis of 12 (O, OH). However, microprobe data, which do not yield H_2O values, should be reduced assuming 11 oxygens (22 negative charges, equivalent to $O_{10}(OH)_2$). Good microprobe analyses should have Ca plus Na approximately equal to two and Si, Al, Fe^{3+}, Ti, Mg, Fe^{2+}, Mn approximately equal to five.

QUARTZ-TRIDYMITE-CRISTOBALITE

Papike and Cameron [1976] reviewed aspects of the crystal chemistry of the silica polymorphs, quartz, tridymite, cristobalite, coesite, and stishovite. Much of the discussion presented here for quartz, tridymite, and cristobalite is abstracted from that paper.

High (or β) quartz is hexagonal, with space group $P6_222$ or $P6_422$ [*Bragg and Gibbs*, 1925]. Unit cell dimensions are $a = 5.01$ Å, $c = 5.47$ Å, and $Z = 3$. Si occupies special positions at heights 0, $\frac{1}{3}$, and $\frac{2}{3}$, and the oxygens lie in coplanar pairs $c/6$ above and below the Si atoms. The SiO_4 tetrahedra are arranged in hexagonal and trigonal helices with axes parallel to the c axis (Figure 10*a*). Right-handed helices result in the structurally right-handed space group $P6_222$, and left-handed helices in the structurally left-handed space group $P6_422$. It is not possible to determine the structural hand of quartz by ordinary X ray techniques, but *De Vries* [1958] showed that it can be established by examination of anomalous scattering produced by Si irradiated by CrK_α radiation.

Low (or α) quartz is trigonal and occurs with either space

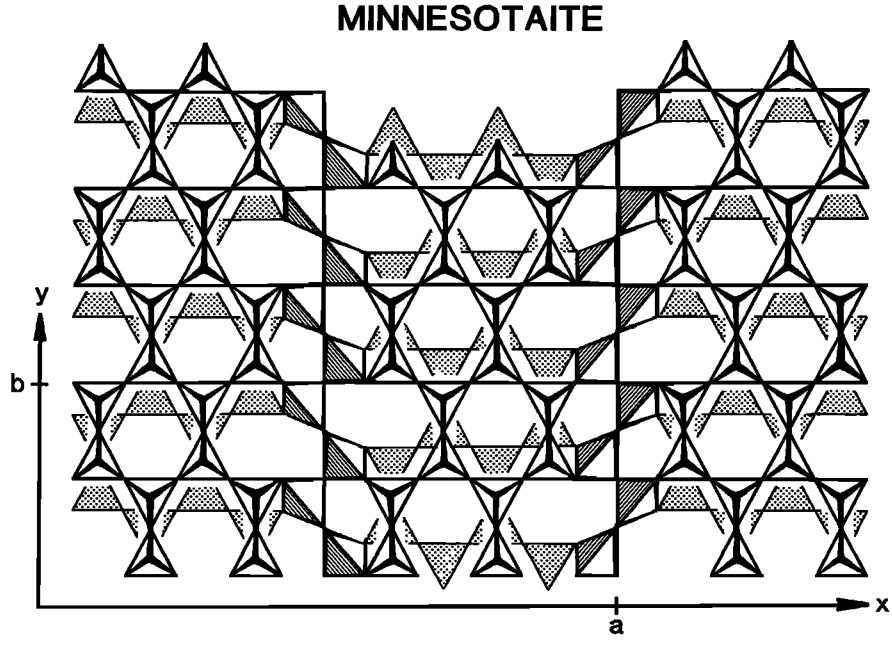

Fig. 7*a*. Crystal structure of minnesotaite *P* cell [after *Guggenheim and Eggleton*, 1986].

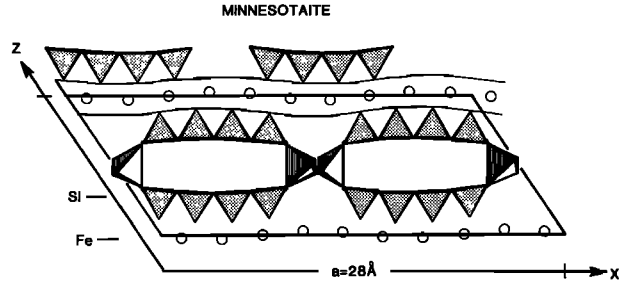

Fig. 7b. Crystal structure of minnesotaite P cell projected down b [after *Guggenheim and Eggleton*, 1986].

group $P3_12$ or space group $P3_22$ [*Gibbs*, 1926; *Wei*, 1935]. Unit cell dimensions [*Deer et al.*, 1963*b*] are $a = 4.91$ Å, $c = 5.40$ Å, and $Z = 3$. The SiO_4 tetrahedra form helices that lie on three-fold screw axes (Figure 10*b*). The oxygens are no longer coplanar above and below each Si atom but are located at the general position (xyz). *Young and Post* [1962] refined the atomic positional coordinates of α quartz.

The high (or β) tridymite structure was first investigated by *Gibbs* [1927], who concluded that it was hexagonal with space group $P6_3/mmc$ ($a = 5.03$ Å and $c = 8.22$ Å). The structure proposed by *Gibbs* [1927] consists of sheets of tetrahedra parallel to (001). The tetrahedra within each sheet share corners to form six-membered rings in which the apices of adjacent tetrahedra point alternately in the $+c$, $-c$, $+c$, $-c$ directions (Figure 10*c*). Adjacent sheets share apical oxygens and are related to one another by mirror planes passing between them. Reinvestigation of another high tridymite [*Dollase*, 1967] at 220°C showed an orthorhombic structure (space group $C222_1$) with strong hexagonal pseudosymmetry and a cell that is dimensionally hexagonal. This structure is very similar to (but more distorted than) the ideal high tridymite structure proposed by Gibbs. The tetrahedral rings in adjacent layers do not directly superimpose but are offset slightly along the b axis (Figure 10*d*). The super structure of a low tridymite was solved by *Dollase and Baur* [1976]. This low tridymite is monoclinic with space group Cc ($a = 18.52$ Å, $b = 5.00$ Å, $c = 23.81$ Å, and $\beta = 105.8°$). It is a collapsed and distorted version of tridymite composed of a relatively complex array of ditrigonal and oval-shaped six-membered rings of tetrahedra.

TABLE 9. Minnesotaite Analyses

	Sample 1*a*	Sample 3*a*	Sample 7
	Major Oxides		
SiO_2	51.79	50.14	53.85
Al_2O_3	1.46	0.37	0.15
Fe_2O_3	0.61	2.00	
MgO	3.21	4.39	9.68
FeO	35.65	36.68	30.53
MnO	0.78	0.27	0.53
CaO	0.10	0.10	0.03
Na_2O	0.06	0.05	0.15
K_2O	0.44	0.15	0.17
H_2O^+	5.03	5.24	
Total	99.13	99.39	95.09
	Number of Ions Based on 11 Oxygens		
Si	4.00	3.91	3.98
Al	0.13	0.03	0.01
Σ tetrahedra	4.13	3.94	3.99
Fe^{3+}	0.04	0.12	
Mg	0.37	0.51	1.07
Fe^{2+}	2.30	2.40	1.89
Mn^{2+}	0.05	0.02	0.03
Σ octahedra	2.76	3.05	2.99
Ca	0.01	0.01	0.01
Na	0.01	0.01	0.02
K	0.04	0.02	0.02
Σ others	0.06	0.04	0.05
OH	2.60	2.96	

Analyses are from *Guggenheim and Eggleton* [1986].

High cristobalite (Figure 10*e*) is cubic, with space group $Fd3m$ ($a = 7.13$ Å) [*Wyckoff*, 1925; *Peacor*, 1973]. The structure determined by *Wyckoff* [1925], often described as the "ideal" high cristobalite structure, contains sheets of six-membered silicate tetrahedra stacked parallel to (111). Adjacent sheets share apical oxygens as in high tridymite, but the basal oxygens of tetrahedra in adjacent sheets are rotated 60°, thus producing an ABCABC ··· sequence. Because this idealized structure contains exceptionally short Si-O distances (1.54 Å), *Nieuwenkamp* [1937] proposed a model based on disordering of the oxygen atom. In his model the oxygen atom is randomly distributed on a circle of radius 0.3–0.55 Å, with the plane of the circle bisecting the Si-Si axis. An investigation of the structure at high temperatures [*Peacor*, 1973] places Si at the special position ($\frac{1}{8}$ $\frac{1}{8}$ $\frac{1}{8}$) and oxygen on a circle of radius 0.45 Å oriented normal to a line between adjacent silicons. Results from the same study also indicate $\frac{1}{6}$-oxygen occupancy of six different equally spaced positions, rather than random distribution on the circle. The refined structure, although similar to that proposed by *Wyckoff* [1925], has more reasonable Si-O distances and Si-O-Si angles.

Low cristobalite is tetragonal, with space group $P4_12_1$ ($a = 4.97$ Å and $c = 6.95$ Å) or the enantiomorph space group, $P4_32_1$ [*Dollase*, 1965; *Peacor*, 1973]. In space group $P4_12_1$ the Si atom lies at ($xx0$), and the oxygen atom is at general position (xyz). Alternate selection of a C-centered tetragonal cell produces a pseudoisometric cell that is dimensionally similar to the high cristobalite cell. A structural study of the low-high cristobalite inversion [*Peacor*, 1973] showed that the coefficient of thermal expansion is larger for low cristobalite than for high cristobalite. With increasing temperature the positions of the oxygen and silicon atoms in low cristobalite change regularly toward those that the atoms occupy in high cristobalite.

The composition of quartz closely approximates 100% SiO_2, but tridymite and cristobalite, which have more open structures, may contain as little as 95% SiO_2 [*Deer et al.*, 1963*b*]. Substitution for Si usually involves a coupled mechanism in which Si is replaced by a trivalent ion, very commonly Al^{3+}, and ions of the appropriate size are introduced into vacant interstitial positions to maintain charge balance. The resultant structures are called stuffed derivatives, and their composition corresponds to a formula such as $(\square_{1-x}A_x)(Si_{1-x}B_x)O_2$, where □ represents an interstitial vacancy; A, a monovalent ion; and B, a trivalent ion [*Frondel*, 1962]. Stuffed forms of silica include nepheline, $KNa_3Al_4Si_4O_{16}$, a derivative of the high tridymite structure, and carnegieite, $NaAlSiO_4$, a derivative of the high cristobalite structure.

Table 12 presents four quartz and two tridymite analyses from *Deer et al.* [1963*b*]. The cations are calculated on the

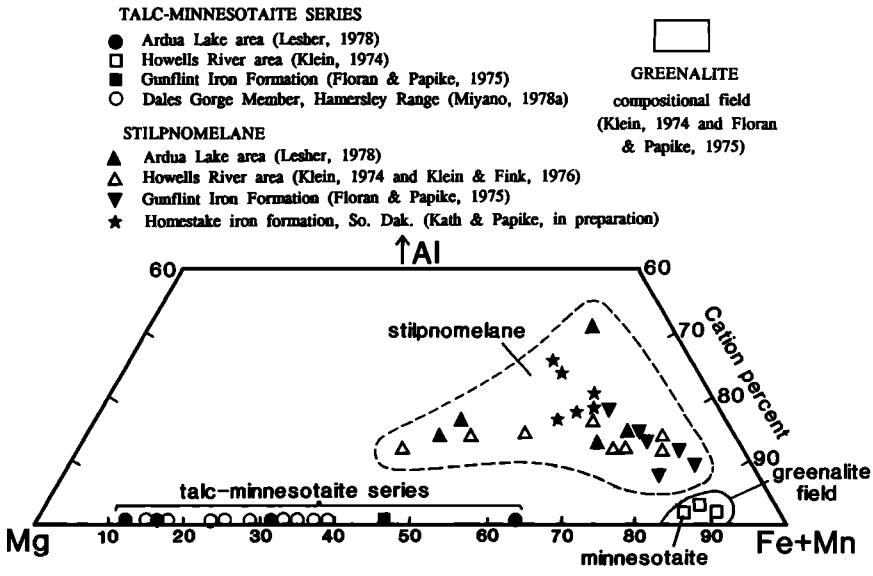

Fig. 8*a*. Compositional ranges of stilpnomelane, talc-minnesotaite series, and greenalite [after *Klein*, 1983].

basis of two oxygens, which is also the way microprobe analyses should be reduced. Good quartz analyses will have Si approximately equal to one. However, tridymite analyses may show Al, Fe^{3+}, and Ti^{4+} in tetrahedral coordination. These cation substitutions result in charge deficiencies at the tetrahedral sites, e.g., one charge deficiency for each ^{IV}Al and $^{IV}Fe^{3+}$. Thus the following charge balance equation should be obeyed:

$$\underset{\text{site charge deficiency}}{^{IV}Al + {}^{IV}Fe^{3+}} = \underset{\text{site charge excess}}{2(Mg, Fe^{2+}, Mn^{2+}, Ca) + Na + K}$$

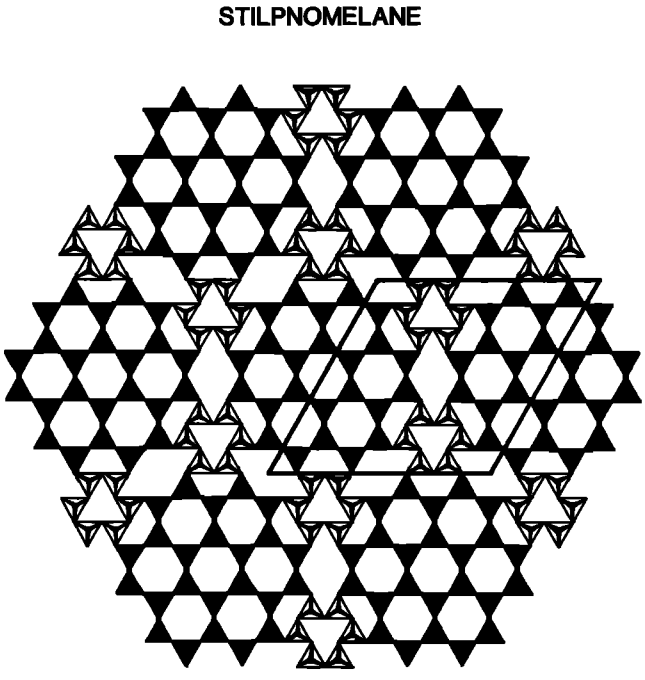

Fig. 8*b*. The modulated tetrahedral sheet of stilpnomelane [after *Eggleton*, 1972].

FELDSPAR

This discussion of feldspar crystal chemistry draws heavily on a paper by *Papike and Cameron* [1976]. For a more complete and in-depth review the reader is referred to *Ribbe* [1983].

The compositions of most natural feldspars can be represented in the ternary system $KAlSi_3O_8$ (Or)-$NaAlSi_3O_8$(Ab)-$CaAl_2Si_2O_8$(An). Members of the series between $KAlSi_3O_8$ and $NaAlSi_3O_8$ are called alkali feldspars, and those between $NaAlSi_3O_8$ and $CaAl_2Si_2O_8$ are plagioclase feldspars. Each series is further subdivided into smaller compositional ranges; however, the names of the subdivisions are now used less commonly than the specific feldspar components An-Ab-Or.

Alkali feldspars generally contain less than 10 mol % An; likewise, plagioclases generally contain less than 10 mol % Or [*Deer et al.*, 1963*b*]. Ions that substitute in limited amounts for the major cations include Fe^{3+} and Ti^{4+} for ^{IV}Al; Rb and Cs for K, Na; Mg, Fe^{2+}, Sr, and Mn for Ca; and Ba for K. The less common barium feldspars form an isomorphous series between $KAlSi_3O_8$ and $BaAl_2Si_2O_8$ (celsian); intermediate members of the series are called hyalophane.

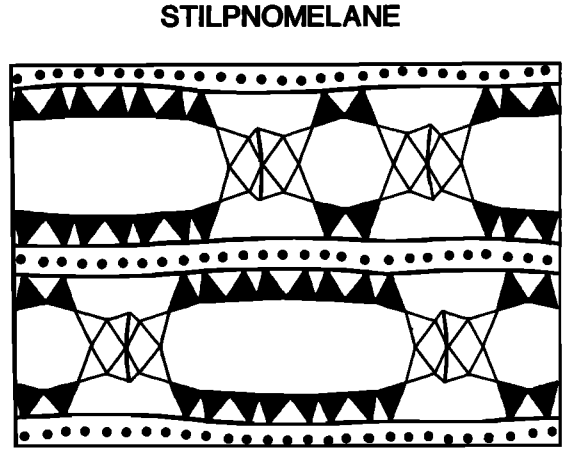

Fig. 8*c*. Crystal structure of stilpnomelane [after *Eggleton*, 1972].

TABLE 10. Stilpnomelane Analyses

	Sample N	Sample P	Sample J	Sample F	Sample V	Sample A
			Major Oxides			
SiO_2	44.74	46.37	48.21	45.99	44.88	42.69
Al_2O_3	6.10	6.30	4.35	4.98	6.69	5.58
Fe_2O_3	2.92	5.38	13.03	20.98	25.46	33.70
MgO	5.00	8.07	9.11	3.42	7.16	3.89
FeO	24.52	20.77	14.00	12.85	2.73	0.30
MnO	4.40	0.66	0.27	0.59	0.53	2.43
CaO	0.00	0.28	0.28	0.12	0.79	0.13
Na_2O	0.30	0.13	0.06	0.42	0.12	0.07
K_2O	3.42	2.58	1.99	1.40	1.54	1.81
H_2O^+		8.87	8.46	7.32	8.80	7.83
Total	91.40	99.41	99.76	98.07	98.7	98.43
			Cations Based on (Si, Al, Fe^{3+}, Mg, Fe^{2+}, Mn^{2+}) = 15			
Si	7.82	7.92	8.17	8.22	7.90	7.74
Al	1.18	1.08	0.83	0.78	1.10	1.20
Σ tetrahedra	9.00	9.00	9.00	9.00	9.00	8.94
Al	0.08	0.19	0.03	0.27	0.29	
Fe^{3+}	0.39	0.69	1.65	2.82	3.37	4.60
Mg	1.30	2.06	2.29	0.91	1.88	1.04
Fe^{2+}	3.58	2.96	1.98	1.92	0.40	0.05
Mn	0.65	0.11	0.04	0.09	0.08	0.37
Σ octahedra	6.00	6.01	5.99	6.01	6.02	6.06
Ca	0.00	0.05	0.05	0.03	0.15	0.03
Na	0.05	0.04	0.03	0.15	0.04	0.03
K	0.76	0.57	0.43	0.32	0.34	0.42
Σ others	0.81	0.66	0.51	0.50	0.53	0.48

All analyses are from *Eggleton and Chappell* [1978].

Adequate characterization of a feldspar requires knowledge of both the chemical composition and the structural state (distribution of Al and Si over distinct tetrahedral sites). Structural state depends on temperature of crystallization and on subsequent thermal history. In general, feldspars that crystallized at low temperatures or cooled slowly from high temperatures have low structural states (highly ordered Si-Al distributions).

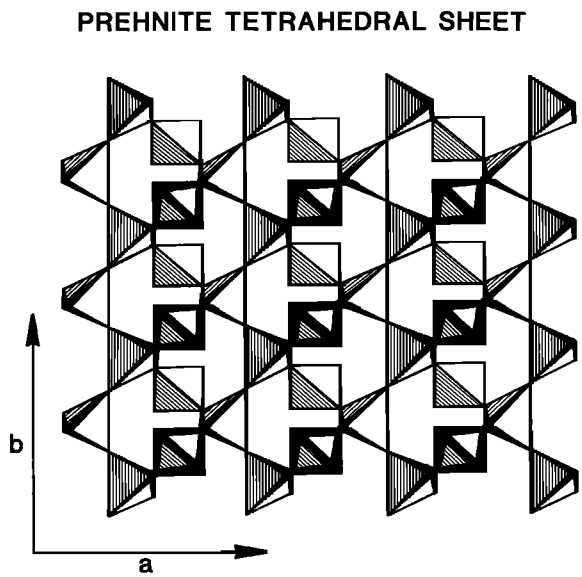

Fig. 9*a*. Idealized tetrahedral sheet of prehnite projected down *c* [after *Quint*, 1987].

Those that cooled rapidly following crystallization at high temperatures have high structural states (disordered Al-Si distributions). A continuum of structural states exists, each state differing principally in the distribution of Si and Al over the independent tetrahedral sites in the crystal structures.

The two limiting structural states of potassium feldspar, $KAlSi_3O_8$, are (1) high-temperature sanidine, which is monoclinic and has a completely disordered Si-Al distribution, and (2) low-temperature maximum microcline, which is triclinic and has an ordered Si-Al distribution. The monoclinic triclinic transition takes place between 300° and 500°C, but the transition temperature as determined in different studies varies considerably.

Adularia is a potassium feldspar that is distinctive because of its morphology and restricted paragenesis (e.g., pegmatites). Both triclinic and monoclinic varieties occur naturally, and optical and structural parameters may vary in different parts of a single grain.

The structures of the $KAlSi_3O_8$ polymorphs can be described as variants of the high-temperature sanidine structure. Table 13*a* summarizes unit cell data for alkali feldspars. Sanidine has space group symmetry *C2/m*, and each unit cell contains four $KAlSi_3O_8$ formula units. The 16 (Si, Al) atoms in the unit cell are distributed randomly over two crystallographically distinct tetrahedral sites, T1 and T2, and the four potassium atoms occupy special positions on mirror planes perpendicular to *b* (Figure 11). The 32 oxygen atoms occur at special positions (four on two-fold axes and four on mirror planes) and at general positions. Potassium atoms occupy large irregularly shaped cavities within this tetrahedral framework. In sanidine each K is coordinated by six oxygens within 2.953 Å and by an additional four within 3.14 Å.

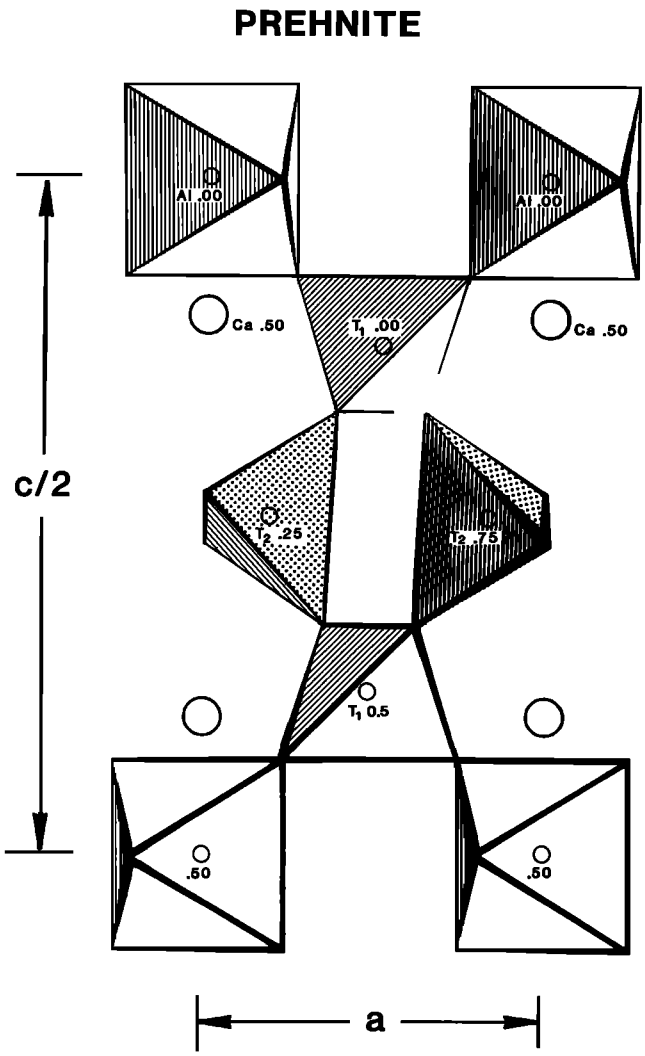

Fig. 9*b*. Average crystal structure of prehnite in space group *Pncm*. Al is confined to T2 tetrahedron (hatched and stippled) [after *Papike and Zoltai*, 1967].

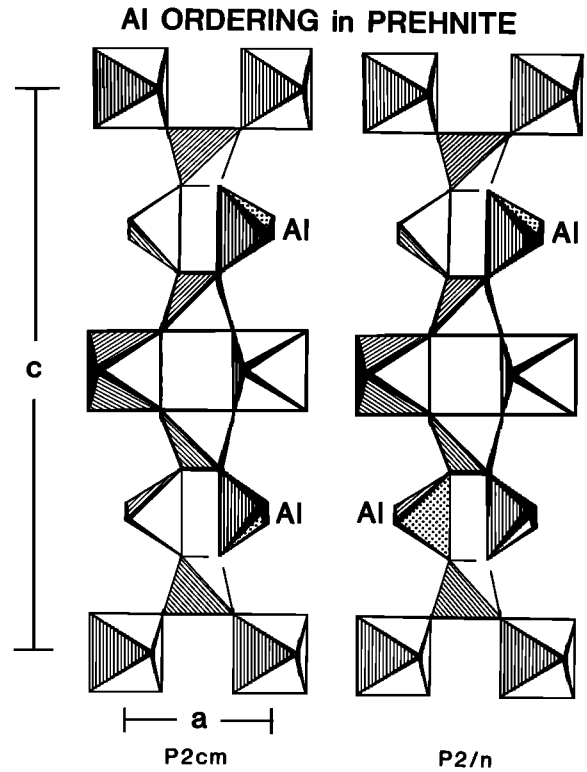

Fig. 9*c*. Possible ordering schemes for tetrahedral Al in space groups *P2cm* and *P2/n*. Al tetrahedra are indicated by both hatching and stippling [after *Papike and Zoltai*, 1967].

The structures of the lower-temperature polymorphs differ from the structure of sanidine principally in the degree of Si-Al ordering. Concentration of Al at a particular tetrahedral site results in the loss of both a twofold axis of rotation and a mirror plane, with a concomitant transition from monoclinic to triclinic symmetry. The two tetrahedral sites of the monoclinic phase become four symmetrically distinct tetrahedral sites (T1o, T1m, T2o, and T2m) in the triclinic phase. In monoclinic sanidine the 16 tetrahedral cations (4Al + 12Si) are distributed randomly over eight T1 and eight T2 sites. In a monoclinic orthoclase, Al is partially ordered at the T1 site. Triclinic maximum microclinic has Al strongly ordered at the T1o site.

$NaAlSi_3O_8$ has two extreme polymorphic modifications that occur in nature, high and low albite. Low albite, which is structurally analogous to microcline, is triclinic and has a highly ordered Si-Al distribution. High albite is triclinic to very high temperatures and thus is not structurally analogous to sanidine. Its Si-Al distribution is also highly disordered. Monoclinic albite, termed monalbite, is stable above ~1000°C.

The calcium end-member, anorthite, is primitive (space group $P\bar{1}$) at room temperature, with $a = 8.18$ Å, $b = 12.88$ Å,

TABLE 11. Prehnite Analyses

	Sample 1 (DHZ264-1)	Sample 2 (DHZ264-3)	Sample 3 (DHZ264-6)
	Major Oxides		
SiO_2	42.76	42.86	41.67
Al_2O_3	24.83	24.41	24.44
Fe_2O_3	0.13	0.52	1.03
TiO_2		0.01	0.12
MgO	0.07	0.03	0.25
FeO	1.12	0.28	0.32
MnO	0.05	0.06	
CaO	26.84	26.89	27.25
Na_2O	0.03	0.32	0.18
H_2O^+	4.24	4.45	4.44
Total	100.07	99.83	99.70
	Number of Ions Based on 12 (O, OH)		
Si	2.954	2.965	2.893
Al	1.046	1.035	1.107
Σ tetrahedra	4.000	4.000	4.000
Al	0.976	0.950	0.893
Fe^{3+}	0.006	0.025	0.053
Ti		0.000	0.006
Mg	0.007	0.002	0.026
Fe^{2+}	0.065	0.016	0.019
Mn	0.003	0.004	
Σ octahedra	1.057	0.997	0.997
Ca	1.986	1.986	2.028
Na	0.004	0.040	0.025
Σ others	1.990	2.026	2.053
OH	1.954	2.048	2.057

Analyses are from *Deer et al.* [1962]; for example, DHZ264-1 refers to page 264, column 1 of Deer et al.

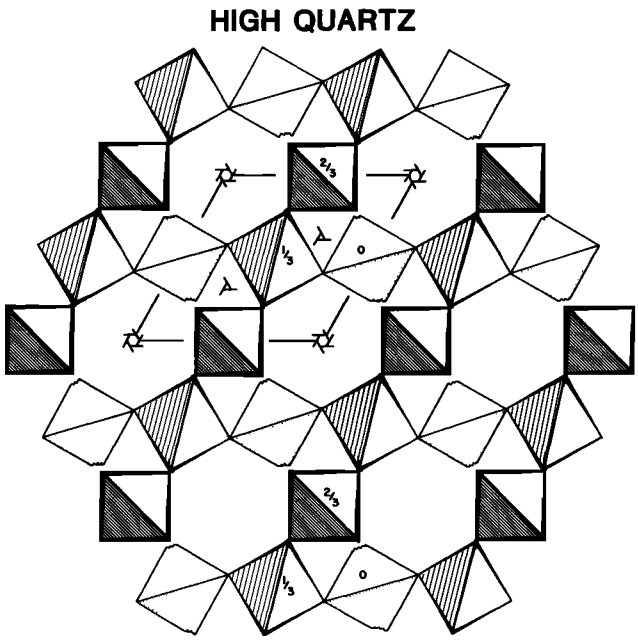

Fig. 10*a*. Crystal structure of high quartz projected down *c* [from *Papike and Cameron*, 1976].

$c = 14.17$ Å, $\alpha = 93.2°$, $\beta = 115.8°$, $\gamma = 91.2°$, and $Z = 8$ [*Deer et al.*, 1963*b*]. Si and Al tetrahedra alternate throughout the structure, and this causes a doubling of the *c* axis. This ordering is nearly perfect and is believed to persist up to melting temperatures. Intermediate plagioclase compositions have complex modulated structures with variable Al-Si ordering patterns and Ca-Na occupancies.

Table 13*b* gives some representative feldspar analyses from *Deer et al.* [1963*b*]. Microprobe analyses should be normalized to eight oxygens. Analyses so reduced will have Na, K, Ca, Ba, Fe^{2+}, Mg approximately equal to one and Al, Si, Fe^{3+}, Ti approximately equal to four.

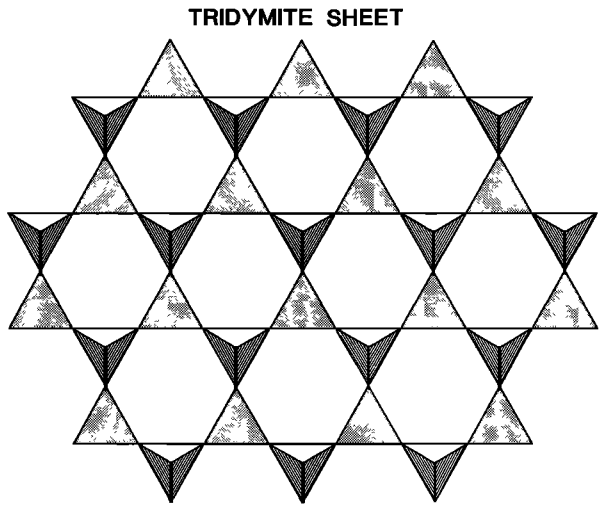

Fig. 10*c*. Portion of idealized tetrahedral sheet in high tridymite projected down *c* [from *Papike and Cameron*, 1976].

NEPHELINE-KALSILITE

The discussion of nepheline presented here is condensed from a review by *Papike and Cameron* [1976]; however, a new expanded discussion of kalsilite has been added. Natural nephelines, $Na_3KAl_4Si_4O_{16}$, are intermediate members of a solid solution series that extends between the pure sodium end-member $NaAlSiO_4$ and $KAlSiO_4$ (kalsilite). Experimental work on this system by *Tuttle and Smith* [1958] showed that pure sodium nepheline transforms at ~900°C to a high-temperature modification that inverts at 1245°C to the polymorph carnegieite, whose structure is similar to that of cristobalite. Nepheline and kalsilite are not isomorphous, but the study by *Tuttle and Smith* [1958] showed that the substitution

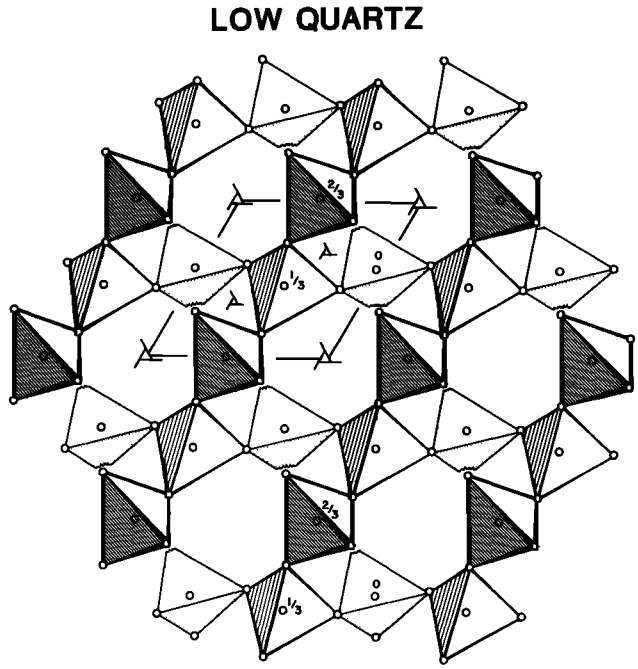

Fig. 10*b*. Crystal structure of low quartz projected down *c* [from *Papike and Cameron*, 1976].

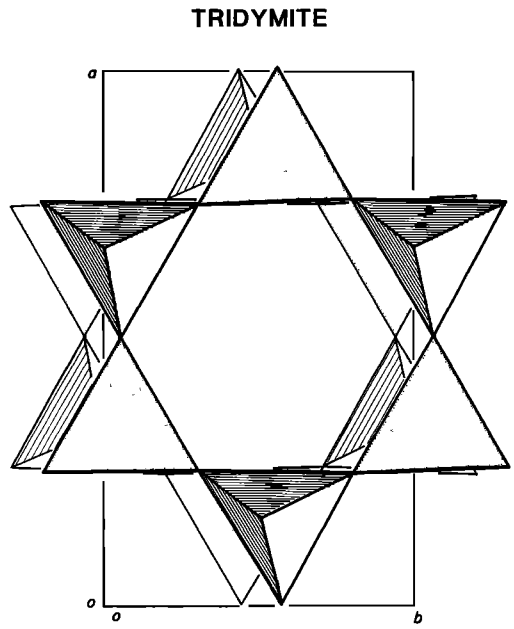

Fig. 10*d*. Projection of the high tridymite structure down *c* [from *Papike and Cameron*, 1976].

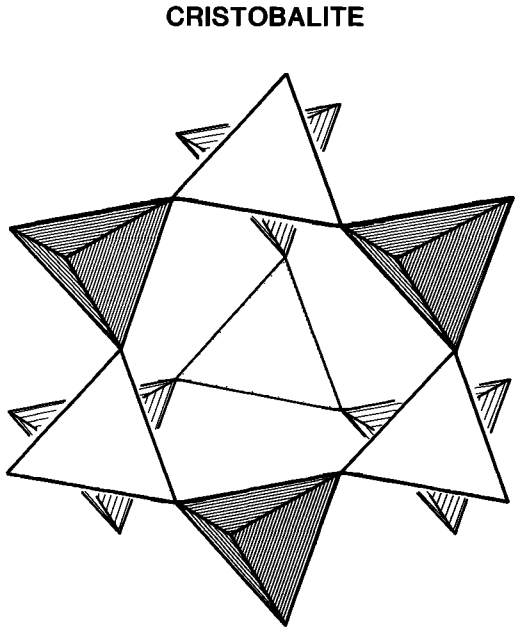

Fig. 10e. Projection of a portion of the high cristobalite structure onto (111) [from *Papike and Cameron*, 1976].

of K for Na in the nepheline structure increases from ~25 mol % at 24°C to ~70 mol % at 1070°C, whereas the substitution of Na for K in the kalsilite structure increases from zero to 25 mol % over the same temperature interval.

TABLE 13*a*. Cell Parameters of Alkali Feldspars

	a, Å	*b*, Å	*c*, Å	α, deg	β, deg	γ, deg
Sanidine	8.56	13.03	7.17	90	116	90
Orthoclase	8.56	13.00	7.19	90	116	90
Intermediate microcline	8.58	12.96	7.21	90.3	116	89.1
Maximum microcline	8.57	12.98	7.22	90.7	116	87.5
High albite	8.15	12.88	7.11	93.4	116.3	90.3
Low albite	8.14	12.79	7.16	94.3	116.6	87.6

From *Deer et al.* [1963*b*].

The nepheline structure can be described as a stuffed derivative of high tridymite, in which Al replaces approximately one half of the Si, and atoms such as K, Na, and Ca occupy interstitial voids to maintain charge balance. *Buerger et al.* [1954] originally determined the structure, and *Hahn and Buerger* [1955] further refined it. Nepheline is hexagonal and has space group symmetry $P6_3$ ($a = 10.0$ Å, $c = 8.4$ Å, and $Z = 2$ [*Deer et al.*, 1963*b*]), although some specimens possess high pseudosymmetry close to $P6_3/m$ [*Dollase*, 1970; *Foreman and Peacor*, 1970]. There are four nonequivalent tetrahedral sites per unit cell: T1 and T2 occupy special positions on three-fold axes, and T3 and T4 occupy general positions. The T2-T3 and T1-T4 tetrahedra point in opposite directions along the *c* axis (Figure 12*a*). Within this tetrahedral framework are two distinct types of interstitial sites. One fourth of the sites are nearly hexagonal in geometry and are occupied

TABLE 12. Quartz-Tridymite Analyses

	Quartz				Tridymite	
	Sample 1 (DHZ192-1)	Sample 2 (DHZ192-2)	Sample 3 (DHZ192-3)	Sample 4 (DHZ192-4)	Sample 5 (DHZ192-5)	Sample 6 (DHZ192-6)
			Major Oxides			
SiO_2	99.79	99.78	99.53	99.00	95.1	95.1
Al_2O_3	0.042		0.02		2.4	2.70
Fe_2O_3	0.007	0.07	0.05		0.36	0.25
TiO_2	0.048	0.015			0.26	0.28
MgO	0.008	0.09			0.3	0.03
FeO		0.04	0.05	0.36		
MnO	0.009			0.02	0.003	0.00
CaO	0.010				0.40	0.2
Na_2O					0.80	0.67
K_2O					0.37	0.75
Total	99.91	100.0	99.65	99.38	99.99	99.98
			Number of Ions Based on Two Oxygens			
Si	0.999	0.999	0.999	0.998	0.967	0.965
Al	0.001		0.000		0.029	0.032
Fe^{3+}	0.000	0.001	0.000		0.003	0.002
Ti^{4+}	0.000	0.000			0.002	0.002
Σ tetrahedra	1.000	1.000	0.999	0.998	1.001	1.001
Mg	0.000	0.001			0.005	0.001
Fe^{2+}		0.000	0.000	0.003		
Mn^{2+}	0.000			0.000	0.000	0.000
Ca	0.000				0.004	0.002
Na					0.016	0.013
K					0.005	0.010
Σ others	0.000	0.001	0.000	0.003	0.030	0.026

All analyses are from *Deer et al.* [1963*b*]; for example, DHZ192-1 refers to page 192, column 1 of Deer et al.

TABLE 13*b*. Feldspar Analyses

	Alkali Feldspar				K Feldspar*		Plagioclase Feldspar						Ba Feldspar
	Sample 1 (DHZ39-13)	Sample 2 (DHZ37-15)	Sample 3 (DHZ40-6)	Sample 4 (DHZ36-1)	Sample 5 (DHZ45-5)	Sample 6 (DHZ45-8)	Sample 7 (DHZ108-1)	Sample 8 (DHZ109-8)	Sample 9 (DHZ112-6)	Sample 10 (DHZ115-14)	Sample 11 (DHZ117-14)	Sample 12 (DHZ120-6)	Sample 13 (DHZ171-14)
						Major Oxides							
SiO_2	64.40	63.01	64.40	65.76	64.76	64.25	68.30	67.39	64.10	56.10	52.06	43.54	33.01
Al_2O_3	19.09	19.73	19.50	20.23	17.22	16.06	19.64	18.97	22.66	27.66	30.09	35.66	27.16
Fe_2O_3	0.31	0.62	0.35	0.18	1.50	2.93	0.08	1.30	0.14	0.08	0.41	0.58	0.28
TiO_2			0.27	0.08	0.00		0.00		0.00	0.04	0.07		
MgO	0.04	0.19	0.07	0.10	0.04	0.00	0.00	0.38	0.25	0.06	0.18	0.06	0.14
FeO			0.05		0.00	0.25			0.17	0.15	0.25	0.00	
MnO	0.01						0.00	0.14	0.00				
CaO	0.05	0.26	1.19	1.19	0.06		0.03	0.40	3.26	9.70	13.00	19.53	0.06
BaO		0.50	0.27	0.63						0.02	0.04		38.53
Na_2O	1.09	1.51	4.19	8.44	0.47	0.44	11.65	10.67	9.89	5.48	3.64	0.26	0.15
K_2O	15.26	14.53	9.40	3.29	16.00	16.15	0.08	0.11	0.05	0.62	0.35		0.54
Total	100.25	100.35	99.69	99.90	100.05	100.08	99.78	99.36	100.52	99.91	100.09	99.63	99.87
						Number of Ions Based on Eight Oxygens							
Si	2.964	2.912	2.933	2.930	3.004	3.003	2.989	2.974	2.817	2.526	2.364	2.024	2.028
Al	1.036	1.075	1.046	1.062	0.942	0.885	1.013	0.986	1.174	1.468	1.611	1.954	1.967
Fe^{3+}	0.011	0.022	0.012	0.006	0.052	0.103	0.002	0.043	0.004	0.002	0.016	0.020	0.013
Ti			0.009	0.003						0.001	0.002		
Σ tetrahedra	4.011	4.009	4.000	4.001	3.998	3.991	4.004	4.003	3.995	3.997	3.993	3.998	4.008
Mg	0.008	0.013	0.005	0.007	0.003			0.025	0.016	0.004	0.012	0.004	0.013
Fe^{2+}			0.002			0.010			0.006	0.006	0.010		
Ca	0.002	0.013	0.058	0.057	0.003		0.001	0.019	0.154	0.468	0.633	0.973	0.004
Ba		0.010	0.005	0.011						0.001	0.001		0.928
Na	0.097	0.135	0.370	0.729	0.042	0.040	0.988	0.913	0.842	0.478	0.320	0.024	0.018
K	0.896	0.857	0.546	0.187	0.947	0.963	0.004	0.006	0.003	0.036	0.020		0.042
Σ others	1.003	1.028	0.986	0.991	0.995	1.013	0.993	0.963	1.021	0.993	0.996	1.001	1.005
						Mineral Composition, mol %							
Cn†													92.4
Or	89.8	84.3	55.9	20.0	89.9	84.7	0.5	0.6	0.3	3.6	2.1		4.2
Ab	9.7	13.2	37.5	73.6	4.2	4.9	99.4	94.3	82.5	48.3	32.1	2.4	1.7
An	0.5	2.5	6.6	6.4	0.6		0.1	5.1	17.2	48.1	65.8	97.6	1.7
Fe-Or					5.3	10.4							

All analyses are from *Deer et al.* [1963*b*]; for example, DHZ39-13 refers to page 39, column 13 of Deer et al.
*Fe-rich.
†Celsian.

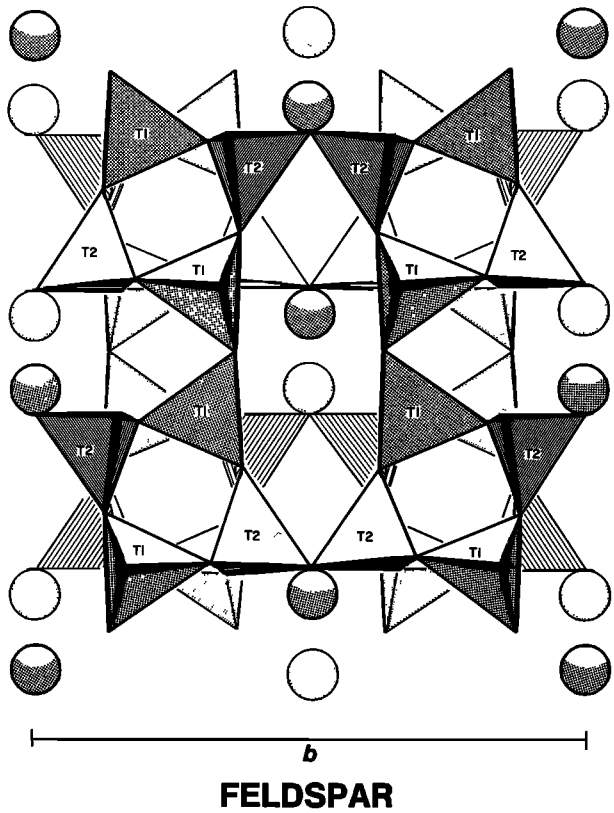

Fig. 11. Projection of a portion of the high sanidine structure [from *Papike and Cameron*, 1976].

principally by K; the remaining three fourths are occupied by Na. The larger K atom is coordinated by nine oxygen atoms, whereas Na is coordinated by either seven or eight oxygens [*Dollase*, 1970]. The O1 atom, which is bonded to Na, is disordered to maintain local charge balance. It is displaced from the threefold axis and statistically occupies each of three different off-axis positions [*Simmons and Peacor*, 1972].

Si and Al are ordered over the tetrahedral sites in nepheline. In general, the T1 and T4 sites are Al-rich, and the T2 and T3 sites are Si-rich [*Dollase and Peacor*, 1971; *Simmons and Peacor*, 1972; *Foreman and Peacor*, 1970]; thus Al tetrahedra share corners with Si tetrahedra, and Si tetrahedra share corners with Al tetrahedra. Structure refinements of five crystals with different thermal histories indicate a variable degree of Si-Al ordering depending on crystallization history [*Dollase and Peacor*, 1971]. The Al and Si in a nepheline from a low-temperature pegmatitic environment [*Foreman and Peacor*, 1970] are highly ordered over all four tetrahedral sites, with T1 and T4 containing most of the Al and T2 and T3 most of the Si. In contrast, the Si-Al distribution in a volcanic nepheline [*Simmons and Peacor*, 1972] shows considerable disorder between T1 and T2 but a high degree of order between T3 and T4.

Kalsilite, $KAlSiO_4$, crystallizes in space group $P6_3mc$ or $P6_3$ ($a = 5.15$ Å, $c = 8.68$ Å, and $Z = 2$ [*Dollase and Freeborn*, 1977]). The structure of a $P6_3mc$ kalsilite was reported by *Dollase and Freeborn* [1977], who showed that the structure is similar to that of $P6_3$ kalsilite but with positionally disordered oxygen atoms. This disorder is attributed to a domain structure. The crystal structure of a $P6_3$ kalsilite was reported by *Perrotta and Smith* [1965].

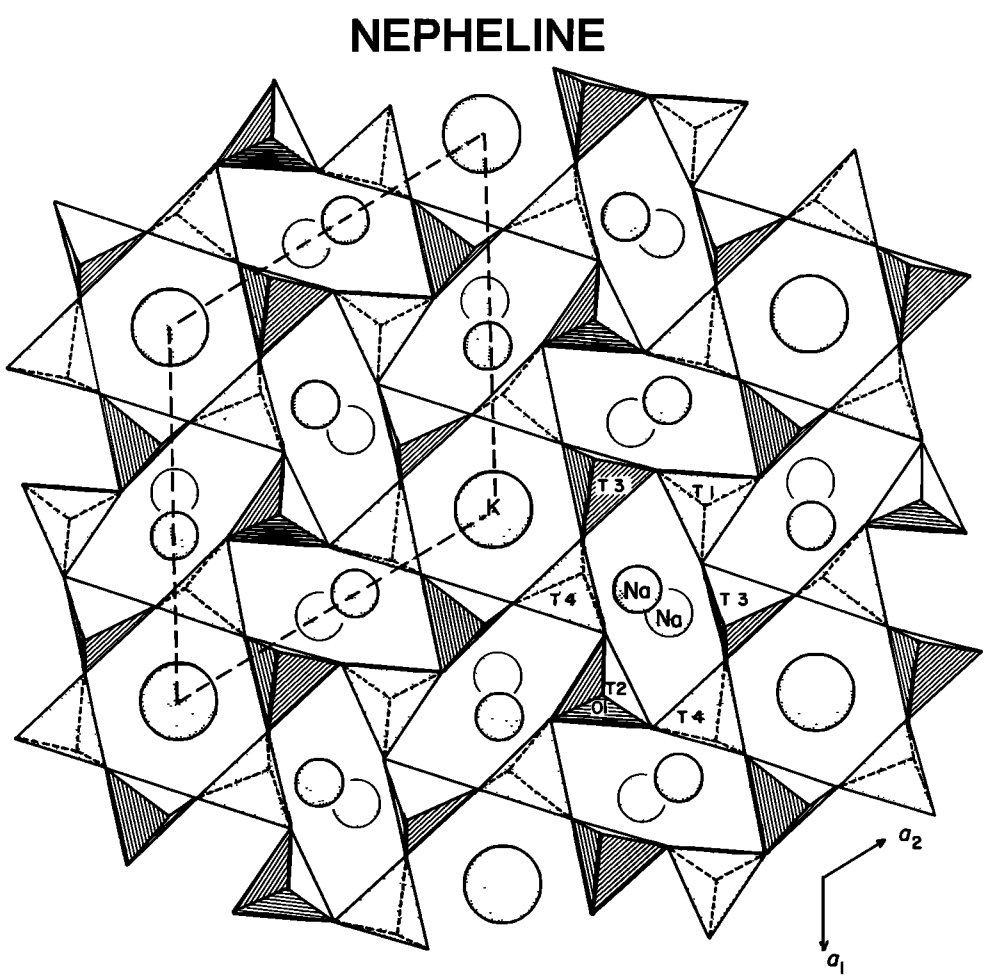

Fig. 12*a*. Projection of the crystal structure of nepheline down *c* [from *Papike and Cameron*, 1976].

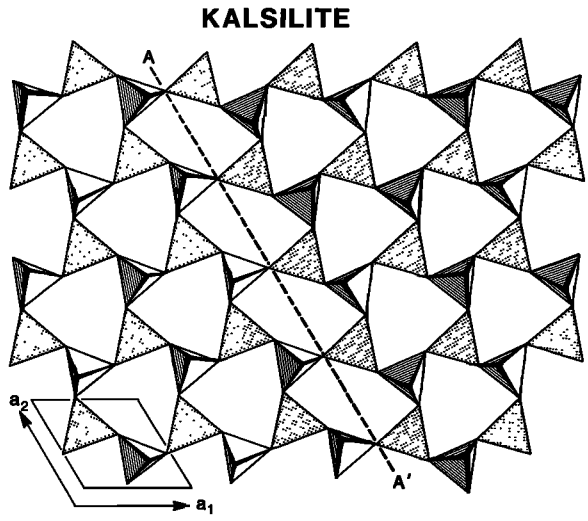

Fig. 12*b*. Projection of the tetrahedral sheet of $P6_3mc$ kalsilite down *c* [after *Dollase and Freeborn*, 1977].

The structure of $P6_3mc$ kalsilite is shown in Figure 12*b*. In this drawing of the structure, regions farthest from the line AA′ display the ideal $P6_3$ kalsilite structure, the unit cell of which is shown. This structure is represented by layers of six-membered rings of SiO_4 and AlO_4 tetrahedra, with K atoms (not shown) occupying sites at the centers of the rings. The Si tetrahedra point out of the paper, whereas the Al tetrahedra point into the paper. In ideal $P6_3$ kalsilite, all of the ditrigonal rings of tetrahedra (the centers look like arrowheads which show a direction) and oriented in the same direction in any one tetrahedral layer. In $P6_3mc$ kalsilite the orientation of the ditrigonal rings changes at the domain boundary AA′.

Table 14 lists some representative nepheline-kalsilite analyses from *Deer et al.* [1963*b*]. *Deer et al.* [1963*b*] show that nepheline contains more Si and less Al than would be represented by a strict solid solution between $NaAlSiO_4$ and $KalSiO_4$. In natural nepheline calculated on the basis of 16 oxygens the nontetrahedral sites sum to 3.3–4.0 occupancy, which indicates some vacancies in these sites [*Deer et al.*, 1963*b*]. *Donnay et al.* [1959] give the general formula, reflecting the importance of vacancies, as $K_xNa_yCa_z\square_{8-(x+y+z)}Al_{(x+y+2z)}Si_{16-(x+y+2z)}O_{32}$ based on a double formula unit.

Microprobe analyses should be reduced on a 16-oxygen basis. Good analyses, so reduced, should have $Si + Al + Fe^{3+}$ approximately equal to eight.

LEUCITE-ANALCITE

Leucite, $KAlSi_2O_6$, is tetragonal (space group $I4_1/a$, $a = 13.0$ Å, $c = 13.8$ Å, and $Z = 16$ [*Deer et al.*, 1963*b*]) with pseudocubic symmetry. At approximately 600°C it transforms into a cubic structure with space group symmetry $Ia3d$ [*Peacor*, 1968; *Sadanaga and Ozawa*, 1968; *Taylor and Henderson*, 1968]. In the low-temperature modification [*Wyart*, 1938, 1940, 1941; *Náray-Szabó*, 1942], as described by *Deer et al.* [1963*b*], the tetrahedra share corners to form both four- and six-membered rings (Figure 13) that are perpendicular to the fourfold and the "pseudothreefold" axes, respectively. The 12-coordinated K atoms occur in large cavities along a line joining the centers of the six-membered rings. At low temperatures the K atoms are presumably too small to fill the large cavities that they occupy, but at higher temperatures, thermal vibrations increase the K atoms' effective size. This, in turn, results in an expansion of the collapsed structure and an increase in symmetry. *Peacor* [1968] refined the structure of the high-temperature polymorph.

TABLE 14. Nepheline-Kalsilite Analyses

	Nepheline			Kalsilite	
	Sample 1 (DHZ242-3)	Sample 2 (DHZ242-6)	Sample 3 (DHZ244-14)	Sample 4 (DHZ253-2)	Sample 5 (DHZ253-3)
			Major Oxides		
SiO_2	44.40	45.02	41.06	38.48	37.98
Al_2O_3	33.14	32.72	33.93	31.01	31.73
Fe_2O_3	0.18	0.52	0.83	1.12	0.98
TiO_2	0.00	0.04	0.00	0.05	0.05
MgO	0.05	0.06	0.00	0.00	0.00
CaO	0.36	0.60	0.19	0.03	0.00
Na_2O	17.17	16.36	15.92	0.30	0.87
K_2O	3.72	4.70	7.14	28.33	27.99
Total	99.02	100.02	99.07	99.32	99.60
			Number of Ions Based on 16 Oxygens		
Si	4.252	4.284	4.024	4.062	3.998
Al	3.742	3.671	3.920	3.860	3.940
Fe^{3+}	0.012	0.038	0.061	0.089	0.038
Ti		0.003		0.004	0.004
Σ tetrahedra	8.006	7.996	8.005	8.015	7.980
Mg	0.007	0.008			
Ca	0.037	0.056	0.020	0.003	
Na	3.188	3.018	3.025	0.062	0.178
K	0.454	0.571	0.893	3.818	3.762
Σ others	3.686	3.653	3.938	3.883	3.940

All analyses are from *Deer et al.* [1963*b*]; for example, DHZ242-3 refers to page 242, column 3 of Deer et al.

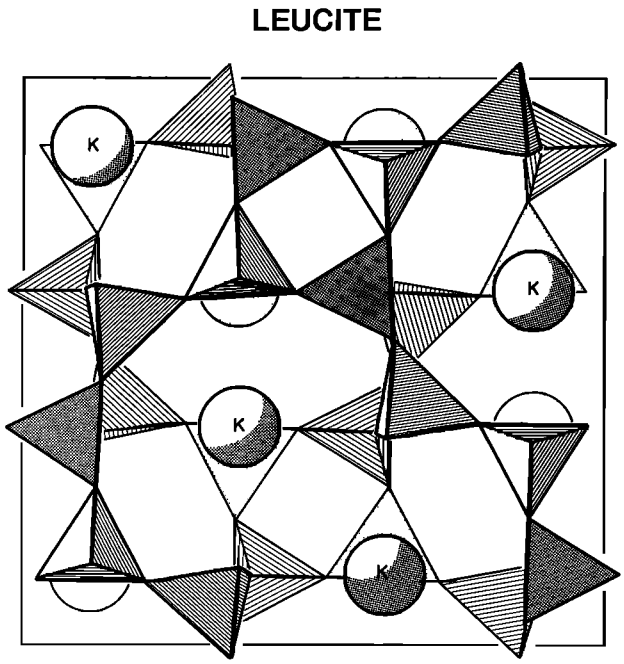

Fig. 13. Projection of a portion of the leucite structure down c [from *Papike and Cameron*, 1976].

Selected analyses for leucite are presented in Table 15. Leucite compositions are close to ideal, with the main substitution involving Na for K. Microprobe analyses should be normalized to six oxygens. Good analyses will have K, Na, Ca approximately equal to one and Si, Al, Fe^{3+}, Ti approximately equal to three.

Analcite, $NaAlSi_2O_6 \cdot H_2O$, crystallizes in space group *Ia3d*, with $a = 13.7$ Å and $Z = 16$ [*Deer et al.*, 1963*b*]; it is isostructural with leucite and pollucite, $CsAlSi_2O_6$ [*Cerný*, 1974]. The structure of analcite was determined by *Taylor* [1930]. The framework of analcite is the same as that of leucite (Figure 13) and contains a set of 16 large cavities which form continuous channels parallel to three-fold symmetry axes. These channels are occupied by H_2O groups. Adjacent to these 16 large cavities are 24 smaller ones occupied by Na. The Na cations are octahedrally coordinated by four coplanar oxygens and two H_2O groups. A neutron diffraction study of analcite [*Ferraris et al.*, 1972] confirms that the structure has cubic symmetry.

Representative chemical analyses of analcite are presented in Table 15. The chemical compositions are quite constant [*Deer et al.*, 1963*b*], with the only appreciable substitution involving K and Ca for Na. Microprobe analyses should be reduced on the basis of six oxygens, and it is safe to assume that one H_2O group per formula unit is also present. The analyses of Table 15 [*Deer et al.*, 1963*b*] are reduced on the basis of seven oxygens because H_2O was determined. Good microprobe analyses will have Na, K, Ca approximately equal to one and Al, Si approximately equal to three.

Sodalite Group

The most important members of the sodalite group are sodlite, $Na_8[Al_6Si_6O_{24}]Cl_2$; nosean, $Na_8[Al_6Si_6O_{24}]SO_4$; and haüyne, $(Na, Ca)_{4-8}(Al_6Si_6O_{24})(SO_4, S)_{1-2}$. Names and formu-

TABLE 15. Leucite-Analcite Analyses

	Leucite			Analcite	
	Sample 1 (DHZ280-4)	Sample 2 (DHZ280-5)	Sample 3 (DHZ280-7)	Sample 4 (DHZ343-3)	Sample 5 (DHZ343-6)
		Major Oxides			
SiO_2	55.4	54.66	56.39	55.11	54.10
Al_2O_3	23.3	23.15	23.10	22.86	23.68
Fe_2O_3	0.5*	0.36			
TiO_2	0.2	0.17			
MgO	0.0	0.04		0.00	
FeO		0.11			
CaO	1.1	0.11	0.27	0.12	0.45
Na_2O	1.8	0.63	2.17	13.79	13.40
K_2O	18.3	20.04	18.05	0.18	0.34
H_2O				8.20	8.22
Total	100.6	99.27	99.98	100.26	100.19
		Number of Ions†			
Si	1.99	1.992	2.019	2.013	1.981
Al	0.98	0.995	0.975	0.984	1.022
Fe^{3+}	0.01	0.010			
Ti	0.01	0.005			
Mg		0.002			
Fe^{2+}		0.003			
Σ tetrahedra	2.99	3.007	2.994	2.997	3.003
Ca	0.04	0.004	0.010	0.005	0.018
Na	0.13	0.045	0.151	0.977	0.951
K	0.84	0.932	0.825	0.008	0.016
Σ others	1.01	0.981	0.986	0.990	0.985
H^+				1.999	2.008

All analyses are from *Deer et al.* [1963*b*]; for example, DHZ280-4 refers to page 280, column 4 of Deer et al.

*Total iron as Fe^{3+}

†Number of ions is based on six oxygens for leucite and seven oxygens for analcite.

TABLE 16*a*. The Sodalite Group

Mineral	Formula	Z^*	Space Group	Unit Cell Edge, Å
Sodalite	$Na_8[Al_6Si_6O_{24}]Cl_2$	1	$P\bar{4}3n$	8.91
Nosean	$Na_8[Al_6Si_6O_{24}]SO_4$	1	$P\bar{4}3n$	9.05
Haüyne	$(Na, Ca)_{4-8}[Al_6Si_6O_{24}](SO_4, S)_{1-2}$	1	$P\bar{4}3n$	9.13
Lazurite	$(Na, Ca)_8[Al_6Si_6O_{24}](SO_4, S, Cl)_2$	1	$P\bar{4}3n$	9.08
Danalite	$Fe_8^{2+}[Be_6Si_6O_{24}]S_2$	1	$P\bar{4}3n$	8.20
Helvite	$(Mn, Fe^{2+}, Zn)_8[Be_6Si_6O_{24}]S_2$	1	$P\bar{4}3n$	8.21–8.29
Genthelvite	$Zn_8[Be_6Si_6O_{24}]S_2$	1	$P\bar{4}3n$	8.12

From *Deer et al.* [1963*b*]. Space group as reported by *Hassan and Grundy* [1984*a*].
*Number of formula units per unit cell.

lae of other members and space group and unit cell information are given in Table 16*a*.

The structure of sodalite can be described as an aluminosilicate framework with cavities occupied by sodium and chlorine (Figure 14). The configuration of the framework was first determined by *Jaeger* [1929*a*, *b*]. The structure was further described by *Barth* [1932] and *Pauling* [1930*c*]. A modern refinement of sodalite and consideration of crystal chemical aspects of the sodalite group are given by *Hassan and Grundy* [1984*a*]. The structural framework is composed of corner-shared alternating SiO_4 and AlO_4 tetrahedra. Cagelike cuboctahedral units are formed bounded by six four-membered tetrahedral rings parallel to the six (100) faces and

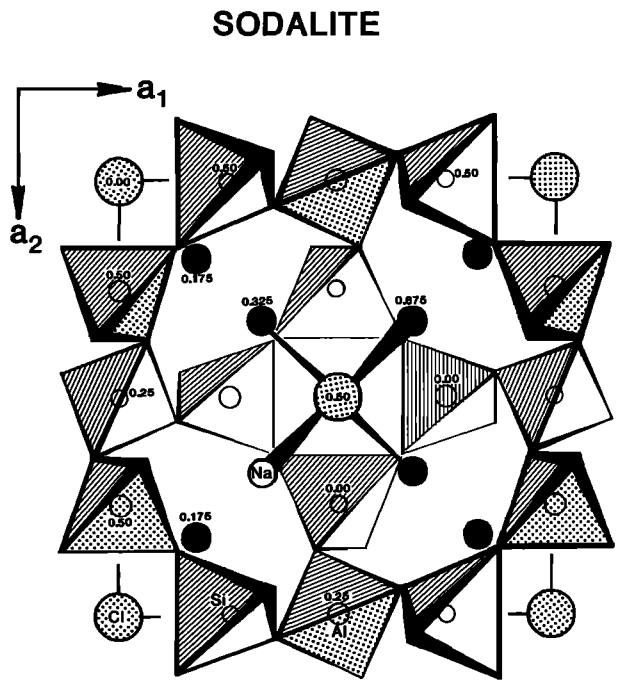

Fig. 14. Crystal structure of sodalite [after *Pauling*, 1930*c*].

eight six-membered tetrahedral rings parallel to the eight (111) faces. These cages are stacked in eightfold coordination with each six-membered ring (each ring is parallel to one of the eight (111) faces) shared by two cages. The six-membered rings

TABLE 16*b*. Sodalite Group Analyses

	Sodalite		Nosean	Haüyne	
	Sample 1 (DHZ292-2)	Sample 2 (DHZ292-6)	Sample 3 (DHZ295-1)	Sample 4 (DHZ295-4)	Sample 5 (DHZ295-5)
			Major Oxides		
SiO_2	36.99	36.72	36.69	32.18	34.04
Al_2O_3	31.77	31.17	28.45	27.11	28.27
Fe_2O_3	0.17	0.70	0.47		
CaO			0.63	10.26	9.51
Na_2O	25.84	24.53	23.90	16.34	10.39
K_2O	0.16	1.13		0.08	5.44
Cl	6.44	7.22	1.05	0.31	0.76
S	0.39				
SO_3			7.30	14.10	10.02
Total	101.76	101.47	98.49	100.38	98.43
Minus O = Cl, S	1.64	1.63	0.23	0.07	0.17
New total	100.12	99.84	98.26	100.31	98.26
	Number of Ions Based on the 21 Oxygens Associated With Six Al and Six Si				
Si	5.959	5.961	6.203	6.018	6.055
Al	6.034	5.965	5.670	5.976	5.927
Fe^{3+}	0.020	0.086	0.060		
Σ tetrahedra	12.013	12.012	11.933	11.994	11.982
Ca			0.114	2.056	1.813
Na	8.070	7.721	7.834	5.924	3.583
K	0.033	0.234		0.019	1.233
Σ X cations	8.103	7.955	7.948	7.999	6.629
Cl	1.756	1.986	0.301	0.098	0.229
S	0.118				
SO_4			0.926	1.979	1.336
Σ Cl, S, SO_4	1.874	1.986	1.227	2.077	1.565

All analyses are from *Deer et al.* [1963*b*]; for example, DHZ292-2 refers to page 292, column 2 of Deer et al.

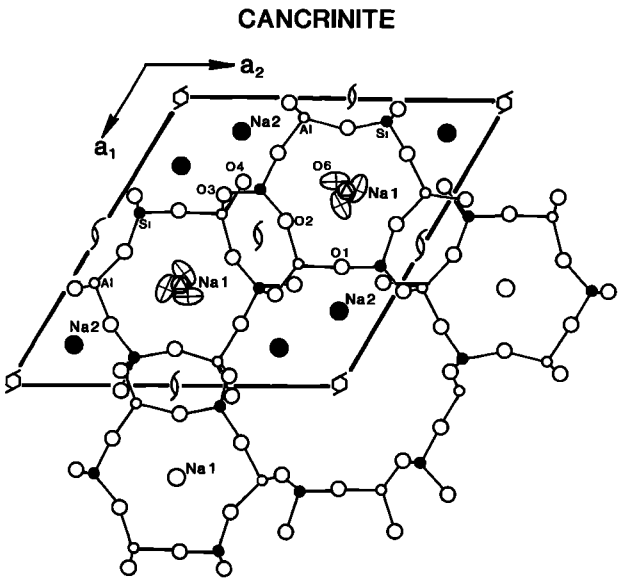

Fig. 15. Crystal structure of cancrinite showing four-, six- and 12-membered rings of alternating silicon and aluminum tetrahedra [after *Grundy and Hassan*, 1982].

thus form channelways parallel to the cube diagonals; these channelways are efficient diffusion paths.

The large central cavities are occupied by Cl^- in sodalite, and these chlorine ions are tetrahedrally coordinated by sodium cations which lie on the cube diagonals (four near the chlorine at the center of the unit cell and four near the chlorines at the cube corners) [*Deer et al.*, 1963*b*]. The eight sodium ions per unit cell are symmetrically equivalent, and each is coordinated by one chlorine and three framework oxygens.

In a detailed study of the sodalite group minerals, *Hassan and Grundy* [1984*a*] present a geometric model for the sodalite group which enables (1) prediction of atomic coordinates of all members of the sodalite group minerals at both room and high temperatures, (2) prediction of the chemical limits of stability, and (3) prediction of thermal expansion data.

Table 16*b* gives representative chemical analyses for sodalite, nosean, and haüyne [*Deer et al.*, 1963*b*]. The formulae are calculated on the basis of 21 oxygens (=42 negative charges, e.g., those charges necessary to balance six Al and six Si, which equal 42 positive charges). However, I recommend microprobe analyses be normalized to 12 (Si + Al + Fe^{3+}) cations. In sodalites there is a small amount of substitution of K and Ca for Na and of Fe^{3+} for Al. Microprobe analyses calculated on the basis of 12 (Si + Al + Fe^{3+}) cations have few criteria for good analyses because the X cations (Na, Ca, etc.) can sum to less than eight and the cage anions (Cl^-, SO_4^{2-}, etc.) are also variable. Provisionally, the microprobe data should be compared with analyses in Table 16*b*.

Cancrinite Group

The cancrinite-vishnevite minerals form a solid solution series in which the major substitutions involve $CO_3^{2-} \leftrightarrows SO_4^{2-}$ and Ca ⇆ Na [*Deer et al.*, 1963*b*]. The carbonate-rich members of the series contain more calcium atoms per formula unit than the sulphate varieties. The reason for this will be explained below. Deer et al. give the end-member formula for cancrinite as $(Na, Ca)_{7-8}[Al_6Si_6O_{24}](CO_3, SO_4, Cl)_{1.5-2.0} \cdot 1\text{–}5H_2O$ and for vishnevite as $(Na, Ca, K)_{6-7}[Al_6Si_6O_{24}](SO_4, CO_3, Cl)_{1\ 0-1.5} \cdot 1\text{–}5H_2O$. They give the general formula for the series as $(Na, Ca, K)_{6-8}[Al_6Si_6O_{24}](CO_3, SO_4, Cl)_{1-2} \cdot 1\text{–}5H_2O$.

However, *Hassan and Grundy* [1984*b*] give the ideal formula for end-member vishnevite as $Na_8Al_6Si_6O_{24} \cdot SO_4 \cdot 2H_2O$ with space group $P6_3$, $a = 12.68$ Å, $c = 5.18$ Å, and $Z = 1$. In addition, they suggest an ideal end-member composition for cancrinite as $Ca_2Na_6Al_6Si_6O_{24}(CO_3)_2 \cdot 2H_2O$. The Ca cations provide two excess charges relative to vishnevite to balance the two excess negative charges resulting from two CO_3 groups relative to one SO_4 group in vishnevite.

The general features of the cancrinite structure were determined by Pauling [1930*a*] and further defined by *Jarchow* [1965]. The crystal structure of a carbonate-rich cancrinite was refined by *Grundy and Hassan* [1982]. Another refinement of cancrinite was reported by *Pahor et al.* [1982]. *Hassan and Grundy* [1984*b*] report a refinement of the vishnevite structure and discuss important crystal chemical aspects of the cancrinite-vishnevite solid solution series.

The cancrinite group of minerals is characterized by an ordered framework of alternating AlO_4 and SiO_4 tetrahedra (Figure 15). The hexagonal symmetry, $P6_3$, is the result of close packing of interconnected and parallel sixfold rings of tetrahedra in an ABAB stacking sequence [*Grundy and Hassan*, 1982]. The sodalite minerals show strong structural similarities to the cancrinite group. However, the sodalite minerals have stacking sequence ABCABC, which leads to cubic instead of hexagonal symmetry. Also, in the cancrinite group the different stacking sequence results in a large continuous channel parallel to the *c* axis. In sodalite this channel is offset by the C-type layer to give a network of large cages instead of

TABLE 17. Cancrinite Group Analyses

	Cancrinite		Vishnevite	
	Sample 1 (DHZ312-1)	Sample 2 (DHZ312-4)	Sample 3 (DHZ313-7)	Sample 4 (DHZ313-8)
	Major Oxides			
SiO_2	33.64	33.98	34.76	35.29
Al_2O_3	29.82	29.11	30.81	28.79
MgO	0.39			0.10
CaO	8.64	4.80	3.87	1.49
Na_2O	15.41	18.69	18.90	15.65
K_2O	0.50	0.64	1.29	4.15
CO_2	6.79	7.00	1.90	1.01
SO_3	0.03	1.37	5.93	5.76
Cl		0.42		
Total	95.22	96.01	97.46	92.24
O = Cl		0.10		
New total	95.22	95.91	97.46	92.24
	Number of Ions Based on 12 (Si, Al)			
Si	5.867	5.971	5.866	6.118
Al	6.130	6.032	6.129	5.886
Σ tetrahedra	11.997	12.003	11.995	12.004
Mg	0.102			0.026
Ca	1.614	0.904	0.700	0.277
Na	5.210	6.368	6.182	5.260
K	0.111	0.144	0.278	0.919
Σ others	7.037	7.416	7.16	6.482
C	1.617	1.679	0.438	0.239
S	0.004	0.180	0.751	0.749
Cl		0.125		
Σ C, S, Cl	1.621	1.984	1.189	0.988

All analyses are from *Deer et al.* [1963*b*]; for example, DHZ312-1 refers to page 312, column 1 of Deer et al.

TABLE 18. Scapolite Analyses

	Sample 1 (DHZ324-2)	Sample 2 (DHZ324-5)	Sample 3 (DHZ325-8)	Sample 4 (DHZ325-9)	Sample 5 (DHZ325-14)
			Major Oxides		
SiO_2	57.89	54.73	52.10	51.83	47.17
Al_2O_3	21.62	22.85	23.79	24.29	26.29
CaO	4.81	8.29	11.13	11.66	14.31
Na_2O	10.50	8.55	6.86	6.40	3.82
K_2O	1.16	1.08	0.87	1.16	1.01
CO_2	1.11	1.69	2.14	2.28	2.66
SO_3	0.03	0.39	0.80	0.72	1.42
Cl	2.96	2.19	1.85	1.66	0.56
Total	100.08	99.77	99.54	100.00	97.24
O = Cl, F	0.67	0.49	0.46	0.38	0.14
New total	99.41	99.28	99.08	99.62	97.1
			Number of Ions Based on 12 (Si, Al)		
Si	8.331	8.042	7.799	7.729	7.241
Al	3.668	3.958	4.200	4.271	4.758
Σ tetrahedra	11.999	12.000	11.999	12.000	11.999
Ca	0.742	1.305	1.785	1.863	2.353
Na	2.930	2.436	1.990	1.849	1.136
K	0.212	0.202	0.166	0.220	0.198
Σ others	3.884	3.943	3.941	3.932	3.687
C	0.218	0.339	0.437	0.464	0.557
S	0.003	0.043	0.090	0.081	0.163
Cl	0.722	0.545	0.470	0.419	0.146
Σ C, S, Cl	0.943	0.927	0.997	0.964	0.866

All analyses are from *Deer et al.* [1963*b*]; for example, DHZ324-2 refers to page 324, column 2 of Deer et al.

continuous channels. Cancrinite also has small cages centered around the three-fold axes (Figure 15).

The cancrinite-vishnevite structures are composed of four-, six-, and 12-membered rings of alternating AlO_4 and SiO_4 tetrahedra. In vishnevite [*Hassan and Grundy*, 1984*b*] the cage (around the three-fold axis) contains one Na^+ (Na1 in Figure 15) and one H_2O group disordered around the three-fold axis (O6 oxygen in Figure 15). The important differences between the cancrinite and the vishnevite structures concern the large channel which contains the remaining cations. In vishnevite the remaining cations (Na, Ca, K) are disordered over the six equivalent cation positions (indicated as Na2 in Figure 15), and the SO_4^{2-} groups are disordered over two alternative positions. Because of space limitations in the unit cell, only one SO_4 group per unit cell can be accommodated [*Hassan and Grundy*, 1984*b*], whereas two CO_3 groups can be accommodated in cancrinite. The CO_3 groups in cancrinite and the SO_4 groups in vishnevite are disordered over two positions in the unit cell, with one triangular face of the SO_4^{2-} tetrahedra taking an orientation similar to that of the triangular CO_3^{2-} group. Because of the alternate orientations of the CO_3 and SO_4 groups in the large channelways, each Na2 cation (Na, Ca, K) is coordinated either by a trigonal pyramid or by an octahedral array of oxygen atoms contributed both by the framework and by the CO_3 and SO_4 groups.

Table 17 presents representative chemical analyses [*Deer et al.*, 1963*b*] of the cancrinite-vishnevite series. The analyses are normalized to 12 (Si + Al) atoms, and this is also the recommended way to normalize microprobe analyses. Because the numbers of Na, Ca, K cations and CO_3, SO_4, Cl anions are variable, criteria for good microprobe analyses are difficult to define. Provisionally, microprobe analyses should be compared with the representative analyses given in Table 17.

SCAPOLITE

Scapolites, a group of rock-forming silicates that exhibit many structural complexities, can, as a first approximation, be considered as solid solutions between marialite, $Na_4Al_3Si_9O_{24}Cl$, and meionite, $Ca_4Al_6Si_6O_{24}CO_3$. These formulae are written in the form most consistent with the scapolite structure but marialite and meionite can also be written as $3NaAlSi_3O_8 \cdot NaCl$, and $3CaAl_2Si_2O_8 \cdot CaCO_3$, respectively, to show an analogy with plagioclase feldspar chemistry. Three coupled substitutions are evident in this solid solution series: $Na^+ \leftrightarrows Ca^{2+}$, $Si^{4+} \leftrightarrows Al^{3+}$, and $Cl^- \leftrightarrows CO_3^{2-}$. All three substitutions are active in the more sodic part of the series ($Ca/(Ca + Na) < 0.75$), whereas in the less sodic part ($Ca/(Ca + Na) > 0.75$), the substitution is $NaSi \leftrightarrows CaAl$, as in the plagioclase feldspars [*Evans et al.*, 1969]. At $Ca/(Ca + Na) > 0.75$ the anion site is filled with CO_3^{2-} [*Papike*, 1964; *Evans et al.*, 1969].

The first reasonably complete structure models of scapolite were reported by *Pauling* [1930*a*] and *Schiebold and Seumel* [1932]. The structure of a Na-rich scapolite was first refined by *Papike and Zoltai* [1965], and that of a Ca-rich scapolite by *Papike and Stephenson* [1966]. *Lin and Burley* [1973*a*, *c*, 1975] reported three additional structural refinements. The ideal end-members, marialite and meionite, display diffraction symmetry consistent with space group *I4/m*, but intermediate compositions have reflections that violate this symmetry and reduce the space group to a primitive type. *Papike and Stephenson* [1966] reported diffuse reflections violating the body-

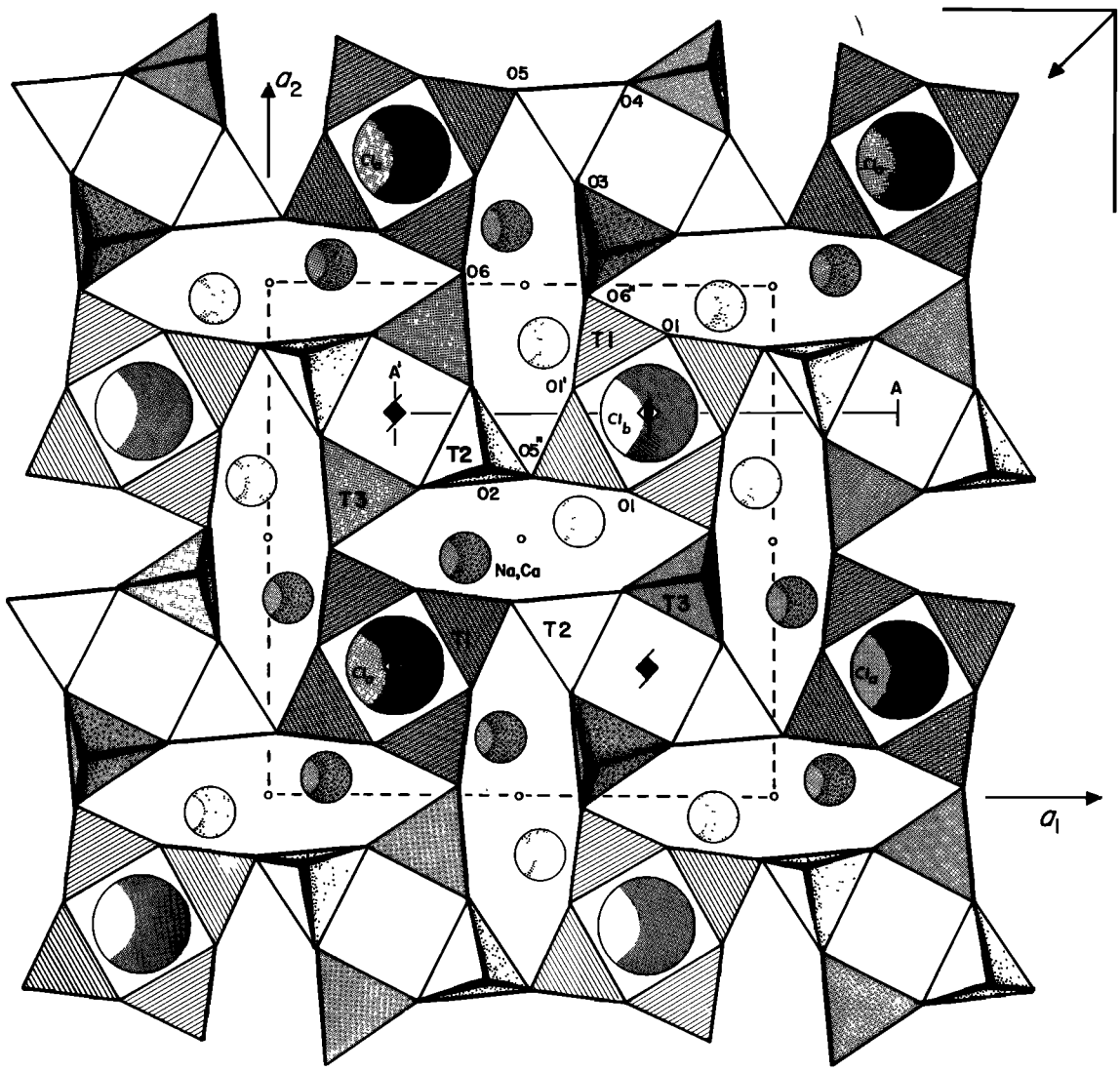

Fig. 16*a*. Crystal structure of the $P4_2/n$ marialite scapolite projected down *c* [from *Levien and Papike*, 1976].

centered symmetry but did not treat them in the structural refinement. *Lin and Burley* [1973*a*, *b*, *c*, 1975] state that the true space group is $P4_2/n$, and their three refinements are reported in this space group, even though they did not observe reflections violating $I4/m$ symmetry in their meionite-rich scapolite. *Ulbrich* [1973] also states that the space group for intermediate compositions is $P4_2/n$. However, *Phakey and Ghose* [1972] and *Buseck and Iijima* [1974] conclude from electron diffraction studies that the space group for intermediate compositions is $P4$ or $P4/m$. Despite the number of space groups reported for various scapolites, most of the structural features are consistent with space group $P4_2/n$, and until proven otherwise, I will assume that all scapolites have this symmetry.

Infrared spectra [*Papike*, 1964; *Schwarcz and Speelman*, 1965] suggest that the carbonate group is a trigonal group similar to those in other substances. The role of a trigonal carbonate group in a tetragonal mineral was first addressed by *Papike and Stephenson* [1966], who suggested that the carbonate group in each unit cell is displaced off the fourfold axis ($I4/m$) and disordered over four different positions in the (001) plane.

Levien and Papike [1976] studied a scapolite derived from a slowly cooled metamorphic rock to study the Al-Si distributions and the thermal expansion and to determine the precise location of the carbonate group. The unit cell information for this scapolite (Table 18, sample 2) is space group $P4_2/n$, with $a = 12.07$ Å, $c = 7.58$ Å, and $Z = 2$. This structural discussion is abstracted from the work of *Levien and Papike* [1976]. The scapolites are framework aluminosilicates with a unique arrangement of four-membered tetrahedral rings which form two distinct types of channels, the first of which contains either Na^+ or Ca^{2+}. These oval-shaped channels run parallel to the *c* axis and are best shown in Figures 16*a* and 16*b*, projections down the *c* axis of marialite and meionite, respectively. The second channel type contains the volatile constituent CO_3^{2-}, shown in Figure 16*b*, or Cl^-, shown in Figures 16*a* and 16*c*. Figure 16*c*, which is a projection down the a_2

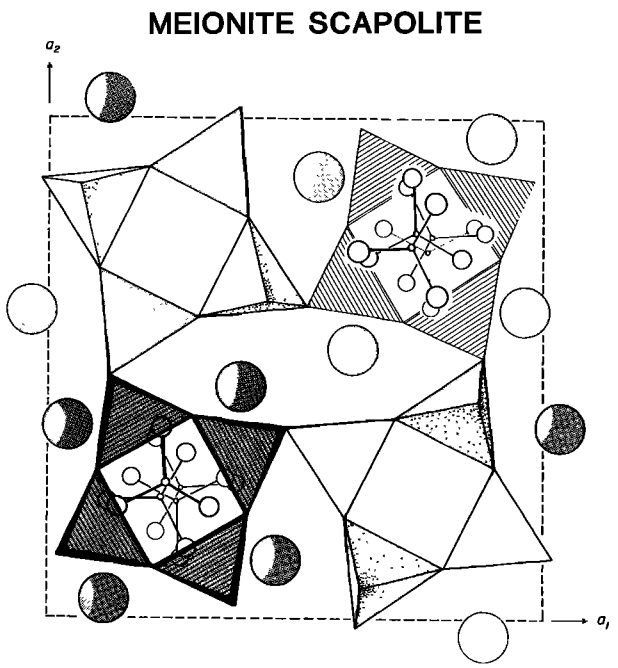

Fig. 16*b*. Crystal structure of a portion of the meionite scapolite structure showing the disordered CO_3^{2-} group [from *Levien and Papike*, 1976].

axis perpendicular to section AA′ in Figure 16*a*, shows the five-membered tetrahedral rings in which Al-O-Al linkage occurs. The refinement results indicate that the trigonal carbonate group is disordered in a manner consistent with $P4_2/n$ symmetry and that the carbonate group is very close to being in the (001) plane, tilting less than 3°.

Five representative analyses of scapolite are reported in Table 18. The analyses are reduced on the basis of 12 (Si + Al), and this is also the way microprobe analyses should be reduced. Because the nonframework cations (largely Na, Ca) and cage anions (largely Cl, CO_3^{2-}) have variable occupancy, there are no good criteria for acceptable microprobe analyses. Therefore, once again, I recommend comparison of the microprobe analyses to the analyses reported in this review paper (Table 18 for scapolite).

CONCLUDING STATEMENT

Within time and space constraints I have attempted to convey structural chemical essentials of 16 groups of multiple-chain, sheet, and framework silicates. The purpose of this exercise, as with part 1 of this synthesis [*Papike*, 1987], is to provide those using silicate mineral chemistry with a ready reference to the relevant crystal structures. For some of the mineral groups considered, e.g., pyriboles, greenalite, minnesotaite, and stilpnomelane, it is difficult to state rigorous criteria for good microprobe analyses because of the complexity of the structures involved. For others, e.g., sodalite, cancrinite, and scapolite, it is difficult to develop criteria for good microprobe analyses because of the complexity of chemical substitutions and variable occupancy of the nonframework cation and anion sites. Nevertheless, despite these complexities, reference to the relevant crystal structures is essential to extract the maximum chemical information for the common multiple-chain, sheet, and framework silicates.

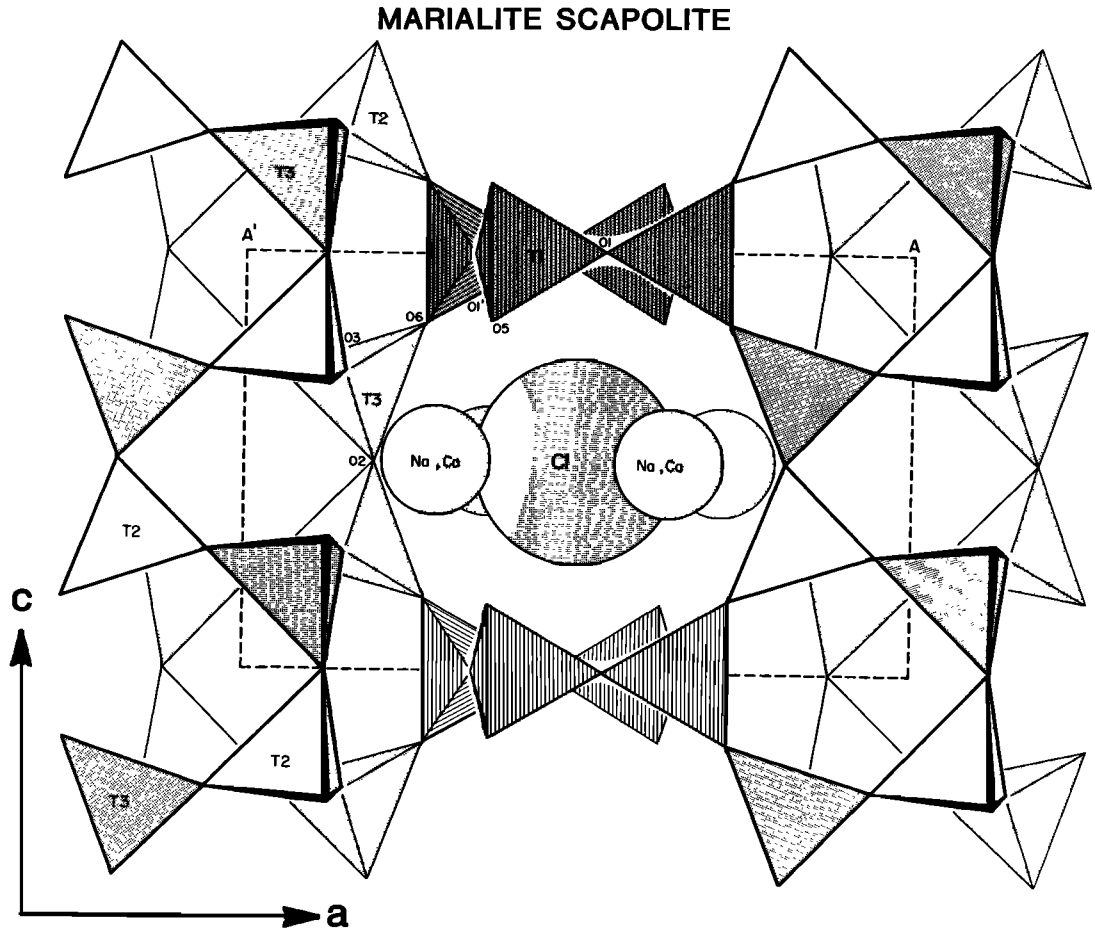

Fig. 16*c*. Projection of the $P4_2/n$ marialite scapolite structure down *a* and onto the AA′ plane [from *Levien and Papike*, 1976].

Acknowledgments. This research was supported by the Institute for the Study of Mineral Deposits, which is gratefully acknowledged. Thanks go to Dolores Nelson for typing the various drafts of this paper and also for carefully typing numerous tables. Genet Duke is acknowledged for her dedicated drafting of complicated structure diagrams. Pauline Papike is thanked for her assistance in technical aspects of putting this review together. Steve Simon's help in reviewing an early draft of this paper is appreciated. Additional detailed reviews by S. Guggenheim, F. Hawthorne, and two anonymous reviewers are gratefully acknowledged.

The Editor thanks David Veblen and Sturges Bailey for their assistance in evaluating this paper.

REFERENCES

Bailey, S. W., Chlorites, in *Soil Components*, vol. II, *Inorganic Components*, edited by Gieseking, pp. 191–263, Springer-Verlag, New York, 1975.

Bailey, S. W., (Ed.), *Reviews in Mineralogy*, vol. 13, *Micas*, 584 pp., Mineralogical Society of America, Washington, D. C., 1984.

Barth, T. F. W., The structures of the minerals of the sodalite family, *Z. Kristallogr., 83*, 405, 1932.

Bayliss, P., Nomenclature of the trioctahedral chlorites, *Can. Mineral., 13*, 178–180, 1975.

Bragg, W. H., and R. E. Gibbs, The structure of α and β quartz, *Proc. R. Soc. London, Ser. A, 109*, 405–427, 1925.

Buerger, M. J., G. E. Klein, and G. Donnay, Determination of the crystal structure of nepheline, *Am. Mineral., 39*, 805–818, 1954.

Buseck, P. R., and S. Iijima, High resolution electron microscopy of silicates, *Am. Mineral., 59*, 1–21, 1974.

Cameron, M., and J. J. Papike, Amphibole crystal chemistry: A review, *Fortschr. Mineral., 57*, 28–67, 1979.

Cerný, P., The present status of the analcime-pollucite series, *Can. Mineral., 12*, 334–341, 1974.

Cerný, P., and D. M. Burt, Paragenesis, crystallochemical characteristics, and geochemical evolution of micas in granite pegmatites, in *Reviews in Mineralogy*, vol. 13, *Micas*, edited by S. W. Bailey, pp. 257–297, Mineralogical Society of America, Washington, D. C., 1984.

Deer, W. A., R. A. Howie, and J. Zussman, *Rock-Forming Minerals*, vol. 3, *Sheet Silicates*, 270 pp., John Wiley, New York, 1962.

Deer, W. A., R. A. Howie, and J. Zussman, *Rock-Forming Minerals*, vol. 2, *Chain Silicates*, 379 pp., John Wiley, New York, 1963*a*.

Deer, W. A., R. A. Howie, and J. Zussman, *Rock-Forming Minerals*, vol. 4, *Framework Silicates*, 435 pp., John Wiley, New York, 1963*b*.

Deer, W. A., R. A. Howie, and J. Zussman, *An Introduction to the Rock-Forming Minerals*, 528 pp., John Wiley, New York, 1966.

De Vries, A., Determination of the absolute configuration of quartz, *Nature, 181*, 1193, 1958.

Dollase, W. A., Reinvestigation of the structure of low cristobalite, *Z. Kristallogr., 121*, 369–377, 1965.

Dollase, W. A., The crystal structure at 220°C of orthorhombic high tridymite from the Steinbach meteorite, *Acta Crystallogr., 23*, 617–623, 1967.

Dollase, W. A., Least-squares refinement of the structure of a plutonic nepheline, *Z. Kristallogr., 132*, 27–44, 1970.

Dollase, W. A., and W. H. Baur, The superstructure of meteoritic low tridymite solved by computer simulation, *Am. Mineral., 61*, 971–978, 1976.

Dollase, W. A., and W. P. Freeborn, The structure of $KAlSiO_4$ with $P6_3mc$ symmetry, *Am. Mineral., 62*, 336–340, 1977.

Dollase, W. A., and D. R. Peacor, Si-Al ordering in nephelines, *Contrib. Mineral. Petrol., 30*, 129–134, 1971.

Donnay, G., J. F. Schairer, and J. D. H. Donnay, Nepheline solid solution, *Min. Mag., 32*, 93–109, 1959.

Drits, V. A., Y. I. Goncharov, V. A. Aleksandrova, V. E. Khadzhi, and A. L. Dmitrik, New type of strip silicate (in Russian), *Kristallografiya, 19*, 1186–1193, 1974. (*Sov. Phys. Crystallogr.*, Engl. Transl., *19*, 737–741, 1974.

Eggleton, R. A., The crystal structure of stilpnomelane, II, The full cell, *Mineral. Mag., 38*, 693–711, 1972.

Eggleton, R. A., and B. W. Chappell, The crystal structure of stilpnomelane, III, Chemistry and physical properties, *Mineral. Mag., 42*, 361–369, 1978.

Evans, B. W., D. M. Shaw, and D. R. Haughton, Scapolite stoichiometry, *Contrib. Mineral. Petrol., 24*, 293–305, 1969.

Ferraris, G., D. W. Jones, and J. Yerkess, A neutron-diffraction study of the crystal structure of analcime, $NaAlSi_2O_6 \cdot H_2O$, *Z. Kristallogr., 135*, 240–252, 1972.

Finger, L. W., The crystal structure and cation distribution of a grunerite, *Mineral. Soc. Am. Spec. Pap., 2*, 95–100, 1969.

Floran, R. J., and J. J. Papike, Petrology of the low-grade rocks of the Gunflint Iron-Formation, Ontario-Minnesota, *Geol. Soc. Am. Bull., 86*, 1169–1190, 1975.

Foreman, N., and D. R. Peacor, Refinement of the nepheline structure at several temperatures, *Z. Kristallogr., 132*, 45–70, 1970.

Foster, M. D., Interpretation of the composition and a classification of the chlorites, *U.S. Geol. Surv. Prof. Pap., 414-A*, 1–33, 1962.

Francke, W., B. Jelinski, and M. Zarei, Hydrothermal synthesis of an ephesite-like sodium mica, *Neues Jahrb. Miner. Monatsh.*, 337–340, 1982.

Frondel, C., *The System of Mineralogy*, vol. 3, *Silica Minerals*, 333 pp., John Wiley, New York, 1962.

Gibbs, G. V., Crystal structure of protoamphibole, *Mineral. Soc. Am. Spec. Pap., 2*, 101–109, 1969.

Gibbs, R. E., Structure of α quartz, *Proc. R. Soc. London, Ser. A, 110*, 443–445, 1926.

Gibbs, R. E., The polymorphism of silicon dioxide and the structure of tridymite, *Proc. R. Soc. London, Ser. A, 113*, 351–368, 1927.

Goldich, S. S., Determination of ferrous iron in silicate rocks, *Chem. Geol., 42*, 343–347, 1984.

Gossner, B., and F. Mussgnug, Röntgenographische untersuchungen an Prehnit und Lawsonit, *Zentralbl. Mineral., Teil 1, 1931A*, 419–423, 1931.

Grundy, H. D., and I. Hassan, The crystal structure of a carbonate-rich cancrinite, *Can. Mineral., 20*, 239–251, 1982.

Gruner, J. W., The crystal structures of talc and pyrophyllite, *Z. Kristallogr., 85*, 412–419, 1934.

Gruner, J. W., The structure and chemical composition of greenalite, *Am. Mineral., 21*, 449–455, 1936.

Gruner, J. W., The composition and structure of minnesotaite, a common iron silicate in iron formations, *Am. Mineral., 29*, 363–372, 1944.

Guggenheim, S., and R. A. Eggleton, Structural modulations in iron-rich and magnesium-rich minnesotaite, *Can. Mineral., 24*, 479–497, 1986.

Guggenheim, S., S. W. Bailey, R. A. Eggleton, and P. Wilkes, Structural aspects of greenalite and related minerals, *Can. Mineral., 20*, 1–18, 1982.

Hahn, T., and M. J. Buerger, The detailed structure of nepheline, $KNa_3Al_4Si_4O_{16}$, *Z. Kristallogr., 106*, 308–338, 1955.

Hassan, I., and H. D. Grundy, The crystal structures of sodalite-group minerals, *Acta Crystallogr., Sect. B, 40*, 6–13, 1984*a*.

Hassan, I., and H. D. Grundy, The character of the cancrinite-vishnevite solid-solution series, *Can. Mineral., 22*, 333–340, 1984*b*.

Hawthorne, F. C., The crystal chemistry of the amphiboles, *Can. Mineral., 21*, 173–480, 1983.

Hurlbut, C. S., Jr., and C. Klein, *Manual of Mineralogy*, 19th ed., 532 pp., John Wiley, New York, 1977.

Jaeger, F. M., Investigations about the structure of ultramarines, IV, On the ultramarines of thallium and on the analogous derivatives of the bivalent metals, calcium, strontium, barium, zinc, manganese, and lead, *Proc. Sect. Sci. Akad. Wiss. Amsterdam, 30*, 249, 1929*a*.

Jaeger, F. M., On the constitution and structure of ultramarine, *Trans. Faraday Soc., 25*, 320, 1929*b*.

Jarchow, O., Atomanordnung und Strukturverfeinerung von Cancrinit, *Z. Kristallogr., 122*, 407–422, 1965.

Johannsen, A., Petrographic terms for field use, *J. Geol., 19*, 317–322, 1911.

Katscher, H., and F. Liebau, Uber die Kristallstruktur von $Ba_2Si_3O_8$, ein Silikat mit Dreifachketten, *Naturwissenschaften, 18*, 512–513, 1965.

Klein, C., Greenalite, stilpnomelane, minnesotaite, crocidolite and carbonates in a very low-grade metamorphic Precambrian iron-formation, *Can. Mineral., 12*, 475–498, 1974.

Klein, C., Diagenesis and metamorphism of Precambrian banded iron-formations, in *Iron-Formation: Facts and Problems*, edited by A. F. Trendall and R. C. Morris, pp. 417–469, Elsevier, New York, 1983.

Klein, C., and R. P. Fink, Petrology of the Sokoman Iron Formation in the Howells River area, at the western edge of the Labrador Trough, *Econ. Geol., 71*, 453–487, 1976.

Leake, B. E., Nomenclature of amphiboles, *Can. Mineral., 16*, 501–520, 1978.

Lee, J. H., and S. Guggenheim, Single crystal X-ray refinement of pyrophyllite—1 *Tc*, *Am. Mineral., 66*, 350–357, 1981.

Lesher, C. M., Mineralogy and petrology of the Sokoman Iron Formation near Ardua Lake, Quebec, Canada, *J. Earth Sci. Leeds, Engl., 15*, 480–500, 1978.

Levien, L., and J. J. Papike, Scapolite crystal chemistry: Aluminum-

silicon distributions, carbonate group disorder, and thermal expansion, *Am. Mineral., 61*, 864–877, 1976.

Liebau, F., Classification of silicates, in *Reviews in Mineralogy*, vol. 5, *Orthosilicates*, edited by P. H. Ribbe, pp. 1–24, Mineralogical Society of America, Washington, D. C., 1980.

Liebau, F., *Structural Chemistry of Silicates, Structure, Bonding, and Classification*, 347 pp., Springer-Verlag, New York, 1985.

Lin, S. B., and B. J. Burley, Crystal structure of a sodium and chlorine-rich scapolite, *Acta Crystallogr., Sect. B, 29*, 1272–1278, 1973*a*.

Lin, S. B., and B. J. Burley, On the weak reflections violating body-centered symmetry in scapolites, *Tschermaks Mineral. Petrogr. Mitt., 20*, 28–44, 1973*b*.

Lin, S. B., and B. J. Burley, The crystal structure of meionite, *Acta Crystallogr., Sect. B, 29*, 2024–2026, 1973*c*.

Lin, S. B., and B. J. Burley, The crystal structure of an intermediate scapolite-wernerite, *Acta Crystallogr., Sect. B, 31*, 1806–1814, 1975.

Miyano, T., Effects of CO_2 on mineralogical differences in some low-grade metamorphic iron-formations, *Geochem. J., 12*, 201–211, 1978.

Moore, P. B., Quartz: Variations on a theme, *Am. Mineral., 71*, 540–546, 1986.

Náray-Szabó, S., Die Struktur des Leucits $KAlSi_2O_6$, *Z. Kristallogr., 104*, 39–44, 1942.

Nieuwenkamp, W., Uber die Struktur von Hoch-Kristobalit, *Z. Kristallogr., 96*, 454–458, 1937.

Nuffield, E. W., Prehnite from Ashcroft, British Columbia, *Toronto Univ. Stud. Geol. Ser., 48*, 49–64, 1943.

Pahor, N. B., M. Calligaris, G. Nardin, and L. Randaccio, Structure of a basic cancrinite, *Acta Crystallogr., Sect. B, 38*, 893–895, 1982.

Papike, J. J., The crystal structure and crystal chemistry of scapolite, Ph.D. thesis, Univ. of Minn., Minneapolis, 1964.

Papike, J. J., Chemistry of the rock-forming silicates: Ortho, ring, and single-chain structures, *Rev. Geophys., 25*, 1483–1526, 1987.

Papike, J. J., and M. Cameron, Crystal chemistry of silicate minerals of geophysical interest, *Rev. Geophys., 14*, 37–80, 1976.

Papike, J. J., and M. Ross, Gedrites: Crystal structures and intracrystalline cation distributions, *Am. Mineral., 55*, 1945–1972, 1970.

Papike, J. J., and N. C. Stephenson, The crystal structure of mizzonite, a calcium- and carbonate-rich scapolite, *Am. Mineral., 51*, 1014–1027, 1966.

Papike, J. J., and T. Zoltai, The crystal structure of a marialite scapolite, *Am. Mineral., 50*, 641–655, 1965.

Papike, J. J., and T. Zoltai, Ordering of tetrahedral aluminum in prehnite, $Ca_2(Al, Fe^{3+})[Si_3AlO_{10}](OH)_2$, *Am. Mineral., 52*, 974–984, 1967.

Papike, J. J., M. Ross, and J. R. Clark, Crystal-chemical characterization of clinoamphiboles based on five new structure refinements, *Mineral. Soc. Am. Spec. Pap., 2*, 117–136, 1969.

Pauling, L., The structure of some sodium and calcium aluminosilicates; *Proc. Natl. Acad. Sic. U. S. A., 16*, 453–459, 1930*a*.

Pauling, L., The structure of chlorites, *Proc. Natl. Acad. Sci. U. S. A., 16*, 578–582, 1930*b*.

Pauling, L., The structure of sodalite and helvite, *Z. Kristallogr., 74*, 213–225, 1930*c*.

Peacor, D. R., A high-temperature single-crystal diffractometer study of leucite, $(K, Na)AlSi_2O_6$, *Z. Kristallogr., 127*, 213–224, 1968.

Peacor, D. R., High-temperature single-crystal study of the cristobalite inversion, *Z. Kristallogr., 138*, 274–298, 1973.

Peng, Sze-Tung, Chou Kung-Du, and Tang You-Chi, The structure of prehnite, *Hua Hsueh Hsueh Pao, 25*, 56–63, 1969.

Perdikatsis, B., and H. Burzlaff, Strukturverfeinerung am Talk $Mg_3[(OH)_2Si_4O_{10}]$, *Z. Kristallogr., 156*, 177–186, 1981.

Perrotta, A. J., and J. V. Smith, The crystal structure of kalsilite, $KAlSiO_4$, *Mineral. Mag., 35*, 588–595, 1965.

Phakey, P. P., and S. Ghose, Scapolite: Observation of anti-phase domain structure, *Nature London Phys. Sci., 238*, 78–80, 1972.

Preisinger, A., Prehnit—Ein neuer Schichtsilikattyp, *Tschermaks Mineral. Petrogr. Mitt., 10*, 491–504, 1965.

Quint, R., Description and crystal structure of amstallite, $CaAl(OH)_2[Al_{0.8}Si_{3.2}O_8(OH)_2] \cdot [(H_2O)_{0.8}Cl_{0.2}]$, a new mineral from Amstall, Austria, *Neues Jahrb. Miner. Monatsh., 6*, 253–262, 1987.

Rayner, J. H., and G. Brown, Structure of pyrophyllite, *Clays Clay Miner., 13*, 73–84, 1964.

Rayner, J. H., and G. Brown, The crystal structure of talc, *Clays Clay Miner., 21*, 103–114, 1973.

Ribbe, P. H. (Ed.), *Reviews in Mineralogy*, vol. 2, *Feldspar Mineralogy*, 2nd ed., 362 pp., Mineralogical Society of America, Washington, D. C., 1983.

Sadanaga, R., and T. Ozawa, Thermal transition of leucite, *Mineral. J., 5*, 321–333, 1968.

Schiebold, E., and G. Seumel, Uber die Kristallstruktur von Skapolith, *Z. Kristallogr., 81*, 110–134, 1932.

Schwarcz, H. P., and E. L. Speelman, Determination of sulfur and carbon coordination in scapolite by infra-red absorption spectrophotometry, *Am. Mineral., 50*, 656–666, 1965.

Seifert, F., and W. Schreyer, Synthesis and stability of micas in the system K_2O-MgO-SiO_2-H_2O and their relation to phlogopite, *Contrib. Mineral Petrol., 30*, 196–215, 1971.

Simmons, W. B., Jr., and D. R. Peacor, Refinement of the crystal structure of a volcanic nepheline, *Am. Mineral., 57*, 1711–1719, 1972.

Smith, J. V., and H. S. Yoder, Jr., Experimental and theoretical studies of the mica polymorphs, *Mineral. Mag., 31*, 209–235, 1956.

Taylor, D., and C. M. B. Henderson, The thermal expansion of the leucite group of minerals, *Am. Mineral., 53*, 1476–1489, 1968.

Taylor, W. H., The structure of analcite ($NaAlSi_2O_6 \cdot H_2O$), *Z. Kristallogr., 74*, 1, 1930.

Thompson, J. B., Jr., Geometrical possibilities for amphibole structures: Model biopyriboles (abstract), *Am. Mineral., 55*, 292–293, 1970.

Thompson, J. B., Jr., Biopyriboles and polysomatic series, *Am. Mineral., 63*, 239–249, 1978.

Tuttle, O. F., and J. V. Smith, The nepheline-kalsilite system, 2, Phase relations, *Am. J. Sci., 256*, 571–589, 1958.

Ulbrich, H. H., Crystallographic data and refractive indices of scapolites, *Am. Mineral., 58*, 81–92, 1973.

Veblen, D. R. (Ed.), *Reviews in Mineralogy*, vol. 9A, *Amphiboles and Other Hydrous Pyriboles—Mineralogy*, 372 pp., Mineralogical Society of America, Washington, D. C., 1981.

Veblen, D. R., and C. W. Burnham, Triple-chain biopyriboles: Newly discovered intermediate products of the retrograde anthophyllite-talc transformation, Chester, VT (abstract), *Eos Trans. AGU, 56*, 1076, 1975.

Veblen, D. R., and C. W. Burnham, New biopyriboles from Chester, Vermont, I, Descriptive mineralogy, *Am. Mineral., 63*, 1000–1009, 1978*a*.

Veblen, D. R., and C. W. Burnham, New biopyriboles from Chester, Vermont, II, The crystal chemistry of jimthompsonite, clinojimthompsonite, and chesterite, and the amphibole-mica reaction, *Am. Mineral., 63*, 1053–1973, 1978*b*.

Veblen, D. R., and P. H. Ribbe (Eds.), *Reviews in Mineralogy*, vol. 9B, *Amphiboles: Petrology and Experimental Phase Relations*, 390 pp., Mineralogical Society of America, Washington, D. C., 1982.

Veblen, D. R., P. R. Buseck, and C. W. Burnham, Asbestiform chain silicates: New minerals and structural groups, *Science, 198*, 359–365, 1977.

Wardle, R., and G. W. Brindley, The crystal structures of pyrophyllite 1*Tc* and of its dehydroxylate, *Am. Mineral., 57*, 732–750, 1972.

Wei, P., The structure of α-quartz, *Z. Kristallogr., 92*, 355–362, 1935.

Wyart, J., Etude sur la leucite, *Bull. Soc. Fr. Mineral., 61*, 228–238, 1938.

Wyart, J., Etude cristallographique d'une leucite artificielle; structure atomique et symmétrie du minéral, *Bull. Soc. Fr. Mineral., 63*, 5–17, 1940.

Wyart, J., Structure atomique de la leucite, *C. R. Acad. Sci., 282*, 356–359, 1941.

Wyckoff, R. W. G., The crystal structure of the high-temperature form of cristobalite (SiO_2), *Am. J. Sci., 9*, 448–459, 1925.

Young, R. A., and B. Post, Electron density and thermal effects in alpha quartz, *Acta Crystallogr., 15*, 337–346, 1962.

J. J. Papike, South Dakota School of Mines and Technology, 501 East Saint Joseph Street, Rapid City, SD 57701.

(Received December 9, 1987;
accepted March 23, 1988.)